Title: SHANK3 controls maturation of social reward circuits in the VTA.
Authors: Bariselli S, Tzanoulinou S, Glangetas C, Prévost-Solié C, Pucci L, Viguié J, Bezzi P, O'Connor EC, Georges F, Lüscher C, Bellone C
Journal: Nature neuroscience
Year: 2016 Jul
Volume: 19
Issue: 7
Pages: 926-34
DOI: 10.1038/nn.4319

SHANK3 controls maturation of social reward circuits in the VTA

Sebastiano Bariselli[1,7], Stamatina Tzanoulinou[1,7], Christelle Glangetas[1–3], Clément Prévost-Solié[1], Luca Pucci[1], Joanna Viguié[4], Paola Bezzi[1], Eoin C O'Connor[4,] François Georges[2,3,6], Christian Lüscher[4,5] & Camilla Bellone[1]

[1]Department of Fundamental Neurosciences, University of Lausanne, Lausanne, Switzerland. [2]Centre National de la Recherche Scientifique, Interdisciplinary Institute for Neuroscience, Bordeaux, France. [3]Université de Bordeaux, Bordeaux, France. [4]Department of Basic Neurosciences, Medical Faculty, University of Geneva, Geneva, Switzerland. [5]Clinic of Neurology, Geneva University Hospital, Geneva, Switzerland. [6]Centre National de la Recherche Scientifique, Neurodegenerative Diseases Institute, Bordeaux, France. [7]These authors contributed equally to this work. Correspondence should be addressed to C.B. (camilla.bellone@unil.ch).

Haploinsufficiency of *SHANK3*, encoding the synapse scaffolding protein SHANK3, leads to a highly penetrant form of autism spectrum disorder. How *SHANK3* insufficiency affects specific neural circuits and how this is related to specific symptoms remains elusive. Here we used shRNA to model *Shank*3 insufficiency in the ventral tegmental area of mice. We identified dopamine (DA) and GABA cell-type-specific changes in excitatory synapse transmission that converge to reduce DA neuron activity and generate behavioral deficits, including impaired social preference. Administration of a positive allosteric modulator of the type 1 metabotropic glutamate receptors mGluR1 during the first postnatal week restored DA neuron excitatory synapse transmission and partially rescued the social preference defects, while optogenetic DA neuron stimulation was sufficient to enhance social preference. Collectively, these data reveal the contribution of impaired ventral tegmental area function to social behaviors and identify mGluR1 modulation during postnatal development as a potential treatment strategy.

Autism spectrum disorders (ASDs) constitute a heterogeneous group of neurodevelopmental conditions characterized by impairments in two core domains: communication and social behavior and repetitive or stereotyped actions[1,2]. Behavioral interventions for social deficits have been suggested, while pharmacotherapy is limited to reducing ASD symptoms such as irritability (for example, risperidone), but fails to address impairments in any of the core domains. To

aid the development of new treatment options, a better understanding of how brain circuits controlling social and repetitive behaviors are altered in ASDs is required.

Brain regions involved in the control of social behavior and repetitive actions show a surprising degree of overlap, encompassing corticolimbic-ventral striatal networks[3,4]. Notably, these regions are subject to modulation by DA neurons of the ventral tegmental area (VTA) and a growing body of literature points to impaired function of this 'reward circuit' as contributing to social deficits in ASDs[5,6]. For example, according to the social motivation hypothesis of autism, social interactions would normally occur because they are inherently rewarding, but individuals with ASDs show a deficit in assigning value to social stimuli resulting in social dysfunction[6]. Midbrain DA neurons signal motivationally relevant stimuli[7,8], and fiber photometry has revealed an increase in VTA DA neuron Ca^{2+} activity during social interactions[9]. However, how genetic risk factors affect VTA function and the mechanisms by which this affects social behavior has not been explored.

Although the etiology of autism is unclear, twin studies highlight a strong genetic component of the disease[10]. Many of the genes implicated in ASDs encode for synaptic proteins and, for this reason, autism is considered a 'synaptopathy'[11]. *SHANK3* is one such gene, encoding the excitatory synapse scaffolding protein SHANK3, whose loss or mutation is associated with Phelan-McDermid syndome[12] and other isolated cases of ASD[13,14]. Through its different domains, SHANK3 orchestrates the layout of metabotropic and ionotropic glutamate receptors at the synapse[15]. For example, the PDZ region is responsible for the indirect link of NMDA receptors (NMDARs) and AMPA receptors (AMPARs), while the proline-rich domain of SHANK3 binds to metabotropic glutamate receptor (mGluR) group I via the Homer protein. In mutant mice with disruptions of distinct SHANK3 domains, a variety of electrophysiological and behavioral phenotypes were reported[16–20]. While such knockout models underscore the importance of *Shank3* deficiency in impairing behavior, how dysfunction in specific brain circuits may contribute to specific behavioral deficits has not been fully resolved.

The peak of *Shank3* gene expression occurs within the first postnatal week and decreases during the second and third weeks, a critical period of development when activity shapes neuronal connectivity and circuit function. We have previously shown that during the first postnatal week in mice, AMPAR transmission to VTA DA

neurons is mainly mediated by GluA2-lacking Ca^{2+} permeable AMPARs[21]. Activation of metabotropic mGluR1 during postnatal development removes these calcium-permeable AMPARs and inserts GluA2-containing receptors. Notably, removal of mGluR1 or exposure to addictive drugs *in utero* impairs the postnatal maturation of glutamatergic transmission to VTA DA neurons, resulting in persistent and aberrant expression of GluA2-lacking AMPARs[21,22]. Given the importance of SHANK3 in orchestrating excitatory synaptic function, we hypothesized that low levels of SHANK3 in the VTA could also affect the maturation of excitatory synapses in this structure, driving long-lasting synaptic, circuit and behavioral deficits that could contribute to the pathology of ASDs.

Here we use a shRNA to induce early postnatal downregulation of SHANK3 specifically in the VTA. The resulting SHANK3 insufficiency impairs the maturation of excitatory synapses onto both VTA DA and GABA neurons. These synaptic changes are concomitant with reduced *in vivo* burst activity of DA neurons, increased activity of GABA neurons and behavioral deficits including impaired social preference that persists into adulthood. Providing a causal link between altered DA neuron activity and social behavior, we find that systemic treatment with a positive allosteric modulator (PAM) of mGluR1 during the postnatal period of synapse maturation normalizes social deficits into adulthood, owing to a specific partial rescue of DA neuron excitatory transmission and activity. Moreover, optogenetic activation of VTA DA neurons increases social preference in SHANK3-deficient mice, confirming sufficiency of DA neuron activity to support social interactions.

RESULTS

SHANK3 insufficiency alters VTA excitatory synaptic transmission

To isolate the potential impact on the VTA caused by global SHANK3 deficiency in some ASD cases, we downregulated SHANK3 (ref. 23) in the VTA of mice before postnatal day (P) 6 using stereotaxic injections of adeno-associated virus (AAV) expressing an shRNA that targets the proline-rich domain encoding a region of *Shank3* mRNA (shShank3), coupled with the ZsGreen reporter (**Fig. 1a**). Construct expression was evident 9 d after the injection (**Supplementary Fig. 1a**), persisted when synapses were mature (more than 20 weeks; data not shown) and was restricted to the VTA, where 61.1% of DA neurons (tyrosine hydroxylase–positive, TH) and 39.5% of non-DA cells (i.e., non-TH cells) were infected (**Supplementary Fig. 1b**).

To better quantify the proportion of VTA GABA cells infected, GAD-Cre mice were injected with AAV-DIO-tdTomato at postnatal day (P) 14 allowing the specific identification of GABA neurons (**Fig. 1b**). Quantification of ZsGreen expression in TH^+ and tdTomato-labeled cells confirmed shShank3 expression in 53.5% of DA neurons and 31.4% of GABA neurons, respectively (**Fig. 1b**). Western-blot analysis of the VTA, dissected at adolescence, showed a significant decrease in SHANK3 expression in AAV-shShank3 mice compared to animals infected with a scrambled sequence (AAV-scrShank3; **Fig. 1c**). No difference in SHANK3 expression was found in the neighboring substantia nigra (**Fig. 1c**), indicating that our manipulation was selective for the VTA. Although we did not examine whether morphological changes occurred in VTA neurons, the number of TH^+ cells did not differ when comparing AAV-shShank3-infected and uninfected sides in the same animal (**Supplementary Fig. 1c**), suggesting that shShank3 expression was not affecting cell survival.

Since SHANK3 is enriched in the postsynaptic density of excitatory synapses[15], we examined whether early postnatal *Shank3* downregulation in the VTA could give rise to alterations in excitatory synaptic transmission to VTA neurons. Whole cell *in vitro* patch clamp recordings from shShank3- or scrShank3-infected cells were performed and excitatory postsynaptic currents (EPSCs) pharmacologically isolated. We recorded from putative DA neurons identified by their high capacitance, low input resistance (**Supplementary Fig. 2a,b**), presence of I_h current and morphology. Recordings were made when the postnatal maturation of VTA DA neuron synapses is normally complete (P18–35; early adolescence)[21]. Putative DA neurons infected with shShank3 exhibited a higher AMPA-to-NMDA ratio compared to scrShank3 or uninfected neurons (**Fig. 2a**). There was no change in the paired pulse ratio (PPR), pointing to a postsynaptic locus of this effect (**Fig. 2b**). Taken together, our data indicate that VTA SHANK3 insufficiency alters glutamatergic transmission to putative DA neurons.

At VTA DA neuron synapses, an aberrant increase in the AMPA/NMDA ratio often reflects functional changes in the AMPAR subunit arrangement[24,25]. To analyze the AMPAR subunit composition, AMPAR-mediated EPSCs were pharmacologically isolated and the rectification index (RI), calculated as the slope of the line between current measured at negative and reversal potentials divided by the corresponding

slope measured at positive potentials[26]. An increase in RI was observed in shShank3-infected putative DA neurons compared to both scrShank3 and uninfected putative DA cells (**Fig. 2c**). Changes in AMPAR can occur together with changes in NMDAR subunit composition[21]. However, no change in sensitivity to the GluN2B antagonist ifenprodil or decay time kinetics was found in shShank3-infected compared to uninfected cells (**Fig. 2d-f**), indicating that the content of GluN2B- or GluN2A-containing NMDARs was not affected by SHANK3 insufficiency. Collectively, these data reveal the presence of GluA2-lacking AMPARs at excitatory synapses onto VTA putative DA neurons of adolescent mice, with no change in NMDAR subunit composition following early postnatal VTA SHANK3 insufficiency.

How does VTA SHANK3 insufficiency alter excitatory transmission? In VTA DA neurons, GluA2-lacking AMPARs contribute to synaptic transmission at birth and are then exchanged for GluA2-containing AMPARs during postnatal synapse maturation[21]. One possibility is that SHANK3 insufficiency prevents this physiological maturation of DA neuron synapses. Alternatively, SHANK3 downregulation could alter synaptic transmission irrespective of any developmental influence. To distinguish between these two scenarios, we introduced AAV-Shank3 into the VTA after the postnatal period of synapse maturation[21] (**Fig. 2g**). When SHANK3 was downregulated in the VTA after P20–24, excitatory transmission recorded at P31–P45 remained unaltered (**Fig. 2g**,**h**). These data suggest that SHANK3 is required for the maturation of excitatory transmission of VTA DA neurons and that, once maturation is completed, basal synaptic transmission becomes independent of SHANK3.

We next examined whether postnatal SHANK3 insufficiency affects excitatory transmission to VTA GABA neurons. Putative GABA neurons were identified by their low capacitance, high input resistance (**Supplementary Fig. 2a**,**b**), absence of I_h and characteristic morphology. The AMPA/NMDA ratio was higher in shShank3-infected putative GABA neurons than in uninfected cells, while RI and PPRs did not differ (**Fig. 3a**–**c**). Thus, VTA SHANK3 insufficiency also alters glutamatergic transmission to VTA putative GABA neurons but, in contrast to putative DA neurons, this manipulation does not affect the content of GluA2-containing AMPARs at these synapses where to the best of our knowledge the

presence of these receptors has never been investigated during development. These data point to cell-type–specific functions of SHANK3 within the VTA.

Positive allosteric modulation of mGluR1

In the VTA, pharmacological activation of mGluR1 on DA neurons promotes the switch from GluA2-lacking to GluA2-containing AMPARs[24,26]. We first asked whether this approach could also reverse the delayed maturation observed with SHANK3 insufficiency. We monitored AMPAR EPSCs in VTA putative DA neurons from adolescent mice infected before P6 and bath applied the group I mGluR agonist DHPG (20 μM). This led to a long-term depression and rendered the current–voltage relationship of AMPAR transmission linear (**Fig. 4a**,**b**).

No long-term changes in AMPAR-mediated transmission or RI were observed after DHPG application in uninfected putative DA cells (**Fig. 4a**,**b**). DHPG induced a transient short-term depression in both shShank3 and uninfected cells, which likely reflects release of endocannabinoids, as previously described[27] (**Fig. 4a**). In VTA GABA putative neurons, DHPG treatment did not induce long-lasting changes in AMPAR EPSCs recorded from shShank3-infected nor uninfected putative GABA neurons (**Supplementary Fig. 3a**). Together, these results show that pharmacological activation of group I mGluRs in acute brain slices partially rescue immature AMPAR-transmission through removal of GluA2-lacking AMPARs in putative DA but not in putative GABA neurons.

Would such treatment also be efficient if administered *in vivo*? For this purpose we used a PAM of mGluR1 (Ro 677476; PAM-mGluR1), which offers several advantages over DHPG, including selectivity for mGluR1 and facilitation of existing endogenous activity[28]. The PAM-mGluR1 was administered systemically (4 mg per kg, intraperitoneal injections) once daily starting from P6 until 24 h before *ex vivo* electrophysiological recordings performed between P18 and P33 (**Fig. 4c**). In PAM-mGluR1-treated shShank3 animals, the AMPA/NMDA ratio and RI in VTA putative DA were no different from those in vehicle scrShank3 mice but significantly lower than those in shShank3 mice treated with vehicle (**Fig. 4c**,**d**). PAM-mGluR1 treatment did not affect baseline transmission to VTA putative DA neurons in scrShank3 mice. Consistent with the *in vitro* DHPG data, the AMPA/NMDA ratio recorded at excitatory inputs to VTA GABA neurons remained elevated following PAM-mGluR1 treatment (**Supplementary Fig. 3b**). These data indicate that *in vivo*

PAM-mGluR1 treatment acts specifically at synaptic inputs to putative DA neurons to normalize the maturation deficit induced by SHANK3 insufficiency.

SHANK3 insufficiency alters VTA neuron activity

Group I mGluRs regulate the firing pattern of DA neurons both *in vivo* and *in vitro*[29,30]. Insufficiency of SHANK3 might therefore lead to altered VTA neuron activity. We performed *in vivo* single-unit recordings in adolescent mice previously injected with AAV-shShank3 virus. We found that the total fraction of VTA putative DA[31] neurons classified as 'burst-firing' was similar in shShank3 mice and scrShank3 controls (**Supplementary Fig. 4a**,**b** and **Fig. 5a**). However, while baseline firing rate did not significantly differ among conditions, within the population of burst-firing neurons the frequency within burst (bursting rate) was significantly lower in shShank3 mice than in controls (**Fig. 5b**–**d**). Conversely, the firing rate of putative GABA neurons (for identification parameters, see Online Methods) was significantly higher in shShank3 mice than in scrShank3 controls (**Fig. 5e**,**f**). Thus, as seen *in vitro*, SHANK3 insufficiency leads to cell-type-specific changes in the activity of VTA neurons. Since VTA GABA neurons provide local inhibition to DA neurons[32], their increased activity may further reduce DA neuron output.

Was PAM-mGluR1 treatment *in vivo* also sufficient to recover VTA putative DA neuron activity following SHANK3 insufficiency? As before, following early postnatal VTA injections of AAV-shShank3 or AAV-scrShank3, we gave mice once-daily injections of PAM-mGluR1 during the period of synapse maturation. After these injections, burst activity of putative DA neurons was not different in shShank3 versus scrShank3 mice (**Fig. 5b**–**d**). Taken together, these findings confirm that the activation of mGluR1 during synapse maturation partially rescues the maturation deficits in VTA DA arising from SHANK3 insufficiency.

VTA SHANK3 insufficiency generates social impairments

Shank3 knockout mice exhibit a variety of behavioral deficits, including increased self-grooming and social interaction deficits[16,18,33]. Since DA neuron activity has been shown to encode social interactions[9], we hypothesized that VTA SHANK3 insufficiency may affect behaviors in the social domain.

First we assayed social preference in mice, using a three-chamber social interaction test[34]. In scrShank3 control mice, social preference was maintained for the

entire duration of the 10-min test (**Fig. 6a**–**c**). In contrast, in shShank3 mice, social preference significantly declined after 5 min (**Fig. 6c**,**d**), suggesting a time-dependent loss of social interest. Further analysis showed that reduced social preference could be explained by a shorter social interaction time and a trend toward decreased number of entries (**Fig. 6e**,**f**) at the expense of a longer object interaction time during the second half of the observation period, T_2 (**Supplementary Fig. 5c)**. These effects were not observed in the first half of the observation period, T_1**]**(**Supplementary Fig. 5a**,**b**). Impaired social preference was also observed in mice injected with a smaller volume of shShank3 virus (50 nL; **Supplementary Fig. 6a**–**g**), while no difference was found in a test of social memory between shShank3 mice and controls (**Supplementary Fig. 6h**–**k**), strengthening the case for specific involvement of VTA in social preference.

To examine whether impaired social preference was accompanied by a generalized anhedonic behavior—that is, a reduction in interest in natural reward—we performed a sucrose preference test by comparing intake of different sucrose concentrations to water (**Supplementary Fig. 6l**–**o**). ShShank3 mice preferred the sucrose solution at a high concentration, but not at a low concentration. However, shShank3 mice consumed significantly more water during the low sucrose concentration condition (**Supplementary Fig. 6m**), which led to the observed decreased sucrose preference ratio (**Supplementary Fig. 6l**). Taken together, it is unclear how broadly VTA SHANK3 insufficiency affects behaviors motivated by natural rewards.

Finally, mice were assessed for general activity levels in an open-field arena. There was no evidence for altered thigmotaxis or locomotor activity between shShank3 mice and controls (**Supplementary Fig. 7a**–**c**). However, during this test, shShank3 mice exhibited higher levels of self-grooming than scrShank3 controls (**Supplementary Fig. 7d**). Although levels of self-grooming were insufficient to induce skin lesions, these observations provide some, albeit limited, evidence for increased repetitive behavior following VTA SHANK3 insufficiency. No differences in body weight were observed between scrShank3 and shShank3 vehicle treated mice (**Supplementary Fig. 7e**,**f**). Collectively, our behavioral analyses indicate that VTA SHANK3 insufficiency leads to behavioral alterations, including decreased time interacting with conspecifics and increased self-grooming.

Requirement for VTA DA neuron activity in social preference

Could impaired social preference be ascribed to altered function of VTA DA or GABA neurons? Since PAM-mGluR1 treatment acted to specifically normalize DA neuron synaptic function and activity (**Figs. 4** and **5**), we took advantage of this finding to examine whether this cell-type-specific rescue would be sufficient to normalize social behavior. Thus, following early postnatal intra-VTA AAV-shShank3 or scrShank3 injections, mice received once-daily systemic injections of PAM-mGluR1 during the period of synapse maturation (P6–P27) until 24 h before the three-chamber social interaction test (**Fig. 6a**). While PAM-mGluR1 treatment did not affect social preference dynamics in scrShank3 control mice, social preference dynamics were partially rescued in shShank3 animals (**Fig. 6b**–**f** and **Supplementary Fig. 5a**–**h**). Locomotor parameters, such as the velocity and distance traveled during the test, did not differ between the groups (**Supplementary Fig. 5i**,**j**). These data indicate that altered VTA putative DA neuron function is a key mechanism by which VTA SHANK3 insufficiency generates impaired social preference.

Is the rescue of postnatal maturation with PAM-mGluR1 permanent? To test this possibility, we downregulated SHANK3 during the early postnatal period, then treated the mice with the PAM-mGluR1 (P6–P27) and looked at synaptic transmission and behaviors in adult animals (**Fig. 7a**). In control shShank3 mice that received vehicle instead of the PAM-mGluR1, we observed a high AMPA/NMDA ratio (**Fig. 7b**) and a reduction in social preference during T_2 (**Fig. 7c**), replicating the findings described above. In contrast, PAM-mGluR1 treatment during early life reduced the AMPA/NMDA ratio (**Fig. 7b**) and normalized social preference (**Fig. 7c**,**d**). Thus, PAM-mGluR1 treatment during postnatal development ameliorates both synaptic alterations and behavioral deficits caused by SHANK3 insufficiency.

This pharmacological rescue suggests that normal VTA DA neuron activity may be sufficient for the maintenance of social preference. We performed optogenetic stimulation of VTA DA neurons during the three-chamber social interaction test in shShank3-injected mice. Channelrhodopsin (ChR2) was selectively expressed in VTA DA neurons by injecting AAV-DIO-ChR2 into the VTA of DAT-Cre mice previously infected with shShank3 or scrShank3 (**Fig. 8a**,**b**). To validate the approach, we determined that blue light stimulation induced reliable bursts of action potentials in VTA DA neurons recorded from acute slices of shShank3 mice (**Fig. 8c**,**d**). *In vivo*,

we stimulated VTA DA neurons[35] during T_2 when mice were in close proximity to the social stimulus (**Fig. 8e**). ShShank3 mice that did not receive optogenetic stimulation showed a reduction in social preference at T_2 (**Fig. 8f**,**g**). However, phasic stimulation of VTA DA neurons increased social preference during T_2 in both scrShank3 and shShank3 mice (**Fig. 8f**) and increased normalized social preference of shShank3 mice to the levels of the scrShank3 control group (**Fig. 8g**). It should be noted that Ro 677476 and optogenetics, perhaps through different mechanisms, have distinct effects on social behavior. These findings demonstrate that DA neuron activity is sufficient to support social preference and show that such stimulation protocols can overcome impaired social behavior attributable to SHANK3 downregulation.

DISCUSSION

With a growing body of evidence pointing to the involvement of VTA in both social behavior and repetitive actions[3,4], our study examines whether and how deficits in these behavioral domains could arise from haploinsufficiency of a gene linked to an ASD. We found that VTA SHANK3 downregulation altered excitatory transmission to both DA and GABA neurons. Together they dampened the firing activity of DA neurons, with an impact on social preference. Treatment with a PAM-mGluR1 during the initial period of postnatal development was sufficient to reverse deficits in social preference, which remained normal in adult animals. Moreover, DA neuron burst firing activity is sufficient to support social preference and overcome social impairments arising from VTA SHANK3 insufficiency. Taken together, these results argue for a central role of perturbed VTA DA neuron maturation in the development of social preference.

Several mouse models have been generated to study the consequences of *Shank3* deletion[33]. Focusing on the postsynaptic density of striatal neurons, a reduction in the expression of GluA2, GluN2A and GluN2B has been observed in *Shank3* knockout mice lacking the PDZ-containing (Protein interaction domain named after a common structure found in PSD-95, Discs Large, and Zona Occludens 1 proteins) SHANK3 isoforms[16]. In mouse models targeting the ankyrin-repeat domain of SHANK3, a reduction in the expression of GluA1 and GluN2A subunits has been reported in the hippocampus, although no changes in basal synaptic transmission were found[18]. Meanwhile, deletion of exon 21 resulted in no major

changes in synaptic ionotropic receptor subunits in whole hippocampal homogenates[19]. Here we find that downregulation of the proline-rich-domain-containing isoforms of SHANK3 has different consequences for basal synaptic transmission depending on the neuronal cell type within the same brain region. Specifically, the AMPAR subunit composition was altered only at excitatory synapses onto DA neurons, where SHANK3 downregulation promoted the insertion of GluA2-lacking AMPARs. However, in VTA GABA neurons, SHANK3 downregulation changed the AMPA/NMDA ratio but left the AMPAR subunit composition unaffected. Taken together, the variety of synaptic alterations reported in different mutant mouse models may reflect disruptions of distinct *Shank3* domains, whose expression is further regulated in a brain-region-specific and cell-type-specific manner.

In VTA DA neurons, activation of mGluR1 during postnatal development drives synaptic maturation by exchanging GluA2-lacking for GluA2-containing AMPARs[21]. This may establish competent DA neuron function, which in adulthood is required to assign emotional valence to salient stimuli[36]. We find that SHANK3 downregulation prevents the postnatal maturation of AMPAR transmission to VTA DA neurons and that affected synapses remain in an immature state. Thus, SHANK3 may serve to guarantee optimal functionality of mGluR1 and its signaling pathway during synaptic maturation of VTA DA neurons. Boosting mGluR1 signaling with a PAM during the period of synaptic development may overcome SHANK3 deficiency and drive the exchange of immature for mature receptors on VTA DA neurons. Surprisingly, at excitatory synapses onto VTA GABA neurons, we did not observe the presence of GluA2-lacking AMPARs when SHANK3 was downregulated, and PAM-mGluR1 treatment was unable to rescue synaptic deficits. These findings are in agreement with our previous observations that mGluR1-LTD (mGluR1-induced Long Term Depression) is contingent on the presence of GluA2-lacking AMPARs at the synapses[26]. A different expression of group I mGluRs[37], a different synaptic localization of SHANK3 or mechanisms of synaptic maturation that may differ between VTA DA and GABA neurons could also explain our results.

Interfering with the expression of *Shank3* in the VTA triggers multiple alterations in synapses and circuits that together reduce DA neuron activity. Other studies have shown that SHANK3 insufficiency can alter cell morphology[15], and DA

and GABA morphological changes should be examined in future studies. At the cellular level, reduced DA neuron activity could arise from a change in mGluR1 signaling following SHANK3 downregulation. Indeed, the burst activity of DA neurons is regulated by NMDAR and group I mGluR activation[29]. Precisely how changes in excitatory synaptic transmission and cell-intrinsic properties interact to determine DA neuron activity warrants further investigation. In addition, VTA DA neurons receive inhibition from local GABA neurons[32,38], whose increased activity following SHANK3 downregulation may further dampen the activity of the DA neurons. Nevertheless, the central role of DA neuron activity in supporting social interactions is supported by our findings that restoring synaptic transmission to DA neurons with PAM-mGluR1 treatment and optogenetic activation of DA neurons were both sufficient to partially rescue normal social behavior in VTA SHANK3-deficient mice.

How might perturbed VTA DA neuron activity lead to deficits in social behavior? Several studies have implicated DA in social bonding[39,40]. It has been suggested that DA neuron activity directly influences social choice[41] and facilitates choice of familiar partners[42]. Recently, it has been shown that activity of DA neurons, measured by monitoring cellular calcium dynamics, increases during social but not object interaction[9]. Since DA neurons project widely throughout the corticolimbic system, it would be of interest to understand how regions downstream of VTA DA neurons contribute to behavioral impairments reported here. Projections to the nucleus accumbens may be particularly relevant, since their activity predicts social interactions in freely moving mice, possibly by controlling the firing of D1 dopamine receptor–expressing medium spiny neurons[9].

In addition to impaired social behavior, VTA SHANK3 downregulation also elevated self-grooming and altered sucrose preference, albeit only at low sucrose concentrations. These findings may reflect a more general deficit in processing natural rewards, which could contribute to the failure of shShank3 mice to maintain social preference. Alternatively, since reduced sucrose preference was seen in the context of increased water consumption, this observation, together with elevated self-grooming, may point to increased repetitive behaviors in VTA SHANK3 mice. Although more robust and precise assays for repetitive behaviors are needed to firmly establish this, repetitive behaviors have been observed in several other Shank3 mouse

models[16,18] and are thought to recapitulate the repetitive behavior observed in patients with ASDs. Dopamine has been linked to repetitive behaviors in several studies via its actions on corticostriatal circuits[43]. Since our manipulation is selective for the VTA, the repetitive behaviors observed may arise from altered function of ventral striatum, producing changes in the motivational aspects of behavioral control. A future challenge is to understand how the encoding of distinct repetitive and social behaviors is distributed across mesocorticolimbic circuits.

Finally, our study confirms mGluR1 activation in VTA DA neurons during the early postnatal period as an essential determinant of postnatal development, which may be deficient in certain forms of ASD. We provide a proof of principle that under conditions of low SHANK3 levels, treatment with a positive allosteric modulator of mGluR1 can overcome deficits in postnatal development. However, it remains unknown whether the VTA dysfunction and response to mGluR1 modulation observed in VTA SHANK3 mice is also present in global loss-of-function *Shank3* mutants that more closely reflect the etiology associated with *SHANK3* mutations found in ASD. Nevertheless, the pharmacological rescue of both neuron function and behavior in VTA SHANK3 mice persists into adulthood and suggests that mGluR1 may be a valid target for the early treatment of some form of ASDs.

ACKNOWLEDGMENTS

We thank M. Mameli, D. Jabaudon and F.Gardoni for the critical reading of the manuscript. C.B is supported by the Swiss National Science Foundation, Pierre Mercier Foundation and NCCR Synapsy. C.L. is supported by the Swiss National Science Foundation and by the European Research Council (MeSSI Advanced grant). This work was supported by a grant from the Simons Foundation (SFARI #239496 to C.L.).

Author Contributions

All VTA SHANK3 infections were performed by S.B. *In vitro* electrophysiology experiments were performed by S.B. Behavioral experiments were performed by S.T., with assistance from C.P.-S., S.B. and E.C.O. S.B. and S.T. performed the statistical analyses for the *in vitro* electrophysiology and the behavioral experiments, and contributed to the statistical analysis of the *in vivo* electrophysiology experiments. *In vivo* recordings were performed by C.G and F.G. Immunohistochemistry was performed by S.B., J.V. and C.G. Western blots were performed by L.P. and P.B. The study was designed and the manuscript written by C.B., with assistance from S.B., E.C.O., C.L. and F.G.

COMPETING FINANCIAL INTERESTS

The authors declare no competing financial interests.

<jrn>1. Volkmar, F.R., State, M. & Klin, A. Autism and autism spectrum disorders: diagnostic issues for the coming decade. *J. Child Psychol. Psychiatry* **50**, 108–115 (2009).</jrn>

<jrn>2. Landa, R.J. Diagnosis of autism spectrum disorders in the first 3 years of life. *Nat. Clin. Pract. Neurol.* **4**, 138–147 (2008).</jrn>

<jrn>3. Ameis, S.H. & Catani, M. Altered white matter connectivity as a neural substrate for social impairment in autism spectrum disorder. *Cortex* **62**, 158–181 (2015).</jrn>

<jrn>4. Wood, J. & Ahmari, S.E. A framework for understanding the emerging role of corticolimbic-ventral striatal networks in OCD-associated repetitive behaviors. *Front. Syst. Neurosci.* **9**, 171 (2015).</jrn>

<jrn>5. Scott-Van Zeeland, A.A., Dapretto, M., Ghahremani, D.G., Poldrack, R.A. & Bookheimer, S.Y. Reward processing in autism. *Autism Res.* **3**, 53–67 (2010).</jrn>

<jrn>6. Chevallier, C., Kohls, G., Troiani, V., Brodkin, E.S. & Schultz, R.T. The social motivation theory of autism. *Trends Cogn. Sci.* **16**, 231–239 (2012).</jrn>

<jrn>7. Schultz, W. Predictive reward signal of dopamine neurons. *J. Neurophysiol.* **80**, 1–27 (1998).</jrn>

<jrn>8. Rodriguez Parkitna, J. & Engblom, D. Addictive drugs and plasticity of glutamatergic synapses on dopaminergic neurons: what have we learned from genetic mouse models? *Front. Mol. Neurosci.* **5**, 89 (2012).</jrn>

<jrn>9. Gunaydin, L.A. *et al.* Natural neural projection dynamics underlying social behavior. *Cell* **157**, 1535–1551 (2014).</jrn>

<jrn>10. Folstein, S.E. & Rosen-Sheidley, B. Genetics of autism: complex aetiology for a heterogeneous disorder. *Nat. Rev. Genet.* **2**, 943–955 (2001).</jrn>

<jrn>11. Zoghbi, H.Y. & Bear, M.F. Synaptic dysfunction in neurodevelopmental disorders associated with autism and intellectual disabilities. *Cold Spring Harb. Perspect. Biol.* **4**, a009886 (2012).</jrn>

<jrn>12. Phelan, K. & McDermid, H.E. The 22q13.3 deletion syndrome (Phelan-McDermid syndrome). *Mol. Syndromol.* **2**, 186–201 (2012).</jrn>

<jrn>13. Gauthier, J. *et al.* Novel de novo SHANK3 mutation in autistic patients. *Am. J. Med. Genet. B. Neuropsychiatr. Genet.* **150B**, 421–424 (2009).</jrn>

<jrn>14. Boccuto, L. *et al.* Prevalence of SHANK3 variants in patients with different subtypes of autism spectrum disorders. *Eur. J. Hum. Genet.* **21**, 310–316 (2013).</jrn>

<jrn>15. Naisbitt, S. *et al.* Shank, a novel family of postsynaptic density proteins that binds to the NMDA receptor/PSD-95/GKAP complex and cortactin. *Neuron* **23**, 569–582 (1999).</jrn>

<jrn>16. Peça, J. *et al.* Shank3 mutant mice display autistic-like behaviours and striatal dysfunction. *Nature* **472**, 437–442 (2011).</jrn>

<jrn>17. Bozdagi, O. *et al.* Haploinsufficiency of the autism-associated Shank3 gene leads to deficits in synaptic function, social interaction, and social communication. *Mol. Autism* **1**, 15 (2010).</jrn>

<jrn>18. Wang, X. *et al.* Synaptic dysfunction and abnormal behaviors in mice lacking major isoforms of Shank3. *Hum. Mol. Genet.* **20**, 3093–3108 (2011).</jrn>

<jrn>19. Kouser, M. *et al.* Loss of predominant Shank3 isoforms results in hippocampus-dependent impairments in behavior and synaptic transmission. *J. Neurosci.* **33**, 18448–18468 (2013).</jrn>

<jrn>20. Zhou, Y. *et al.* Mice with Shank3 mutations associated with ASD and schizophrenia display both shared and distinct defects. *Neuron* **89**, 147–162 (2016).</jrn>

<jrn>21. Bellone, C., Mameli, M. & Lüscher, C. In utero exposure to cocaine delays postnatal synaptic maturation of glutamatergic transmission in the VTA. *Nat. Neurosci.* **14**, 1439–1446 (2011).</jrn>

<jrn>22. Bellone, C. & Lüscher, C. Drug-evoked plasticity: do addictive drugs reopen a critical period of postnatal synaptic development? *Front. Mol. Neurosci.* **5**, 75 (2012).</jrn>

<jrn>23. Verpelli, C. *et al.* Importance of Shank3 protein in regulating metabotropic glutamate receptor 5 (mGluR5) expression and signaling at synapses. *J. Biol. Chem.* **286**, 34839–34850 (2011).</jrn>

<jrn>24. Mameli, M., Balland, B., Luján, R. & Lüscher, C. Rapid synthesis and synaptic insertion of GluR2 for mGluR-LTD in the ventral tegmental area. *Science* **317**, 530–533 (2007).</jrn>

<jrn>25. Argilli, E., Sibley, D.R., Malenka, R.C., England, P.M. & Bonci, A. Mechanism and time course of cocaine-induced long-term potentiation in the ventral tegmental area. *J. Neurosci.* **28**, 9092–9100 (2008).</jrn>

<jrn>26. Bellone, C. & Lüscher, C. Cocaine triggered AMPA receptor redistribution is reversed in vivo by mGluR-dependent long-term depression. *Nat. Neurosci.* **9**, 636–641 (2006).</jrn>

<jrn>27. Bellone, C. & Lüscher, C. mGluRs induce a long-term depression in the ventral tegmental area that involves a switch of the subunit composition of AMPA receptors. *Eur. J. Neurosci.* **21**, 1280–1288 (2005).</jrn>

<jrn>28. Knoflach, F. *et al.* Positive allosteric modulators of metabotropic glutamate 1 receptor: characterization, mechanism of action, and binding site. *Proc. Natl. Acad. Sci. USA* **98**, 13402–13407 (2001).</jrn>

<jrn>29. Prisco, S., Natoli, S., Bernardi, G. & Mercuri, N.B. Group I metabotropic glutamate receptors activate burst firing in rat midbrain dopaminergic neurons. *Neuropharmacology* **42**, 289–296 (2002).</jrn>

<jrn>30. Meltzer, L.T., Serpa, K.A. & Christoffersen, C.L. Metabotropic glutamate receptor-mediated inhibition and excitation of substantia nigra dopamine neurons. *Synapse* **26**, 184–193 (1997).</jrn>

<jrn>31. Ungless, M.A. & Grace, A.A. Are you or aren't you? Challenges associated with physiologically identifying dopamine neurons. *Trends Neurosci.* **35**, 422–430 (2012).</jrn>

<jrn>32. Tan, K.R. *et al.* GABA neurons of the VTA drive conditioned place aversion. *Neuron* **73**, 1173–1183 (2012).</jrn>

<jrn>33. O'Connor, E.C., Bariselli, S. & Bellone, C. Synaptic basis of social dysfunction: a focus on postsynaptic proteins linking group-I mGluRs with AMPARs and NMDARs. *Eur. J. Neurosci.* **39**, 1114–1129 (2014).</jrn>

<jrn>34. Crawley, J.N. Mouse behavioral assays relevant to the symptoms of autism. *Brain Pathol.* **17**, 448–459 (2007).</jrn>

<jrn>35. Pascoli, V., Terrier, J., Hiver, A. & Lüscher, C. Sufficiency of mesolimbic dopamine neuron stimulation for the progression to addiction. *Neuron* **88**, 1054–1066 (2015).</jrn>

<jrn>36. Stuber, G.D. *et al.* Reward-predictive cues enhance excitatory synaptic strength onto midbrain dopamine neurons. *Science* **321**, 1690–1692 (2008).</jrn>

<jrn>37. Merrill, C.B., Friend, L.N., Newton, S.T., Hopkins, Z.H. & Edwards, J.G. Ventral tegmental area dopamine and GABA neurons: Physiological properties and expression of mRNA for endocannabinoid biosynthetic elements. *Sci. Rep.* **5**, 16176 (2015).</jrn>

<jrn>38. van Zessen, R., Phillips, J.L., Budygin, E.A. & Stuber, G.D. Activation of VTA GABA neurons disrupts reward consumption. *Neuron* **73**, 1184–1194 (2012).</jrn>

<jrn>39. Curtis, J.T. & Wang, Z. Ventral tegmental area involvement in pair bonding in male prairie voles. *Physiol. Behav.* **86**, 338–346 (2005).</jrn>

<jrn>40. Liu, Y., Young, K.A., Curtis, J.T., Aragona, B.J. & Wang, Z. Social bonding decreases the rewarding properties of amphetamine through a dopamine D1 receptor-mediated mechanism. *J. Neurosci.* **31**, 7960–7966 (2011).</jrn>

<jrn>41. Aragona, B.J., Liu, Y., Curtis, J.T., Stephan, F.K. & Wang, Z. A critical role for nucleus accumbens dopamine in partner-preference formation in male prairie voles. *J. Neurosci.* **23**, 3483–3490 (2003).</jrn>

<jrn>42. Aragona, B.J. & Wang, Z. Dopamine regulation of social choice in a monogamous rodent species. *Front. Behav. Neurosci.* **3**, 15 (2009).</jrn>

<jrn>43. Langen, M., Kas, M.J.H., Staal, W.G., van Engeland, H. & Durston, S. The neurobiology of repetitive behavior: of mice…. *Neurosci. Biobehav. Rev.* **35**, 345–355 (2011).</jrn>

Editorial Summary
The authors show that downregulation of SHANK3 in the VTA induces cell specific changes in DA and GABA neurons that converge to generate social behavioral deficits. Administration of a positive allosteric modulator of the type 1 metabotropic glutamate receptors (mGluR1) ameliorates synaptic, circuit and behavioral deficits.

METHODS

Accession codes. We used the following shRNA sequence that targets exon 21 of the rat and mouse *SHANK3* gene (GenBank: *Shank3*, NM_021423.3). **[AU: Move shRNA sequence to Online Methods; give only the accession code here, shShank3 sequence now moved in drugs and virus paragraph of Methods]**

Animals.

The study was conducted with wild-type C57Bl/6j (WT), DAT-iresCre (*Slc6a3*$^{tm1.1(cre)Bkmn}$) and GAD-Cre (65-kDa isoform of the *Gad2* locus[44]) male and female mice housed in groups (weaning at P21–P23) under a normal light–dark cycle (lights on at 7.00 a.m.). All the physiology and behavior experiments were performed during the light cycle. All the procedures performed at the UNIL and UNIGE compiled with the Swiss National Institutional Guidelines on Animal Experimentation and were approved by the Swiss Cantonal Veterinary Office Committee for Animal Experimentation. All procedures performed at Bordeaux were conducted in accordance with the European directive 2010-63-EU and with approval from Bordeaux University Animal Care and Use Committee (no. 50120205-A). All experiments were performed blindly to the experimenter, and within each litter the mice were randomly assigned to both virus and pharmacological treatments.

The number of animals used for each experiment is reported per group in each figure legend. No statistical methods were used to predetermine sample sizes, but our sample sizes are similar to those generally employed in the field.

Electrophysiology.

Horizontal midbrain slices 200–250 µm thick containing VTA were prepared following the experimental injection protocols described in the text. Slices were kept in artificial cerebrospinal fluid containing 119 mM NaCl, 2.5 mM KCl, 1.3 mM

$MgCl_2$, 2.5 mM $CaCl_2$, 1.0 mM NaH_2PO_4, 26.2 mM $NaHCO_3$ and 11 mM glucose, bubbled with 95% O_2 and 5% CO_2. Whole-cell voltage-clamp recording techniques were used (30–32 °C, 2–3 ml min^{-1}, submerged slices) to measure the holding currents and synaptic responses of VTA neurons, with recordings made medially to the medial terminal nucleus of the accessory optic tract (MT). Putative DA and GABA neurons were classified according to the following criteria: large/small soma, cell capacitance (for putative DA neuron >28 pF, for putative GABA neuron <27 pF), hyperpolarization step (–60 mV, 500 ms duration immediately after whole-cell patch clamp configuration) induced I_h current presence/absence and input resistance (monitored for 2 min after the whole-cell patch clamp configuration at +40 mV). Recordings were performed from uninfected, shShank3-infected and scrShank3-infected cells (identified by the expression of the green reporter protein) and sorted as putative DA or putative GABA neurons as described above. The internal solution contained 130 mM CsCl, 4 mM NaCl, 2 mM $MgCl_2$, 1.1 mM EGTA, 5 mM HEPES, 2 mM Na_2ATP, 5 mM sodium creatine phosphate, 0.6 mM Na_3GTP and 0.1 mM spermine. Currents were amplified, filtered at 5 kHz and digitized at 20 kHz. The liquid junction potential was small (–3 mV) and traces were therefore not corrected.

Access resistance was monitored by a hyperpolarizing step of –14 mV at each sweep, every 10 s. The cells were recorded at the access resistance from 10–30 MΩ for putative DA neurons and 15–40 MΩ for putative GABA neurons. Data were excluded when the resistance changed >20%. Synaptic currents were evoked by stimuli (0.05–0.10 ms) at 0.1 Hz through a stimulating electrode placed rostral to the VTA. The experiments were carried out in the presence of the $GABA_A$ receptor antagonist picrotoxin (100 µM); the AMPAR EPSCs were pharmacologically isolated by application of the NMDAR antagonist D-APV (50µM) and NMDAR EPSCs were recorded at +40 mV in presence of the AMPAR blocker NBQX (10 µM). Representative example traces are shown as the average of 15–20 consecutive EPSCs typically obtained at each potential. The rectification index of AMPARs is the ratio of the chord conductance calculated at negative potential (–60 mV) divided by the chord conductance at positive potential (+40 mV). The analysis of the decay time of NMDAR-mediated EPSC was conducted as described previously[45] and the ifenprodil sensitivity was calculated as the percentage of NMDAR EPSC amplitude reduction (at +40 mV) after 20–25 min of continuous ifenprodil (3 µM, GluN2B-containing

NMDAR antagonist) bath application compared to baseline. The time interval between the two stimulations for the PPR measurement was 50 ms (interstimulation interval, ISI) and the ratio was obtained by dividing the $EPSC_2$ by $EPSC_1$ amplitude at –60 mV. The *in vitro* validation of the optogenetic protocol (used *in vivo*) was performed in current-clamp configuration, after the assessment of the I_h current and the desensitization current (500 ms pulse duration) in voltage-clamp mode. The internal solution contained 140 mM potassium gluconate, 2 mM $MgCl_2$, 5 mM KCl, 0.2 mM EGTA, 10 mM HEPES, 4 mM Na_2ATP, 0.3 mM Na_3GTP and 10 mM creatine phosphate. Blue light was delivered through the 40× objective focused on the cell soma with a power intensity of 8 mW. Synaptic responses were collected with a Multiclamp 700B amplifier (Axon Instruments, Foster City, CA), filtered at 2.2 kHz, digitized at 5 Hz, and analyzed online using Igor Pro software (Wavemetrics, Lake Oswego, OR).

Stereotaxic injections.

Injections of purified AAV-shShank3, AAV-scrShank3 and AAV-CAG-DIO-tdTomato were performed in mice at different time points. Anesthesia was induced and maintained with a mixture of oxygen and isoflurane (Baxter AG, Vienna, Austria). The animals were then placed on the stereotaxic frame (Angle One; Leica, Germany) and a single or bilateral craniotomy was made over the VTA at following stereotaxic coordinates: for neonatal injections (P2–P5), ML 0.15 mm, AP 0.1 mm, DV –3.8 mm from lambda; for juvenile injections (P14/P21/P24), ML ± 0.5 mm, AP –3.2 mm, DV –4.0 mm from bregma. The virus was injected with graduated pipettes (Drummond Scientific Company, Broomall, PA) at the rate of 100 nl/min for a total volume of 50 and 200 nL for neonatal (as reported in the text) and 400 nL for juvenile animals. For all the experiments the virus was incubated for at least 9 d, at which point expression was clearly identifiable by the reporter protein expression, before proceeding with further manipulations.

In vivo single-unit neuron recordings.

A glass micropipette (tip diameter: 2–3 µm; 4–6 MΩ for VTA dopamine neurons and tip diameter: 1–2 µm, 10–15 MΩ for VTA putative GABA neurons) filled with 2% pontamine sky blue solution in 0.5 M sodium acetate was lowered into the VTA. VTA dopamine neurons were identified according to well-established

electrophysiological features[46–48], which included the following: (1) an action potential with ≥1.1 ms (measured from the start of action potential to the negative trough); (2) slow spontaneous firing rate (≤10 Hz); (3) single and burst spontaneous firing patterns composed of 2–10 spikes *in vivo* . The onset of a burst was defined with an interspike interval lower than 80 ms and the end of the burst with an interspike interval higher than 160 ms (ref. 31). Putative VTA GABA neurons were identified according to well-established electrophysiological criteria: (1) an action potential width <1.1 ms; (2) a location within the VTA, with the VTA boundary defined as 200 μm dorsal to the first VTA DA neuron recorded **[AU: Sentence ok as edited? OK]**[31,32,49,50]. The extracellular potential was recorded with an Axoclamp-2B amplifier and filter (300 Hz / 0.5 kHz)[51]. Single neuron spikes were collected online (CED 1401, SPIKE 2; Cambridge Electronic Design). Four parameters for VTA dopamine neuron firing and bursting activity were analyzed: the cumulative probability distribution of the firing rate, the bursting rate and the index of bursting (burst event frequency × mean spikes per burst). **[AU: Sentence correct as edited? OK].**

Immunohistochemistry and cell counting.

Mice were killed and transcardially perfused with PBS 1× followed by 4% paraformaldehyde prepared in PBS 1×. The brain was removed and left for overnight postfixation at 4 °C. Horizontal VTA slices were cut at 50 μm and washed three times in PBS 1× before incubation in the blocking solution containing 0.3% Triton X-100 and 1% goat serum. The slices were incubated with rabbit anti-TH (Abcam ab112, 1:500) at 4 °C overnight and then washed three times in PBS 1× and incubated for 2 h at room temperature with secondary antibodies, goat anti-rabbit IgG-Alexa 568 (Abcam, 1:500; ab175471) or goat anti-rabbit IgG-Alexa 647 (Abcam, 1:500; ab150079). Finally, the slices were washed three times in PBS 1× before being mounted onto microscope slides with Abcam DAPI mounting medium (Abcam, ab104139). Images were acquired with an LSM-710 confocal microscope.

Cell counting was performed on 50-μm-thick VTA slices from at least 4 WT mice and 3 GAD-Cre mice injected with shShank3 (at P5) and AAV-CAG-DIO-tdTomato (at P14). All slices were collected and immunohistochemistry against TH was performed for every other slice (secondary antibody IgG-Alexa 568 for WT and IgG-Alexa 647 for GAD-Cre:tdTomato mice). Two confocal images of VTA were

acquired bilaterally for each slice, along the whole VTA dorso-ventral axis in the dopaminergic area. For WT, the number of TH^+, $ZsGreen^+$ and $TH^+ZsGreen^+$ cells were counted in at least 6 fields of view per mouse, and a percentage average calculated for each mouse. The total percentage average (**Supplementary Fig. 1b**) was calculated as an average of the values from each mouse. To count the total number of TH-positive cells, the VTA was unilaterally infected and sliced at the juvenile stage and cell counting performed as described above (**Supplementary Fig. 1c**). Cell-counting from GAD-Cre:tdTomato was performed by two independent experimenters. Specifically, the number of TH^+, $TH^+ZsGreen^+$, $tdTom^+$ and $tdTom^+ZsGreen^+$ was counted in each field of view of the VTA along the whole dorso-ventral axis (at least 6 fields). The percentage of cells obtained by each experimenter was averaged for each mouse. The total percentage of infected cells (**Fig. 1b**) was obtained by averaging the percentage obtained for each mouse.

Western blot analysis.

AAV-shShank3-infected and AAV-scrShank3-infected mice (P21–P35) were anesthetized and decapitated. Midbrain slices 350 µm thick were obtained with a vibratome (Leica VT1200S). The VTA and the adjacent SN were dissected in animals that showed virus expression (one mouse was excluded from shShank3 group because it was not infected), isolated and homogenized in a lysis buffer containing 20 mmol/L HEPES, pH 7.4, 10 mmol/L NaCl, 3 mmol/L MgCl2, 2.5 mmol/L EGTA, 0.1 mmol/L dithiothreitol, 50 mmol/L NaF, 1 mmol/L Na_3VO_4, 1% Triton X-100 and a protease inhibitor cocktail (Roche). Lysates were boiled for 5 min and separated on a denaturing 5–9% acrylamide gel. The following primary antibodies were used: Shank3 (H-160) (sc-30193, Santa Cruz Biotechnology, 1:200) and tubulin (sc-8035,Santa Cruz Biotechnology, 1:1,000). The following secondary antibodies were used: goat-anti-rabbit, goat-anti-mouse coupled with IRdye 800 or IRdye 680 (936-32210, 926-32220, LiCor, Lincoln, 1:10,000) **[AU: Please clarify: 30% of what? It was a Typo now removed]**. Protein bands were revealed by the Odyssey infrared image system (LiCor).

Social interaction test.

A three-chambered social preference test was used, comprising a rectangular Plexiglas arena (60 × 40 × 22 cm) (Ugo Basile, Varese, Italy) divided into three

chambers (each 20 × 40 × 22 (h) cm). The walls of the center chamber had doors that could be lifted to allow free access to all chambers. The social preference test was performed similarly as published by Moy *et al.*[52] and the variables were scored and calculated as previously published[53]. Briefly, each mouse was placed in the arena for a habituation period of 10 min, when it was allowed to freely explore the empty arena. At the end of the habituation, the test was performed: two enclosures with metal vertical bars were placed diagonally, one in the bottom left corner of the left compartment and one in the top right corner of the right compartment. One enclosure was empty (serving as an inanimate object) whereas the other contained a social stimulus (unfamiliar juvenile mouse 25 ± 1 d old). The enclosures allowed visual, auditory, olfactory and tactile contact between the experimental mice and the mice acting as social stimuli. The juvenile mice in the enclosures were habituated to the apparatus and the enclosures for a brief period of time on the 3 d preceding the experiment. The experimental mouse was allowed to freely explore the apparatus and the enclosures for 10 min. The position of the empty vs. juvenile-containing enclosures alternated and was counterbalanced for each trial to avoid any bias effects.

Every session was video-tracked and recorded using Ethovision XT (Noldus, Wageningen, the Netherlands), which provided an automated recording of the entries around the enclosures, the distance moved and the velocity. Behavior was also manually scored by an experimenter blind to the treatment of animals. The mice were considered to be exploring the empty and the social stimulus when their nose was directed toward the enclosures' contents at a distance less than approximately 2 cm. The time spent sniffing each enclosure was assessed and then used to determine the preference score for the social target as compared to the empty enclosure (social/(social + empty)). To investigate the dynamics of social preference between groups across time, we divided the test phase into two 5-min bins and calculated the social preference ratios for these two time points (T_1 and T_2). Moreover, the normalized social preference at T_2 (SP_2) was calculated by dividing the social preference score at T_2 by the social preference score for the total testing time. The change in the interaction with the mouse was calculated between T_1 and T_2 (time of interaction with social target at T_2 – time of interaction with social target at T_1), and the change in interaction for the empty enclosure was calculated similarly**[AU:**

Sentence corect as edited? YES]. The arena was cleaned with 1% acetic acid solution and dried between trials.

Social memory task.

For the cohort of mice injected in the VTA with 50 nL of AAV-shShank3 or AAV-scrShank3, a social memory task was performed. Following the social preference test performed as described above, a novel mouse was introduced into the formerly empty enclosure. Mice were exposed to the enclosures containing the novel and the familiar mouse for 10 min. Time spent sniffing each enclosure was assessed and the preference score for the novel mouse compared to the familiar (novel/(novel + familiar)) was calculated. The social memory test was also divided into two 5-min bins and social memory calculated during T_1 and T_2. As reported for the social preference test, the normalized social memory at T_2 (SM_2) was calculated by dividing the social memory score at T_2 by the social memory score for the total testing time. The change in the interaction with the novel mouse was calculated between T_1 and T_2 (time of interaction with novel mouse during T_2 – time of interaction with novel mouse during T_1), and the change in interaction was calculated similarly for the familiar mouse.

Optogenetic stimulation during the social preference test.

AAV-shShank3-infected and AAV-scrShank3-infected DAT-Cre mice underwent a second stereotaxic surgery at 4–5 weeks of age to inject 250–500 nL of AAV5-ef1a-ChR2(H134R)-eYFP into the VTA (–3.2 AP, +0.9 ML and –4.28 DV at a 10° angle), together with a single fiber optic cannula at the same coordinates, but positioned approximately 0.1 mm above the ChR2 infection site[35]. Following at least 2 weeks of recovery, mice were first habituated to a patch cable during 3 × 30 min sessions preceding the social preference test. The social preference test was performed as described above, except that mice assigned to the ‘ON’ condition received phasic blue light stimulation of VTA DA neurons only when they entered in close proximity to the social stimulus during T_2. Laser power was controlled between each test to ensure an estimated 7–10 mW of power at the implanted fiber tip.

Open field test.

The open field was a 75-cm diameter Plexiglas circular arena, divided into three virtual zones (wall, intermediate and center). Animals were allowed to freely explore

the open field for 10 min and their behavior was automatically (Ethovision, Noldus, Wageningen, the Netherlands) and manually scored (for assessing self-grooming behavior). Parameters analyzed with the automated tracking system were distance, velocity and time in the different zones. The arena was cleaned with 1% acetic acid and dried between each test.

Sucrose preference test.

Mice were housed individually for the duration of this task (48 h) and had access to standard lab chow and tap water throughout the experiment. At 18 h they were exposed to two drinking bottles, one with water and the other one containing sucrose solution. During the first testing day, sucrose was given at 1% and 24 h afterwards the bottles were weighed and subsequently the sucrose solution was given to the mice at a concentration of 8% for another 24 h, when the second measurement was taken. Mice were weighed at the beginning of the experiment and water and sucrose bottle positions were counterbalanced between animals to avoid any confounding effect of side preference. Sucrose and water consumption were normalized to 10 g of the body weight of each mouse and the amount of water and sucrose drunk was analyzed. A sucrose preference ratio was calculated as (sucrose consumed/(sucrose consumed + water consumed)).

Drugs and viruses.

Drugs and viruses used were: AAV-shShank3/scrShank3 (AAV5, AAV1; 7.4×10^{13} GC/mL; VectorBioLab; shShank3 sequence: 5′-GGAAGTCACCAGAGGACAAGA-3′), AAV-CAG-DIO-tdTomato (AAV9, gift from Prof. Anthony Holtmaat), rAAV5-Ef1a-DIO-hChR2(H134R)-eYFP (5×10^{12} virus molecules/mL UNC). Ro 677476 (4346, Tocris), D-APV (0106, Tocris), picrotoxin (1128, Tocris), NBQX (0373, Tocris), (R,S)-3,5-DHPG (0342, Tocris) and ifenprodil hemitartrate (0545, Tocris).

Statistical analysis.

The data were analyzed with independent or paired two-tailed samples *t*-tests, one-way, two-way or repeated measures ANOVA followed up by *post hoc* tests (as reported in figure legends). Normality was checked with the Shapiro-Wilk criterion and, when violated, non-parametric statistics were applied (Mann-Whitney and Kruskal-Wallis). Regarding *t*-tests, when Levene's test for the equality of variances was significant, suggesting that equal variances could be not assumed, the adjusted

values and degrees of freedom are reported. All bars and error bars represent the mean ± s.e.m., and significance was set at $P < 0.05$. The data were analyzed using the statistical package SPSS (SPSS, Chicago, IL, USA) versions 17.0 and 22.0 and Graphpad Prism 5 and 6, and the graphs were created using GraphPad Prism 5 and 6 (San Diego, CA, USA). For the behavioral experiments 2 animals out of 60 were excluded from the analysis, as 1 was not infected in the VTA (shShank3:Vehicle) and another did not show any social preference during T_1 (scrShank3:Ro). A **Supplementary Methods Checklist** is available.

Data availability.

The data that support the findings of this study are available from the corresponding author upon request.

<jrn>44. Kätzel, D., Zemelman, B.V., Buetfering, C., Wölfel, M. & Miesenböck, G. The columnar and laminar organization of inhibitory connections to neocortical excitatory cells. *Nat. Neurosci.* **14**, 100–107 (2011).</jrn>

<jrn>45. Bellone, C. & Nicoll, R.A. Rapid bidirectional switching of synaptic NMDA receptors. *Neuron* **55**, 779–785 (2007).</jrn>

<jrn>46. Ungless, M.A., Magill, P.J. & Bolam, J.P. Uniform inhibition of dopamine neurons in the ventral tegmental area by aversive stimuli. *Science* **303**, 2040–2042 (2004).</jrn>

<jrn>47. Grace, A.A. & Bunney, B.S. Intracellular and extracellular electrophysiology of nigral dopaminergic neurons-1. Identification and characterization. *Neuroscience* **10**, 301–315 (1983).</jrn>

<jrn>48. McCutcheon, J.E. *et al.* Dopamine neurons in the ventral tegmental area fire faster in adolescent rats than in adults. *J. Neurophysiol.* **108**, 1620–1630 (2012).</jrn>

<jrn>49. Steffensen, S.C., Svingos, A.L., Pickel, V.M. & Henriksen, S.J. Electrophysiological characterization of GABAergic neurons in the ventral tegmental area. *J. Neurosci.* **18**, 8003–8015 (1998).</jrn>

<jrn>50. Bocklisch, C. *et al.* Cocaine disinhibits dopamine neurons by potentiation of GABA transmission in the ventral tegmental area. *Science* **341**, 1521–1525 (2013).</jrn>

<jrn>51. Georges, F. & Aston-Jones, G. Activation of ventral tegmental area cells by the bed nucleus of the stria terminalis: a novel excitatory amino acid input to midbrain dopamine neurons. *J. Neurosci.* **22**, 5173–5187 (2002).</jrn>

<jrn>52. Moy, S.S. *et al.* Sociability and preference for social novelty in five inbred strains: an approach to assess autistic-like behavior in mice. *Genes Brain Behav.* **3**, 287–302 (2004).</jrn>

<jrn>53. Tzanoulinou, S., Riccio, O., de Boer, M.W. & Sandi, C. Peripubertal stress-induced behavioral changes are associated with altered expression of genes involved in excitation and inhibition in the amygdala. *Transl. Psychiatry* **4**, e410 (2014).</jrn>

Figure 1 Neonatal AAV-shShank3 infections target VTA DA and GABA neurons. (**a**) Top: experiment schematic. Left: representative confocal image of coronal slice obtained from a shShank3-infected WT mouse containing the VTA. Right: high magnification of VTA slice. (**b**) Top: experiment schematic. Left: representative image of staining in GAD-Cre mice infected with shShank3 and DIO-tdTomato, identifying GABA neurons. Right: quantification of viral infection for DA and infected GAD-Cre VTA neurons (see Online Methods). $TH^+/ZsGreen^+$ indicates double-positive TH and ZsGreen neurons. $tdTom^+$/ZsGreen+ refers to double-positive tdTomato and ZsGreen neurons.(**c**) Top: experiment schematic. Left: quantification of SHANK3 downregulation in VTA and Substantia Nigra (SN) for scrShank3- and shShank3-injected WT mice (VTA: Mann-Whitney $U = 3$; SN: Mann-Whitney $U = 10$). Numbers in bars indicate the number of animals. Right: example of SHANK3 expression in scrShank3 or shShank3 VTA and SN, and Western blot of SHANK3 downregulation in VTA and SN for scrShank3- and shShank3-injected WT mice. SHANK3/Tubulin refers to expression levels of SHANK3 normalized to Tubulin. Error bars show SEM.

Figure 2 SHANK3 downregulation alters the postnatal development of AMPAR-mediated transmission. (**a**) Top: experiment schematic. Group mean AMPA/NMDA

ratio calculated in uninfected, shShank3-infected and scrShank3-infected putative DA neurons (Kruskal-Wallis $K_{(2)} = 10.47$, $P = 0.005$, followed by Dunn's *post hoc* test). Right: example traces of evoked AMPAR and NMDAR EPSCs recorded at +40 mV. (**b**) Top: example traces of AMPAR EPSCs at –60 mV. Group mean PPRs for shShank3-infected and uninfected cells ($t_{(18)} = 0.05$, unpaired *t*-test). (**c**) Top: example traces of evoked AMPAR EPSCs recorded at –60, 0 and +40 mV. Group mean RI calculated in uninfected, shShank3-infected and scrShank3-infected putative DA neurons (one-way ANOVA $F_{(2,27)} = 11.66$, $P < 0.001$, followed by Tukey honest significant difference (HSD) *post hoc* test). **[AU: Add text explaining dotted lines in b,c traces. The dotted lines are there for aiding the reader to appreciate rectifying AMPARs in shShank3 condition]**(**d**) Top: example traces of NMDAR EPSCs during ifenprodil (3 μM) bath application. Time course of NMDAR EPSC amplitude during ifenprodil application for uninfected and shShank3-infected putative DA neurons. (**e**) Group mean ifenprodil inhibition calculated in uninfected and shShank3-infected putative DA neurons ($t_{(10)} = –0.21$, unpaired *t*-test). (**f**) Top: scaled example traces of NMDAR-EPSCs at +40 mV for Uninfected and shShank3 infected putative DA neurons Group mean decay times of NMDAR EPSCs ($t_{28} = –0.16$, unpaired *t*-test). (**g**) Top: experiment schematic. Group mean AMPA/NMDA ratio calculated in uninfected and shShank3-infected neurons ($U = 18.50$, Mann-Whitney test). Right: example traces of evoked AMPAR and NMDAR EPSCs recorded at +40 mV. (**h**) Group mean RIs calculated in uninfected and shShank3-infected putative DA neurons ($t_{(12)} = 0.38$, unpaired *t*-test). Top: example traces of evoked AMPAR EPSCs recorded at –60, 0 and +40 mV. Error bars show s.e.m. Example trace scale bars: 20 ms, 20 pANumbers in bars indicate cells, mice.

Figure 3 SHANK3 downregulation affects excitatory transmission to VTA GABA neurons. (**a**) Top: experiment schematic. Group mean AMPA/NMDA ratio calculated in uninfected and shShank3-infected putative GABA neurons ($t_{(14)} = –3.11$, unpaired *t*-test). Right: example traces of evoked AMPAR and NMDAR EPSCs recorded at +40 mV. (**b**) Group mean PPRs for uninfected and shShank3-infected putative GABA neurons ($t_{(25)} = –0.76$, unpaired *t*-test). Top: example traces of AMPAR EPSCs at –60 mV for uninfected and shShank3-infected putative GABA neurons. (**c**) Group mean RIs calculated in uninfected and shShank3-infected putative GABA neurons ($t_{(10)} = 0.01$, unpaired *t*-test). Top: example traces of evoked AMPAR EPSCs recorded at –

60, 0 and +40 mV. Scale bars for all traces**:** 20 ms, 20 pA. The numbers indicate cells and mice.

Figure 4 Stimulation of mGluR1 rescues synaptic deficits (**a**) Top: experiment schematic. Time course of pharmacologically isolated AMPAR EPSCs recorded at –60 mV from uninfected and shShank3-infected putative DA neurons before and after 5 min application of DHPG (20 μM). Insets: example traces of evoked AMPAR EPSCs recorded at –60 mV. (**b**) Top: example traces of evoked AMPAR EPSCs recorded at –60, 0 and +40 mV before and after DHPG application. Group mean RIs before and 25 min after DHPG application (shShank3: $t_{(5)} = 3.60$; uninfected: $t_{(4)} = 1.42$, paired *t*-test). (**c**) Top: experiment schematic. Group mean AMPA/NMDA ratio (two-way ANOVA; virus × drug interaction: $F_{(1,22)} = 6.41$, $P = 0.019$; main effect virus: $F_{(1,22)} = 20.54$, $P < 0.001$; main effect drug: $F_{(1,22)} = 7.02$, $P = 0.015$; followed by Tukey HSD *post hoc* test). Right: example traces of evoked AMPAR and NMDAR EPSCs recorded at +40 mV. (**d**) Top: example traces of evoked AMPAR EPSCs recorded at –60, 0, +40 mV. Group mean RI (two-way ANOVA; virus × drug interaction: $F_{(1,30)} = 4.62$, $P = 0.040$; main effect virus: $F_{(1,30)} = 14.93$, $P = 0.001$; main effect drug: $F_{(1,30)} = 5.26$, $P = 0.029$; followed by Tukey HSD *post hoc* test). Error bars show s.e.m. Example traces scale bar: 20 ms, 20 pA. Numbers in bars indicate cells, mice.

Figure 5 VTA SHANK3 insufficiency alters *in vivo* DA neuron activity (**a**) Top: experiment schematic. Quantification of bursting and non-bursting VTA putative DA neurons from scrShank3 or shShank3 vehicle treated mice. (**b**) Representative traces of a VTA putative DA neuron recorded *in vivo*. Each dot represents a burst event. Scale bar: 1 s (**c**) Group mean and cumulative probability distribution of the firing rate of VTA putative DA bursting cells (Kruskal-Wallis $K_{(3)} = 10.85$, $P = 0.013$, followed by Dunn's *post hoc* test). (**d**) Effect of PAM-mGluR1 (Ro 677476) treatment on bursting activity of VTA putative DA neuron (for bursting rate: Kruskal-Wallis $K_{(3)} = 14.09$, $P = 0.003$, followed by Dunn's *post hoc* test; for index of bursting: Kruskal-Wallis $K_{(3)} = 14.62$, $P = 0.002$, followed by Dunn's *post hoc* test). Error bars show s.e.m. (**e**) Top: experiment schematic. Representative traces of VTA putative GABA neurons recorded *in vivo*. Scale bar: 10 s. (**f**) Group mean ($U = 425.5$, Mann-Whitney test) and cumulative probability distribution of the firing rate of VTA

putative GABA neurons. Numbers above bars indicate cells and mice. Error bars show s.e.m.

Figure 6 VTA SHANK3 insufficiency induces social deficits that are reversed by PAM-mGluR1 treatment. (**a**) Experiment schematic. (**b**) Activity trail plots and experiment schematic (S, social target; O, inanimate object). (**c**) Scatter plots and group mean of social preference during the first half (T_1) and second half (T_2) of the 10-min test (repeated measures two-way ANOVA: time × drug × virus interaction $F_{(1,54)} = 4.48$, $P = 0.039$; between subjects: main effect virus $F_{(1,54)} = 4.99$, $P = 0.030$. Two-way ANOVA between vehicle groups: time main effect $F_{(1,54)} = 0.83$, $P = 0.368$, virus main effect $F_{(1,54)} = 1.54$ $P = 0.220$, time × virus interaction $F_{(1,54)} = 8.30$, $P = 0.006$. Two-way ANOVA between Ro 677476 groups: time main effect $F_{(1,54)} = 0.17$, $P = 0.683$, virus main effect $F_{(1,54)} = 1.63$, $P = 0.207$, time × virus interaction $F_{(1,54)} = 0.40$s, $P = 0.531$. Repeated measures ANOVA within groups main effect of time: scrShank3 vehicle $F_{(1,15)} = 1.36$, shShank3 vehicle $F_{(1,12)} = 7.87$, scrShank3 Ro 677476 $F_{(1,12)} = 0.26$, shShank3 Ro 677476 $F_{(1,15)} = 0.03$). **(d**) Bar graph of social preference during T_2, over the total social preference (normalized SP_2) (two-way ANOVA; virus × drug interaction: $F_{(1,54)} = 5.98$, $P = 0.018$; main effect virus: $F_{(1,54)} = 1.73$, $P = 0.194$; main effect drug: $F_{(1,54)} = 0.03$, $P = 0.875$; followed by Tukey HSD *post hoc* test). (**e**) Time of social interaction during T_2 (two-way ANOVA; virus × drug interaction: $F_{(1,54)} = 1.07$, $P = 0.305$; main effect virus: $F_{(1,54)} = 3.84$, $P = 0.055$; main effect drug: $F_{(1,54)} = 0.27$, $P = 0.606$; followed by Tukey HSD *post hoc* test). (**f**) Number of entries during T_2 (two-way ANOVA; virus × drug interaction: $F_{(1,54)} = 6.76$, $P = 0.012$; main effect virus: $F_{(1,54)} = 0.60$, $P = 0.442$; main effect drug: $F_{(1,54)} = 1.83$, $P = 0.182$; followed by Tukey HSD *post hoc* test). Numbers in bars indicate mice. Error bars show s.e.m.

Figure 7 Synaptic and social deficits persist into adulthood and are reversed by treatment with PAM-mGluR1 during the critical period. (**a**) Experiment schematic. (**b**) Top: example traces of evoked AMPAR and NMDAR EPSCs recorded at +40 mV. Group mean AMPA/NMDA ratio calculated in shShank3-infected mice injected with vehicle or PAM-mGluR1 (Ro 677476, $t_{(8.33)} = 2.30$, unpaired *t*-test). Scale bar: 20 pA, 20 ms. (**c**) Scatter plots and group mean representing the social preference during T_1 and T_2 (repeated measures ANOVA; time × group interaction: $F_{(1,22)} = 5.56$, $P = 0.028$, main effect group $F_{(1,22)} = 0.22$, $P = 0.644$; followed by repeated

measures ANOVA within subjects. Main effect time: shShank3 vehicle, $F_{(1,9)} = 8.58$; shShank3 Ro 677476, $F_{(1,13)} = 0.24$). (**d**) Group mean entries around the social enclosure, time spent sniffing the stimulus mouse during T_2 and normalized social preference at T_2 for shShank3 mice treated with vehicle or Ro 677476 (entries: $t_{(22)} = -2.88$, unpaired *t*-test; time: $U = 39.00$, Mann-Whitney test; normalized SP_2, $t_{(22)} = -2.44$, unpaired *t*-test). Numbers in bars indicate mice. Error bars show s.e.m.

Figure 8 Optical stimulation of VTA DA neurons increases social preference. (**a**) Schematic of the experimental design, injection site and cannula placement. (**b**) Representative image of cannula placement and injection site of the AAV-shShank3 and AAV-DIO-ChR2 in the VTA. Scale bar: 500 μm. (**c**) Whole-cell patch clamp recording of ChR2-infected VTA DA neuron, showing desensitizing photocurrent in response to 500 ms blue light. Scale bar: 100 ms, 1 nA. (**d**) *In vitro* validation of 20-Hz blue light stimulation protocol. Scale bar: 1 s, 10 mV. (**e**) Experiment schematic. Optical stimulation (blue) was applied during the second 5 min of the test (T_2) only when animals were in proximity to the enclosure containing the stimulus mouse. (**f**) Scatter plots and group mean of social preference for each condition (repeated measures two-way ANOVA: time × light × virus interaction $F_{(1,31)} = 1.11$, $P = 0.300$; between subjects: light stimulation × virus interaction $F_{(1,31)} = 5.52$, $P = 0.025$; main effect virus $F_{(1,31)} = 2.28$, $P = 0.141$; main effect of light stimulation $F_{(1,31)} = 14.17$, $P = 0.001$. Two-way ANOVA between off groups: time main effect $F_{(1,38)} = 1.67$, $P = 0.204$; virus main effect $F_{(1,38)} = 9.88$, $P = 0.003$; time × virus interaction $F_{(1,38)} = 4.34$, $P = 0.044$. Two-way ANOVA between on groups: time main effect $F_{(1,24)} = 31.08$, $P < 0.001$; virus main effect $F_{(1,24)} = 0.41$, $P = 0.527$; time × virus interaction $F_{(1,24)} = 0.35$, $P = 0.558$. Repeated measures ANOVA within subjects main effect of time: scrShank3 off, $F_{(1,9)} = 0.23$; shShank3 off, $F_{(1,10)} = 11.77$; scrShank3 on, $F_{(1,7)} = 55.14$; shShank3 on, $F_{(1,5)} = 9.03$). (**g**) Group mean normalized social preference SP_2 (two-way ANOVA; virus × light stimulation interaction: $F_{(1,31)} = 1.28$, $P = 0.267$; main effect virus: $F_{(1,31)} = 4.70$, $P = 0.038$; main effect light stimulation: $F_{(1,31)} = 16.93$, $P < 0.001$; followed by Dunnett *post hoc* test). Error bars show s.e.m. Numbers in bars indicate mice.

a

AAV-shShank3 (200 nL)

<P6 | Juvenile | Adolescent

WT mice

Immunohistochemistry

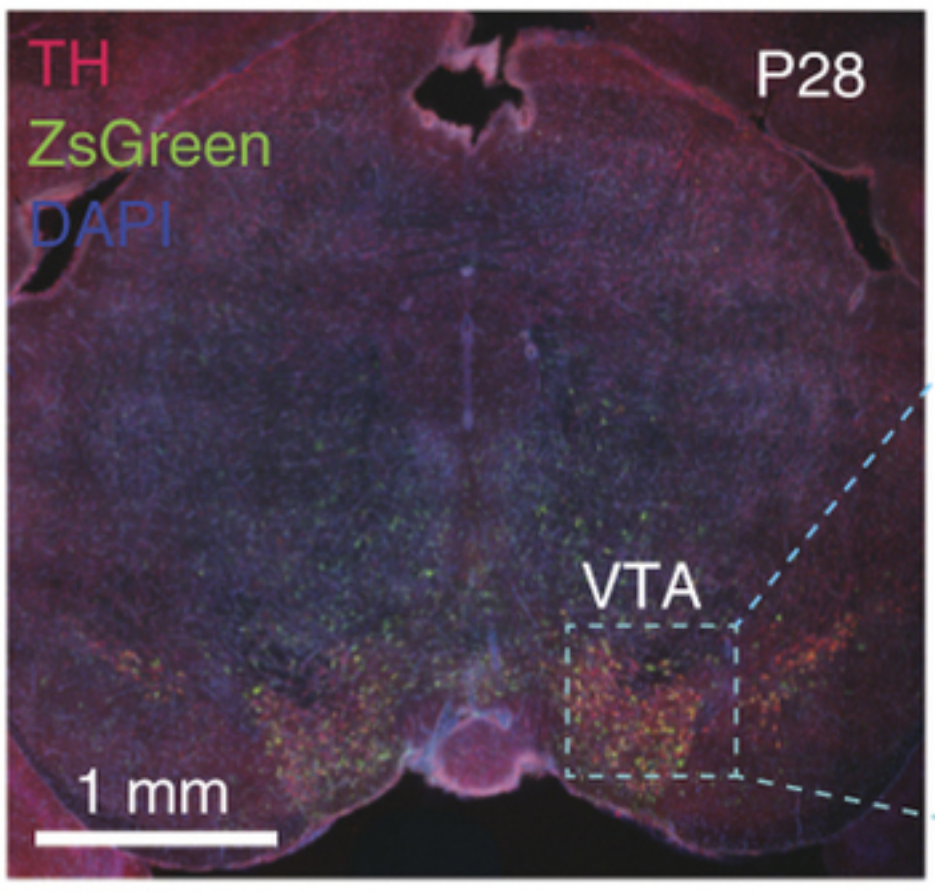

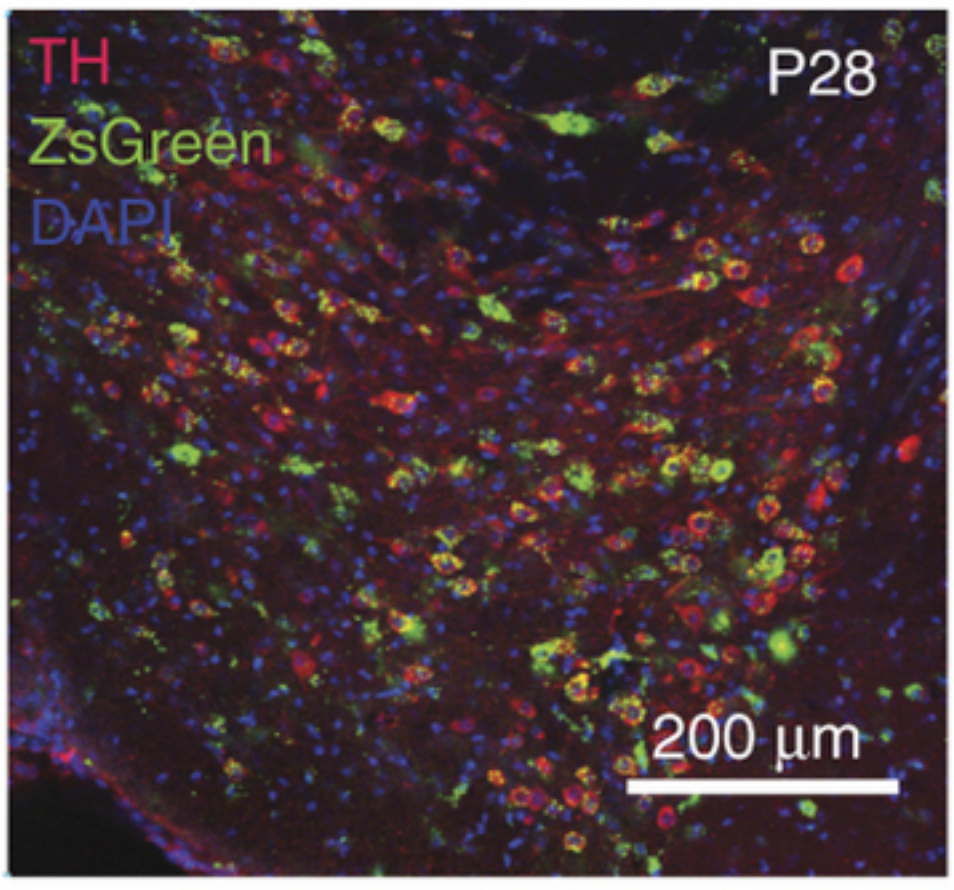

b

AAV-shShank3 AAV-DIO-tdTomato

<P6 | Juvenile | Adolescent

GAD-Cre mice

Immunohistochemistry

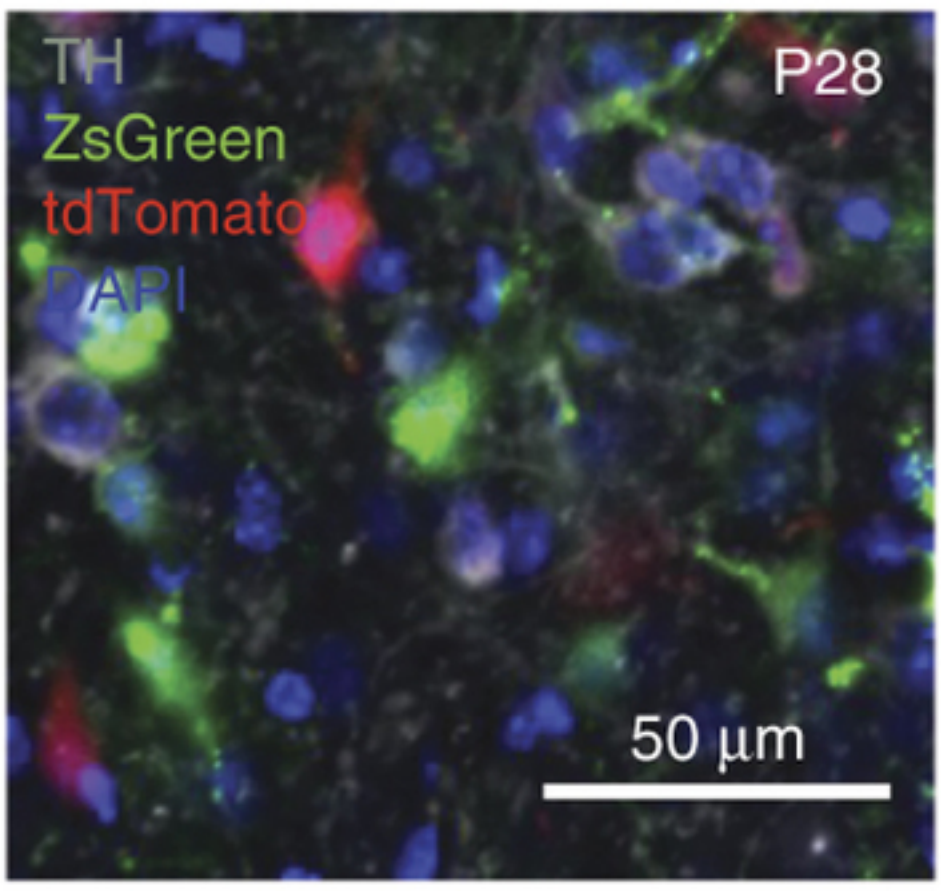

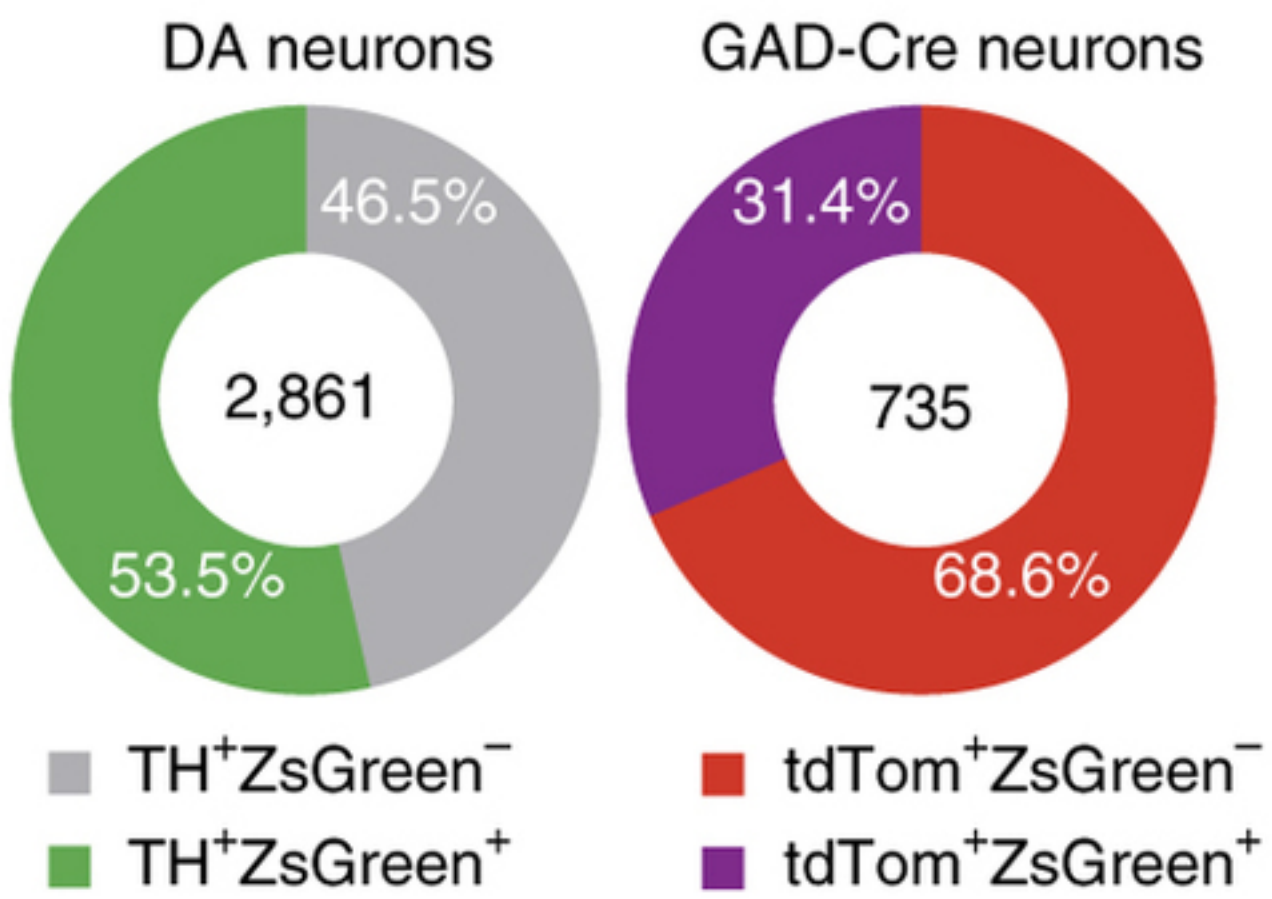

c

AAV-shShank3 or AAV-scrShank3 (200 nL)

<P6 | Juvenile | Adolescent

WT mice

Western blot

P21–P35

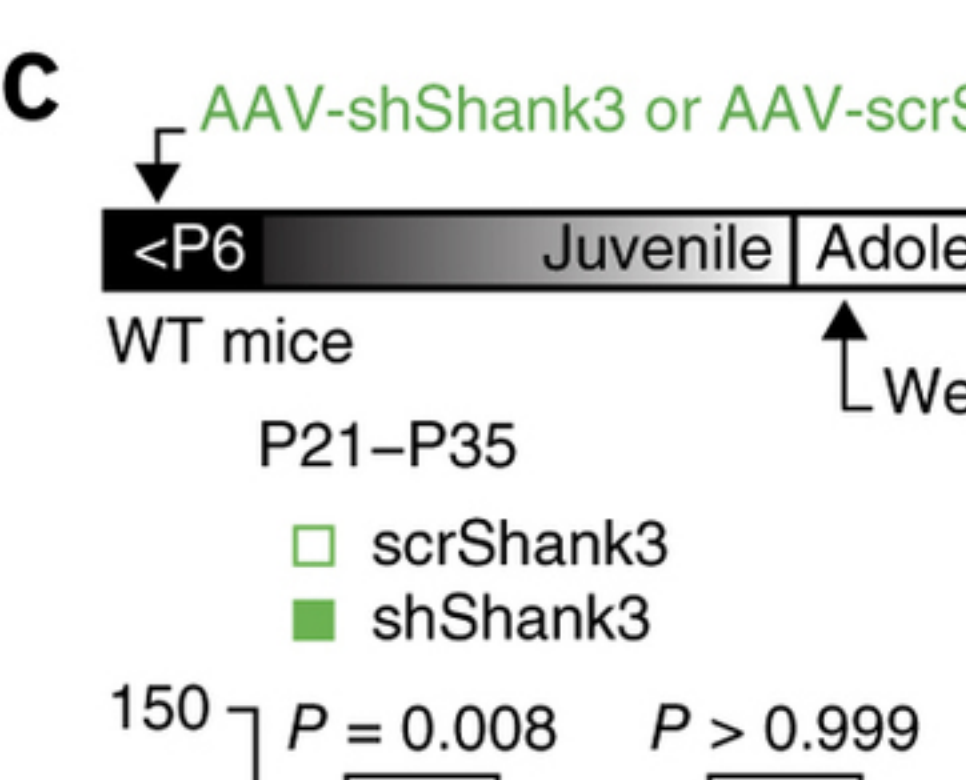

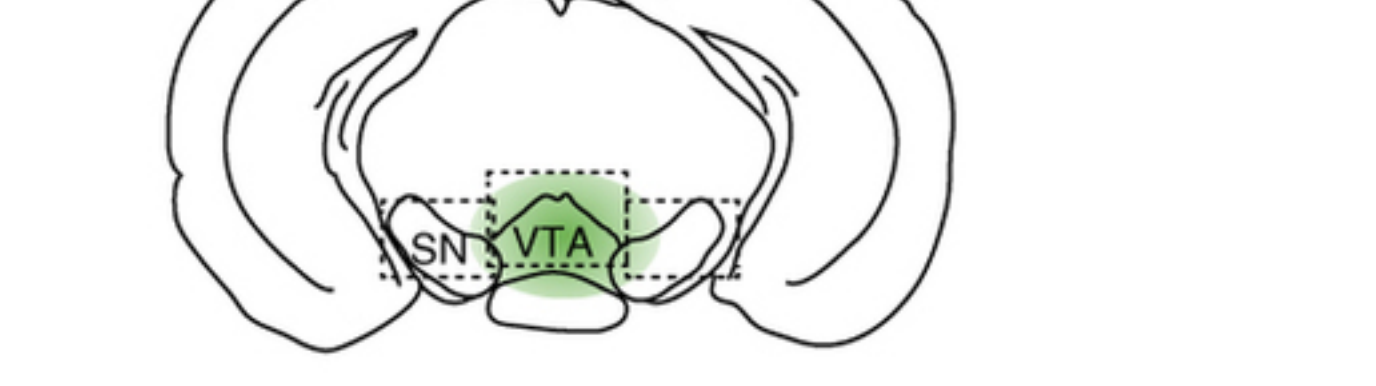

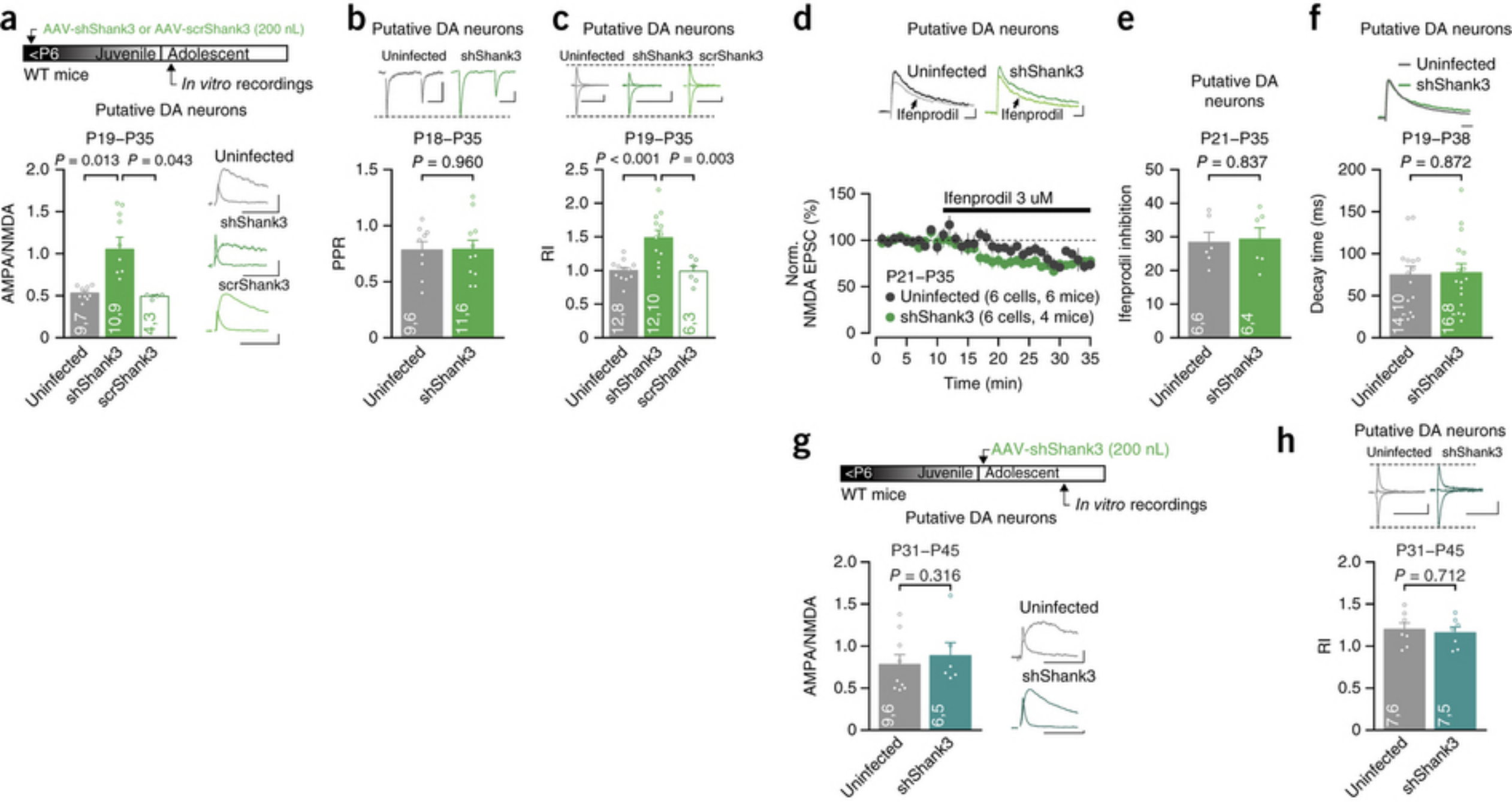
a
AAV-shShank3 or AAV-scrShank3 (200 nL)
<P6
Juvenile
Adolescent
WT mice
In vitro recordings
Putative DA neurons
P19–P35
P = 0.013
P = 0.043
AMPA/NMDA
Uninfected
shShank3
scrShank3
b
Putative DA neurons
Uninfected
shShank3
P18–P35
P = 0.960
PPR
c
Putative DA neurons
Uninfected
shShank3
scrShank3
P19–P35
P < 0.001
P = 0.003
RI
d
Putative DA neurons
Uninfected
shShank3
Ifenprodil
Ifenprodil 3 uM
Norm. NMDA EPSC (%)
P21–P35
Uninfected (6 cells, 6 mice)
shShank3 (6 cells, 4 mice)
Time (min)
e
Putative DA neurons
P21–P35
P = 0.837
Ifenprodil inhibition
f
Putative DA neurons
Uninfected
shShank3
P19–P38
P = 0.872
Decay time (ms)
g
AAV-shShank3 (200 nL)
<P6
Juvenile
Adolescent
WT mice
In vitro recordings
Putative DA neurons
P31–P45
P = 0.316
AMPA/NMDA
Uninfected
shShank3
h
Putative DA neurons
Uninfected
shShank3
P31–P45
P = 0.712
RI

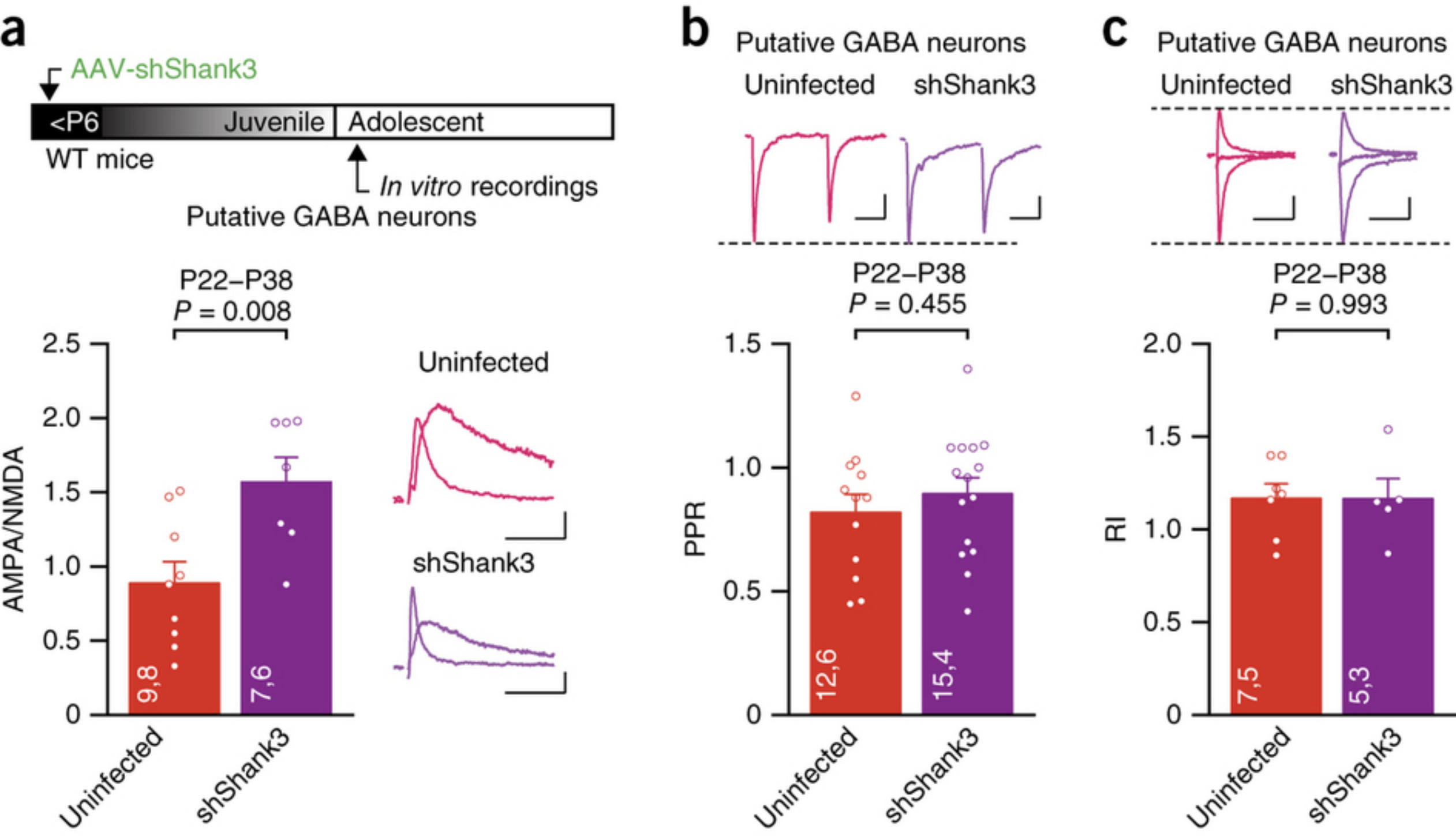
a
AAV-shShank3
<P6
Juvenile
Adolescent
WT mice
In vitro recordings
Putative GABA neurons
P22–P38
P = 0.008
AMPA/NMDA
2.5
2.0
1.5
1.0
0.5
0
9,8
7,6
Uninfected
shShank3
b
Putative GABA neurons
Uninfected
shShank3
P22–P38
P = 0.455
PPR
1.5
1.0
0.5
0
12,6
15,4
c
Putative GABA neurons
Uninfected
shShank3
P22–P38
P = 0.993
RI
2.0
1.5
1.0
0.5
0
7,5
5,3

a

AAV-shShank3

<P6 | Juvenile | Adolescent

WT mice

In vitro recordings

Putative DA neurons

Norm. AMPA EPSC (%)

DHPG

P18–P27

Uninfected (14 cells, 8 mice)

shShank3 (15 cells, 14 mice)

Time (min)

b

Putative DA neurons

shShank3

Uninfected

P18–P27 P = 0.016

P18–P27 P = 0.230

RI

6,5

5,3

Before DHPG

After DHPG

c

AAV-shShank3 or AAV-scrShank3

<P6 | Juvenile | Adolescent

WT mice

In vitro recordings

Ro 677476 or vehicle i.p.

Putative DA neurons

P18–P33

P = 0.554

P < 0.001 P = 0.002

P > 0.999

AMPA/NMDA

5,4 8,3 5,5 8,5

scrShank3 shShank3 scrShank3 shShank3

Vehicle Ro 677476

Vehicle

Ro 677476

scrShank3 shShank3

d

Putative DA neurons

Vehicle Ro 677476

scrShank3 shShank3 scrShank3 shShank3

P18–P33

P = 0.635

P = 0.001 P = 0.010

P > 0.999

RI

9,5 9,3 6,4 10,7

scrShank3 shShank3 scrShank3 shShank3

Vehicle Ro 677476

a

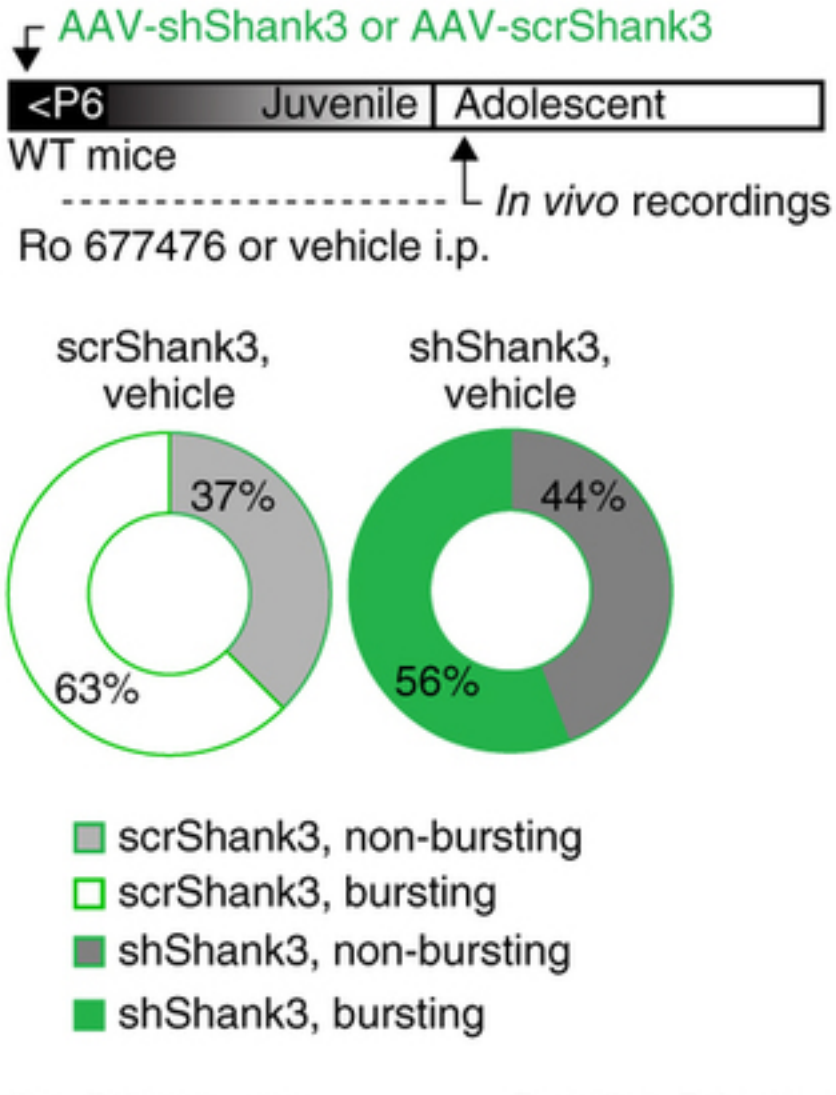
AAV-shShank3 or AAV-scrShank3
<P6
Juvenile
Adolescent
WT mice
In vivo recordings
Ro 677476 or vehicle i.p.
scrShank3, vehicle
shShank3, vehicle
37%
63%
44%
56%
scrShank3, non-bursting
scrShank3, bursting
shShank3, non-bursting
shShank3, bursting

b

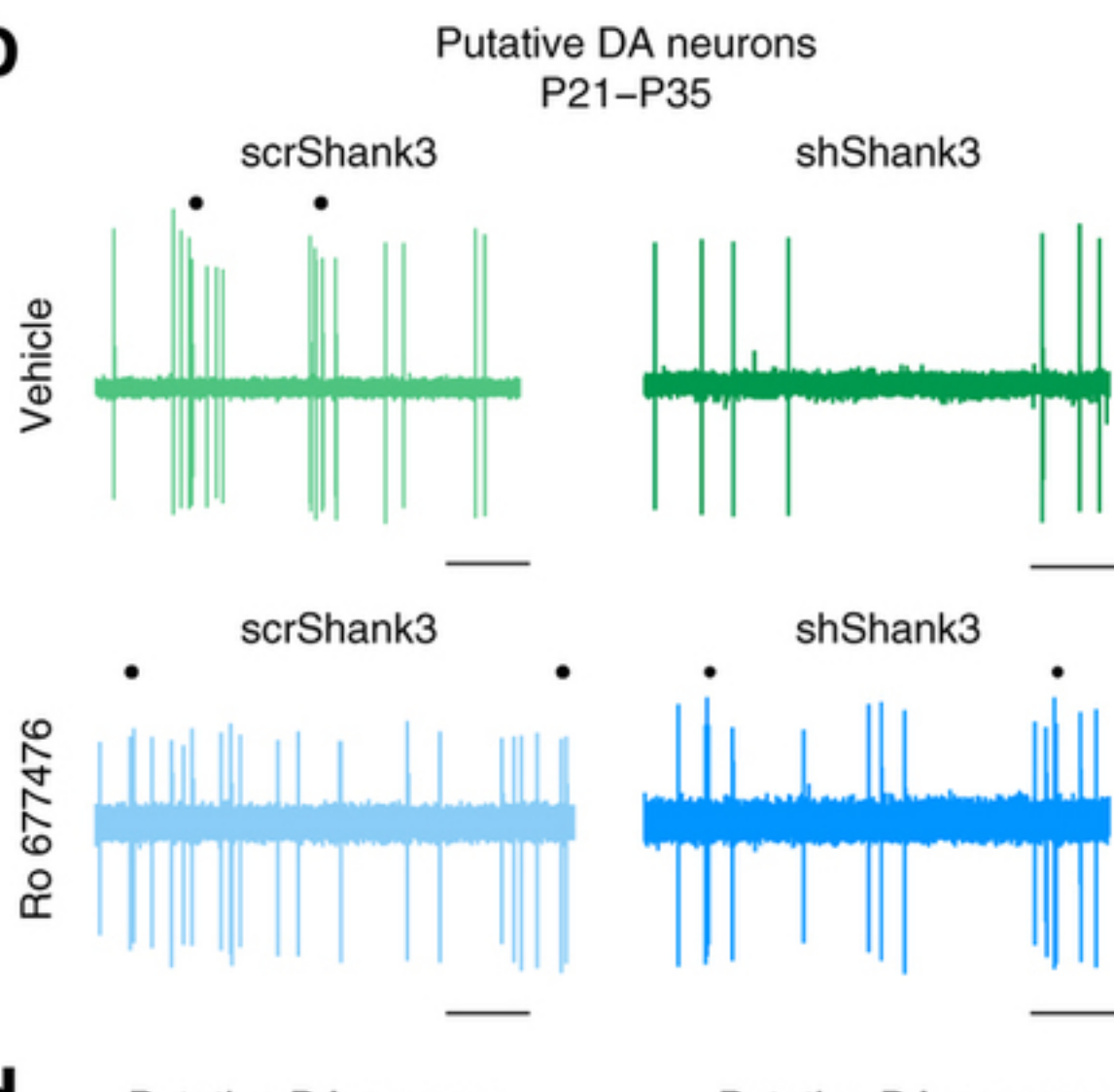
Putative DA neurons
P21–P35
scrShank3
shShank3
Vehicle
Ro 677476

c

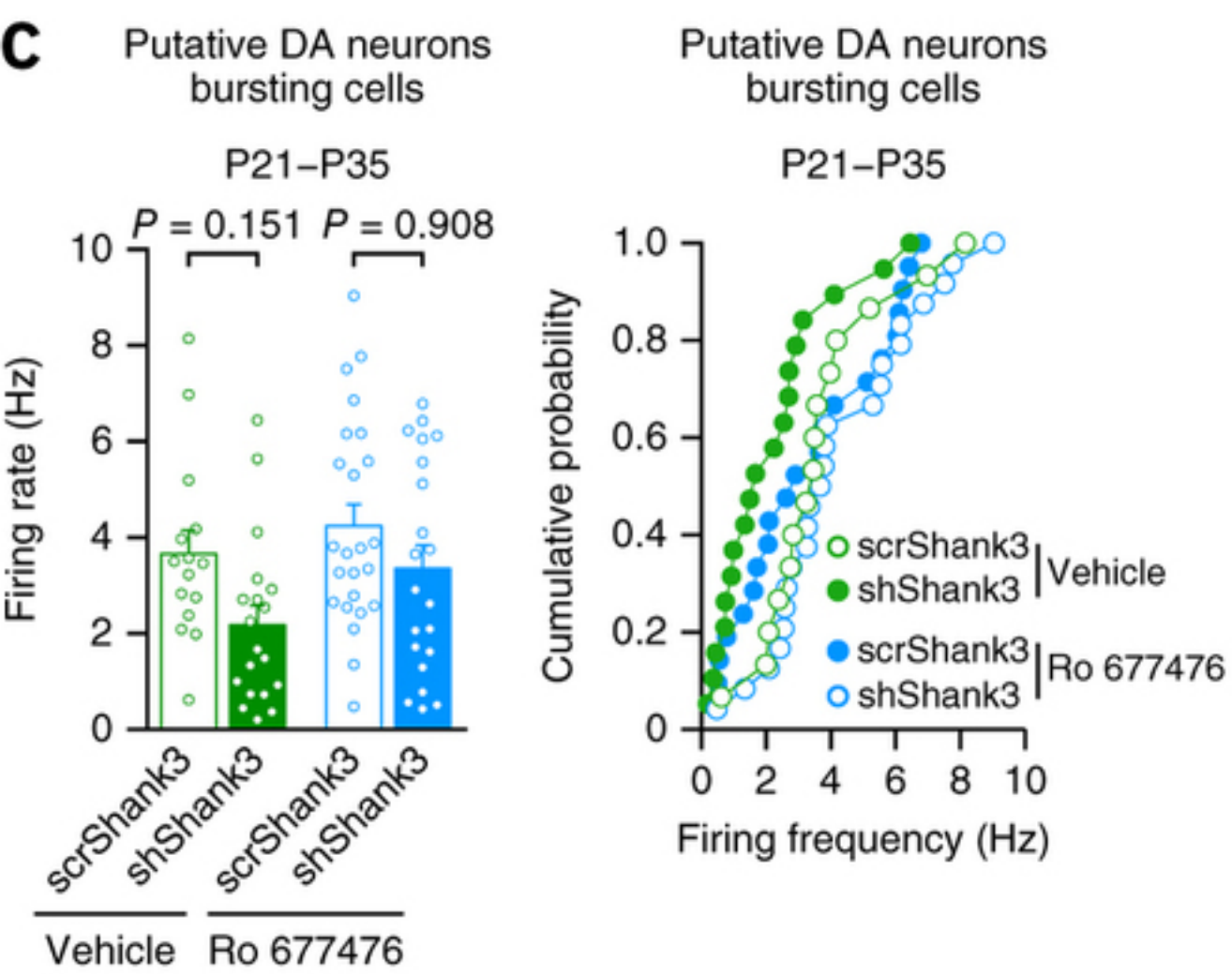
Putative DA neurons
bursting cells
P21–P35
P = 0.151
P = 0.908
Firing rate (Hz)
scrShank3
shShank3
Vehicle
Ro 677476
Cumulative probability
Firing frequency (Hz)

d

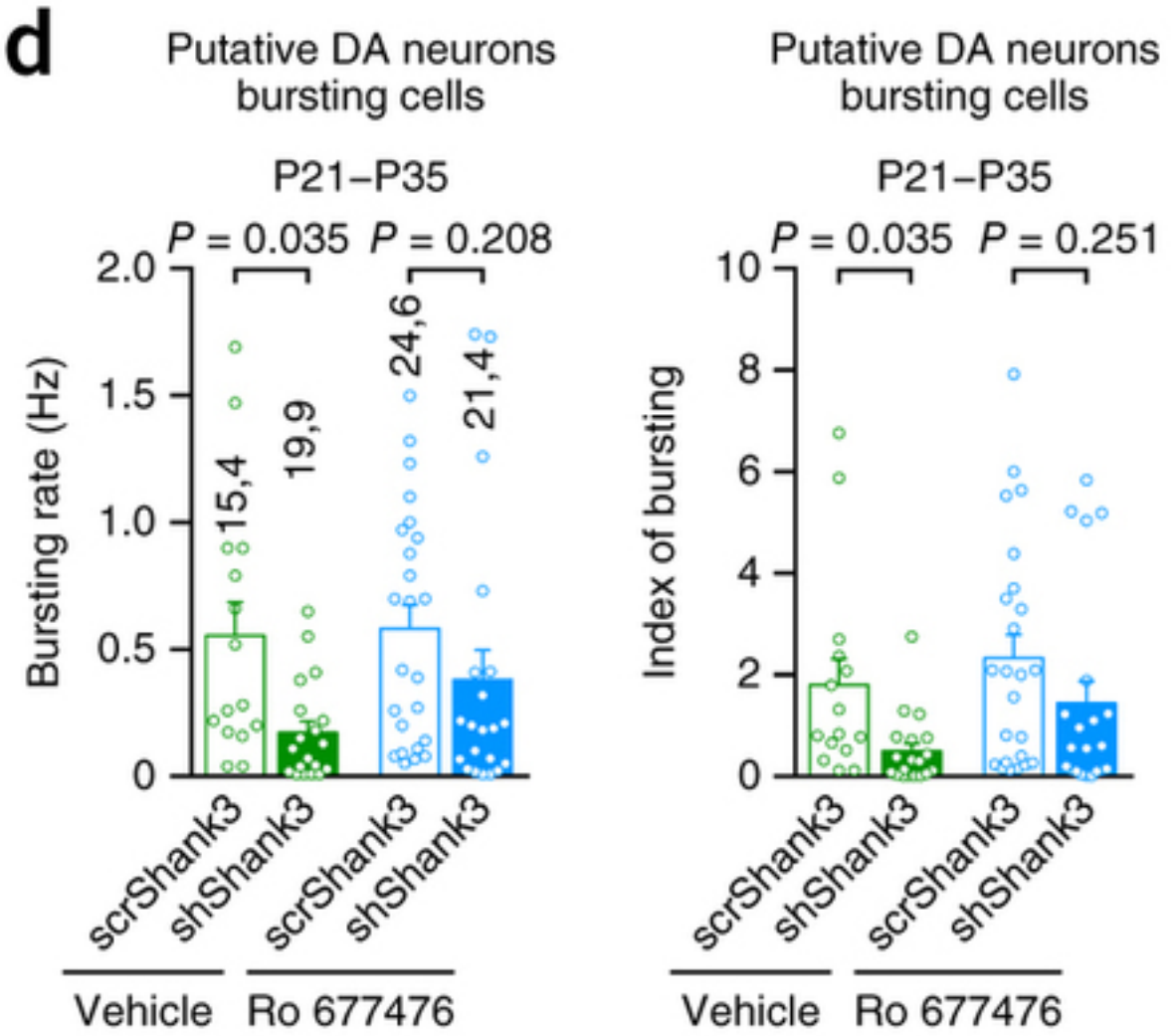
Putative DA neurons
bursting cells
P21–P35
P = 0.035
P = 0.208
P = 0.251
Bursting rate (Hz)
15,4
19,9
24,6
21,4
Index of bursting
scrShank3
shShank3
Vehicle
Ro 677476

e

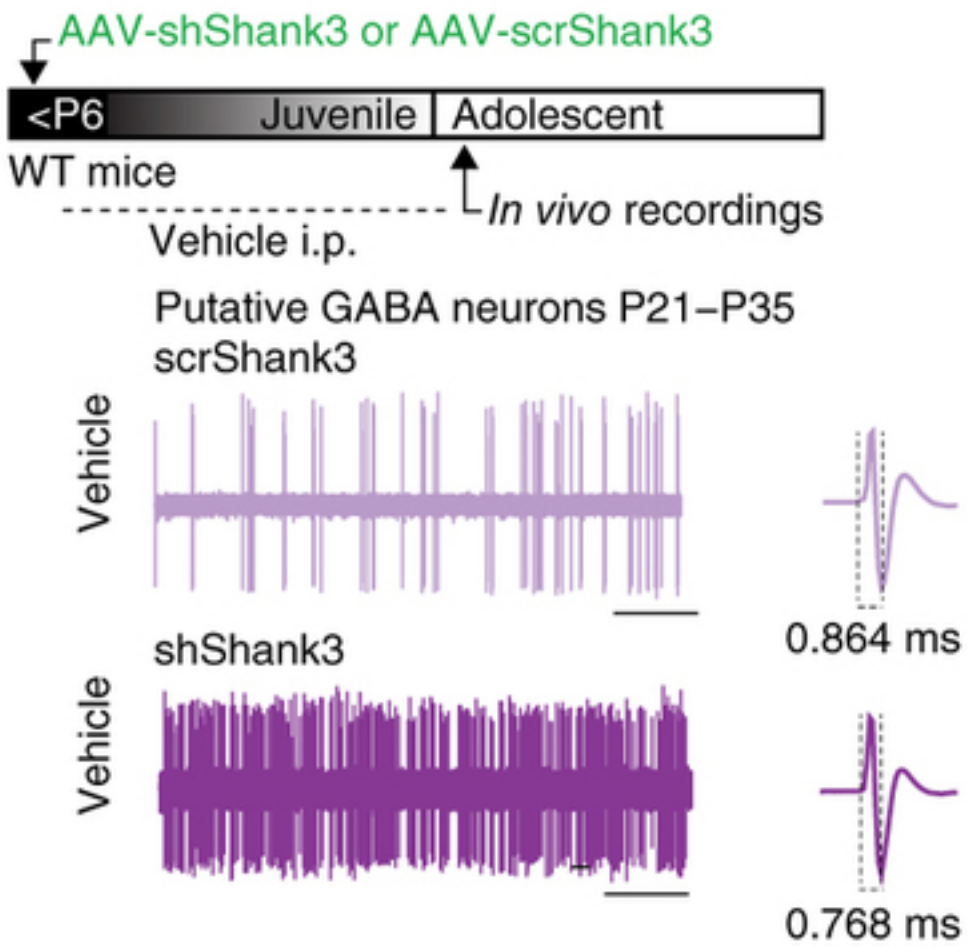
AAV-shShank3 or AAV-scrShank3
<P6
Juvenile
Adolescent
WT mice
In vivo recordings
Vehicle i.p.
Putative GABA neurons P21–P35
scrShank3
Vehicle
shShank3
Vehicle
0.864 ms
0.768 ms

f

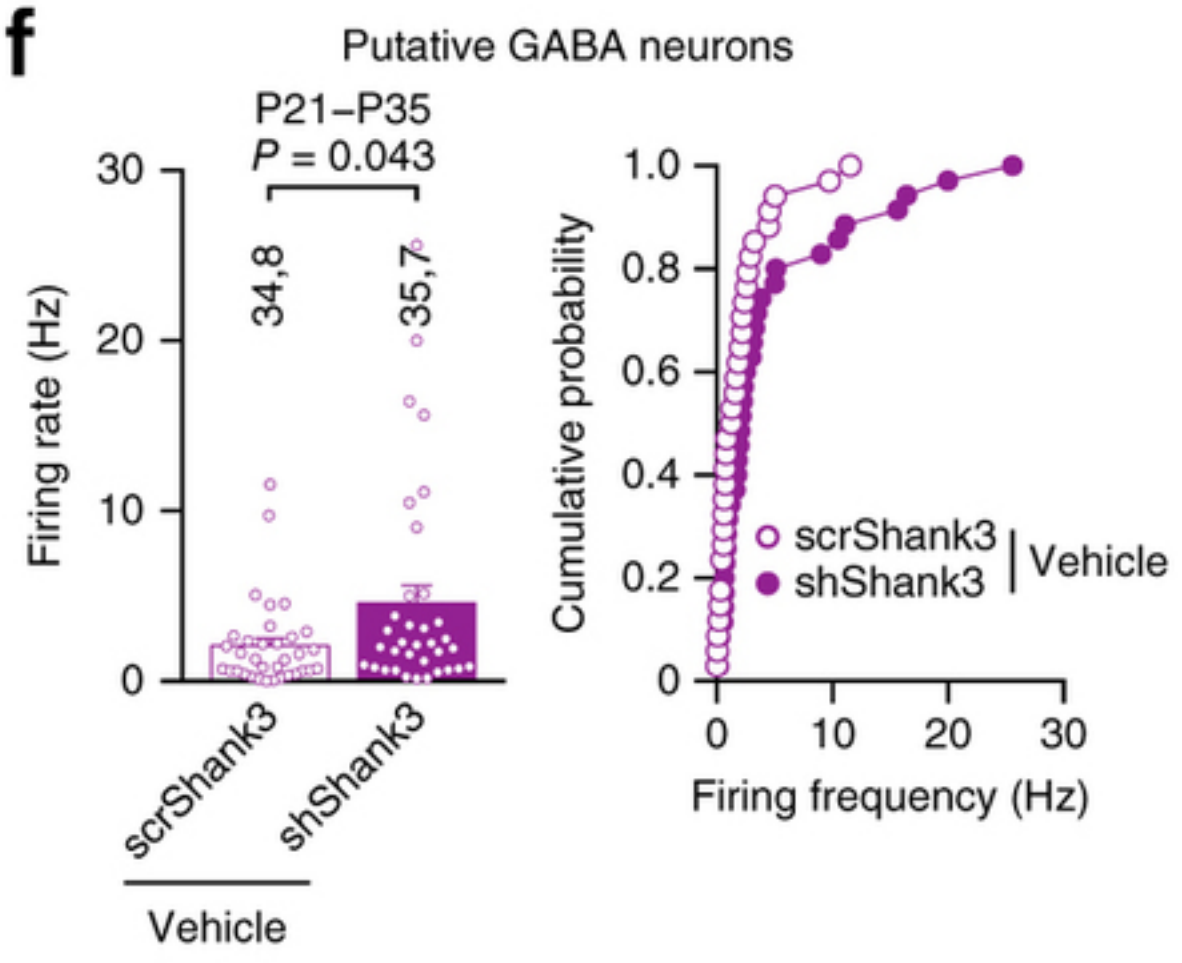
Putative GABA neurons
P21–P35
P = 0.043
Firing rate (Hz)
34,8
35,7
scrShank3
shShank3
Vehicle
Cumulative probability
Firing frequency (Hz)

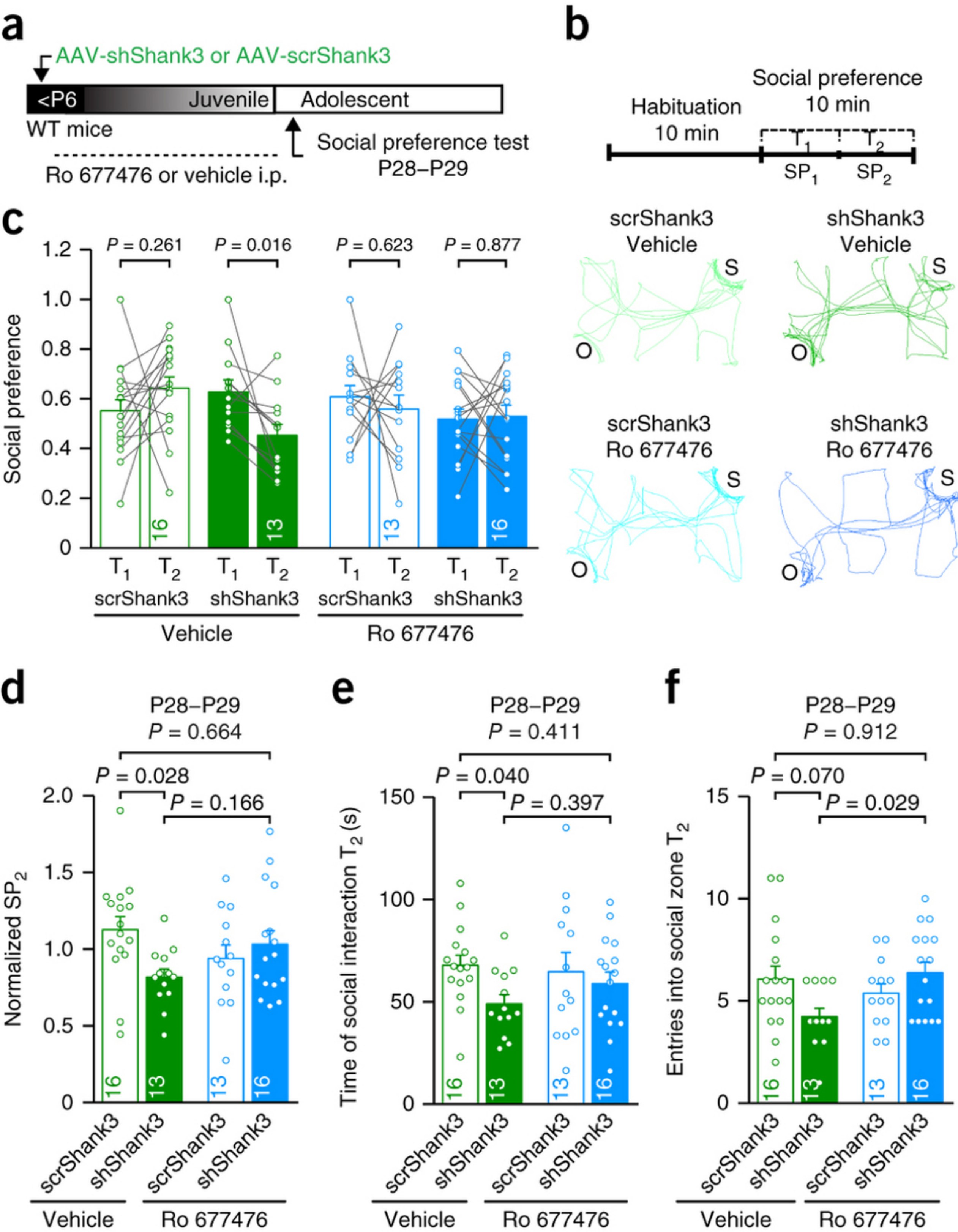
a
AAV-shShank3 or AAV-scrShank3
<P6
Juvenile
Adolescent
WT mice
Social preference test
P28–P29
Ro 677476 or vehicle i.p.
b
Habituation
10 min
Social preference
10 min
T1
T2
SP1
SP2
scrShank3
Vehicle
shShank3
Vehicle
S
O
scrShank3
Ro 677476
shShank3
Ro 677476
c
P = 0.261
P = 0.016
P = 0.623
P = 0.877
Social preference
1.2
1.0
0.8
0.6
0.4
0.2
0
16
13
13
16
T1 T2 T1 T2 T1 T2 T1 T2
scrShank3 shShank3 scrShank3 shShank3
Vehicle
Ro 677476
d
P28–P29
P = 0.664
P = 0.028
P = 0.166
Normalized SP2
2.0
1.5
1.0
0.5
0
16
13
13
16
scrShank3 shShank3 scrShank3 shShank3
Vehicle
Ro 677476
e
P28–P29
P = 0.411
P = 0.040
P = 0.397
Time of social interaction T2 (s)
150
100
50
0
16
13
13
16
scrShank3 shShank3 scrShank3 shShank3
Vehicle
Ro 677476
f
P28–P29
P = 0.912
P = 0.070
P = 0.029
Entries into social zone T2
15
10
5
0
16
13
13
16
scrShank3 shShank3 scrShank3 shShank3
Vehicle
Ro 677476

a

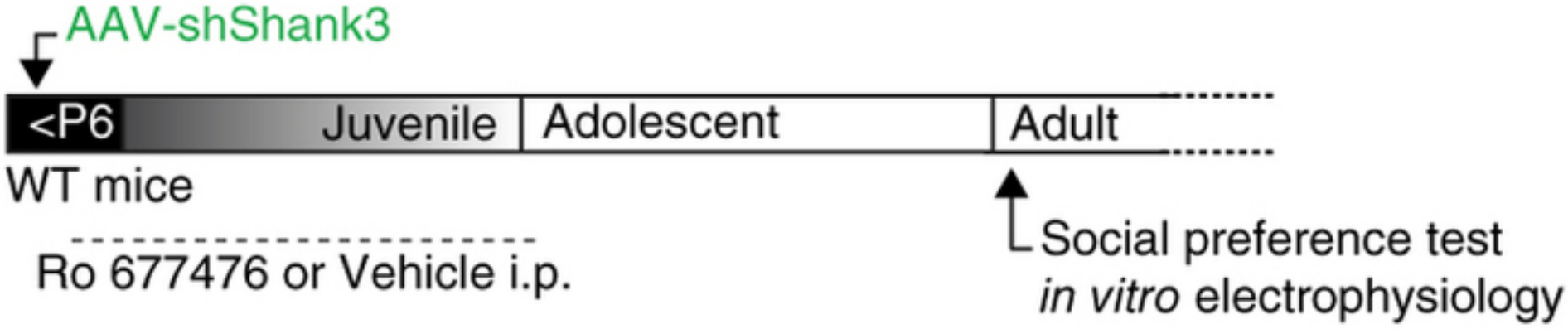
AAV-shShank3
<P6
Juvenile
Adolescent
Adult
WT mice
Ro 677476 or Vehicle i.p.
Social preference test
in vitro electrophysiology

b

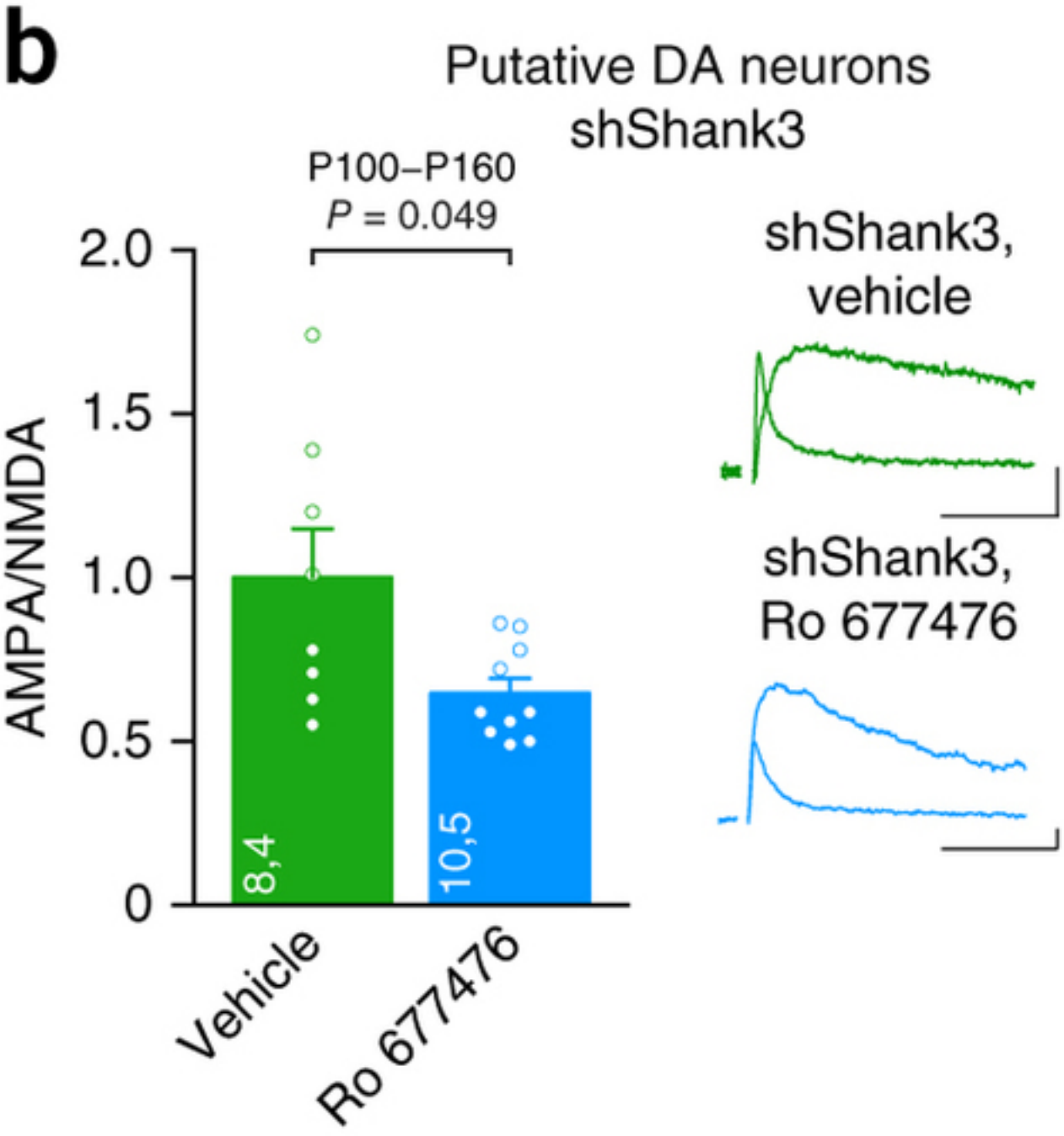
Putative DA neurons
shShank3
P100–P160
P = 0.049
AMPA/NMDA
2.0
1.5
1.0
0.5
0
8,4
10,5
Vehicle
Ro 677476
shShank3,
vehicle
shShank3,
Ro 677476

c

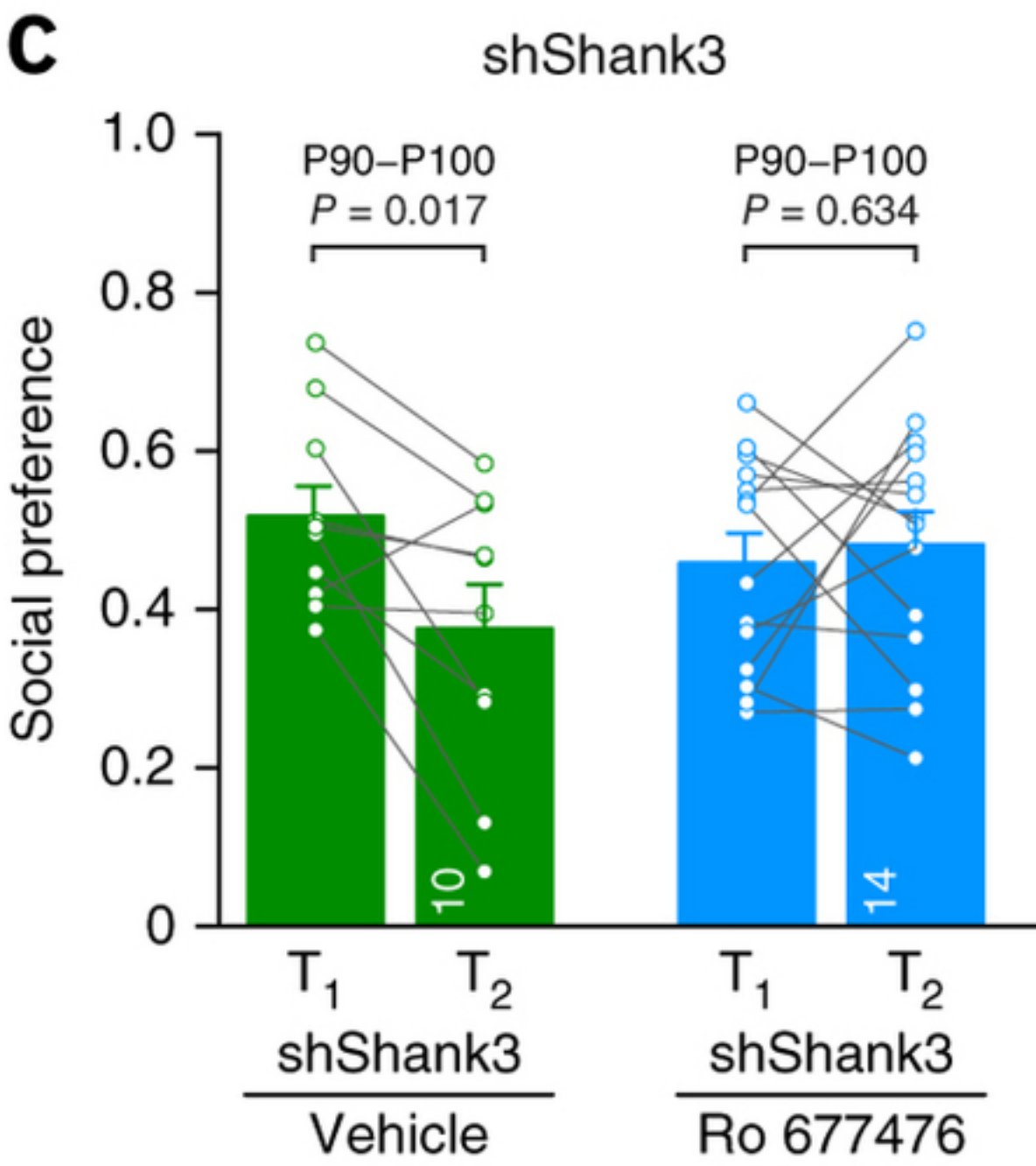
shShank3
P90–P100
P = 0.017
P90–P100
P = 0.634
Social preference
1.0
0.8
0.6
0.4
0.2
0
10
14
T1
T2
shShank3
Vehicle
shShank3
Ro 677476

d

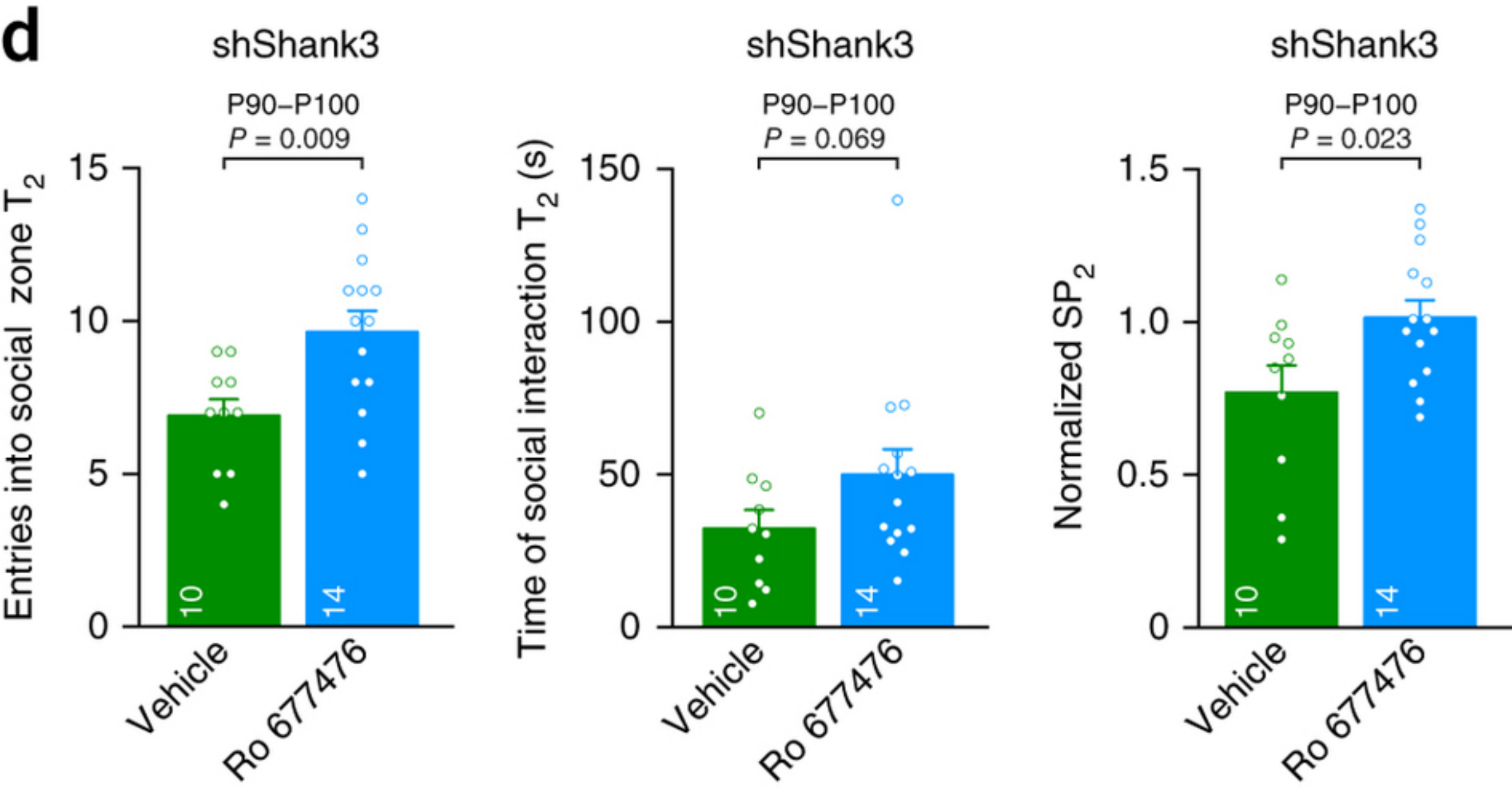
shShank3
P90–P100
P = 0.009
Entries into social zone T2
15
10
5
0
10
14
Vehicle
Ro 677476
shShank3
P90–P100
P = 0.069
Time of social interaction T2 (s
150
100
50
0
10
14
Vehicle
Ro 677476
shShank3
P90–P100
P = 0.023
Normalized SP2
1.5
1.0
0.5
0
10
14
Vehicle
Ro 677476

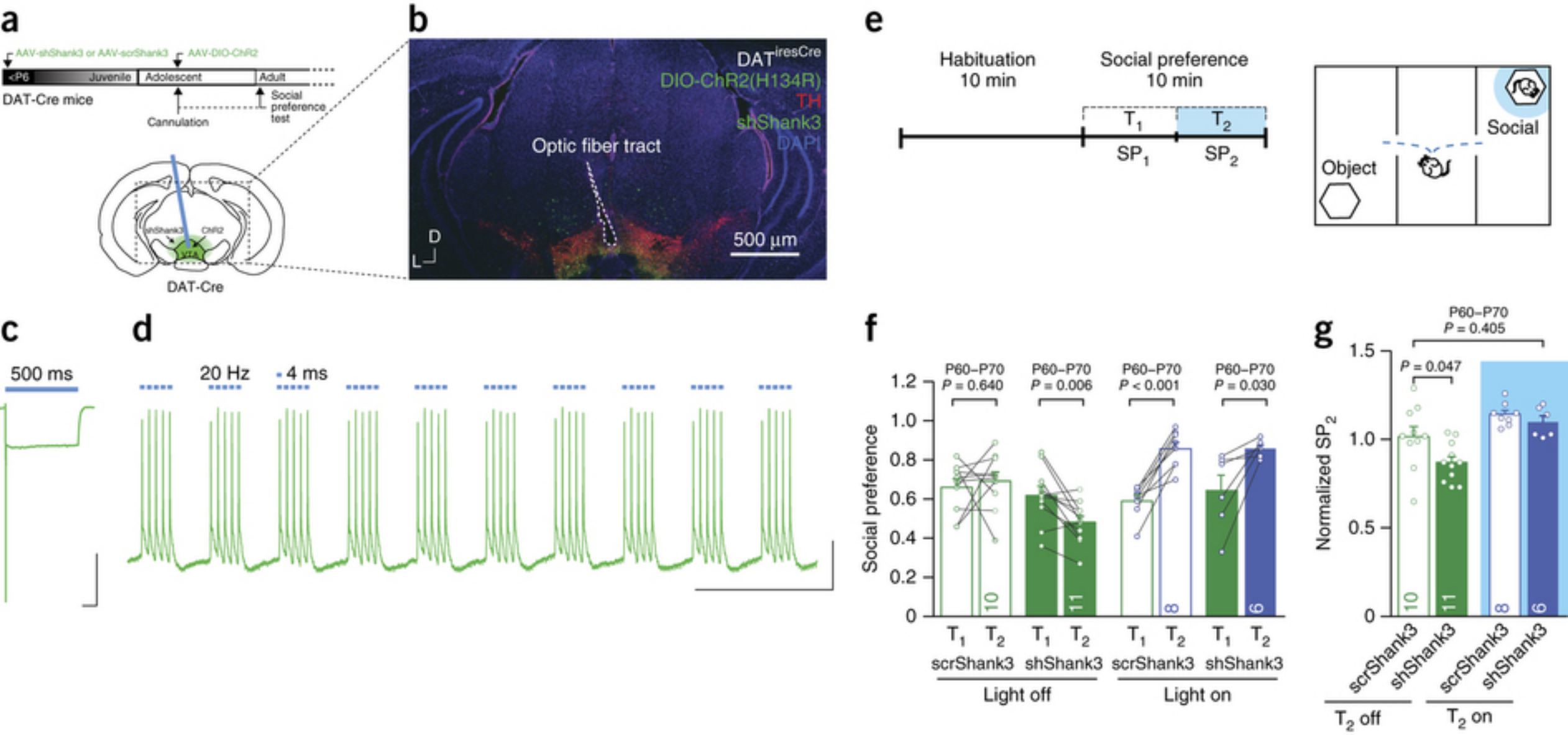
a
AAV-shShank3 or AAV-scrShank3
AAV-DIO-ChR2
<P6
Juvenile
Adolescent
Adult
DAT-Cre mice
Cannulation
Social preference test
shShank3
ChR2
VTA
DAT-Cre
b
DAT iresCre
DIO-ChR2(H134R)
TH
shShank3
DAPI
Optic fiber tract
D
L
500 µm
c
500 ms
d
20 Hz
4 ms
e
Habituation 10 min
Social preference 10 min
T1
T2
SP1
SP2
Social
Object
f
Social preference
P60–P70 P = 0.640
P60–P70 P = 0.006
P60–P70 P < 0.001
P60–P70 P = 0.030
10
11
8
6
T1 T2 T1 T2 T1 T2 T1 T2
scrShank3 shShank3 scrShank3 shShank3
Light off
Light on
g
Normalized SP2
P60–P70 P = 0.405
P = 0.047
10
11
8
6
scrShank3 shShank3 scrShank3 shShank3
T2 off
T2 on

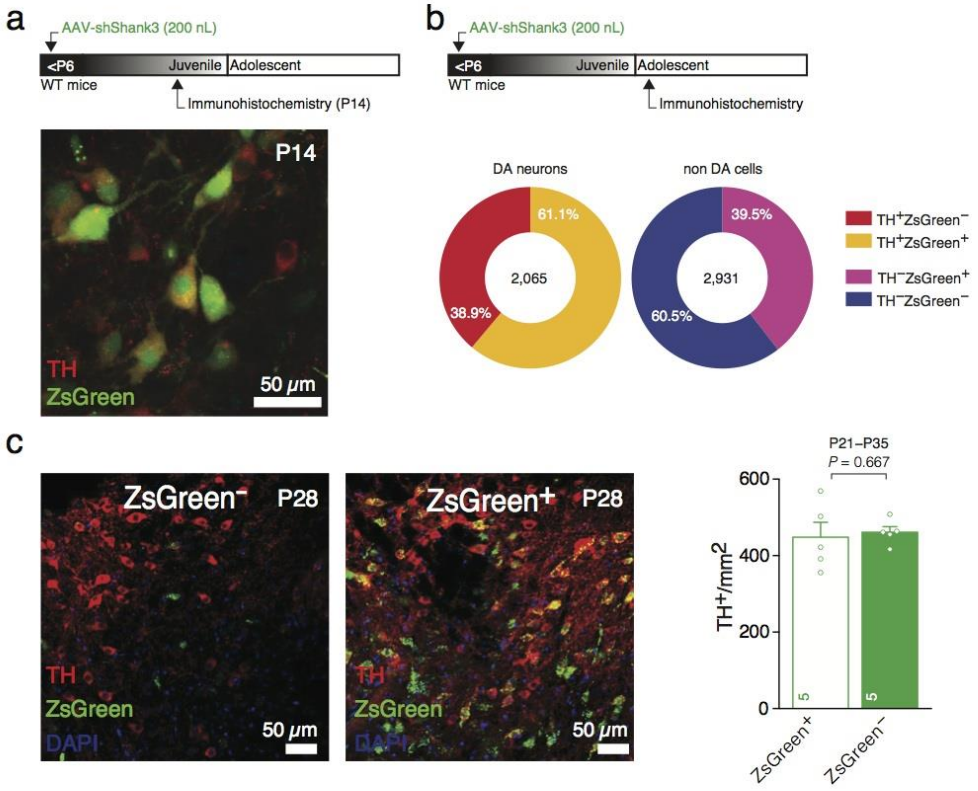

Supplementary Figure 1

AAV-shShank3 targets DA and non-DA neurons within the VTA

(a) Top: schematic of the immunostaining experiment performed at P14 on VTA AAV-shShank3 infected mice. Representative confocal image shows ZsGreen expression in DA neurons (experiment repeated in 3 mice). (**b)** Top: schematic of cell counting experiments performed in adolescent WT animals injected with AAV-shShank3 at P5 (for details see Materials and Methods). Quantification of viral infection in TH^+ (DA neurons; yellow, 61.1% $ZsGreen^+$; red, 38.9% $ZsGreen^-$) and TH^- cells (non DA cells; pink, 39.5% $ZsGreen^+$; blue, 60.5% $ZsGreen^-$). (**c**) Left: representative images of immunostaining experiments performed at P28 on unilaterally injected mice at P5 shows TH and ZsGreen expression for the Uninfected ($ZsGreen^-$) and the shShank3 infected ($ZsGreen^+$) side (experiment repeated in 5 mice). Scale bar: 50 µm. Right: quantification of dopaminergic (TH^+) neurons from infected ($ZsGreen^+$) and Uninfected ($ZsGreen^-$) side (U = 10, Mann-Whitney test). The numbers indicate the mice.

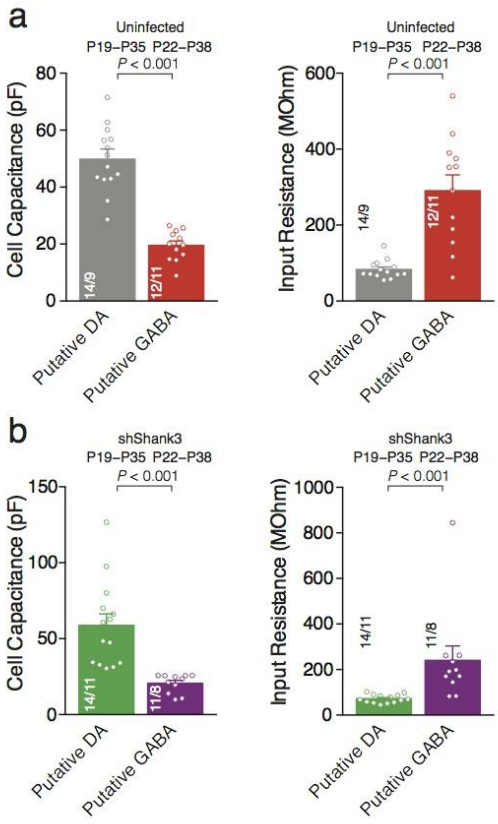

Supplementary Figure 2

Cell capacitance and input resistance in putative DA and GABA neurons

(a) Left: bar graph representing the mean value of cell capacitance of Uninfected Putative DA and GABA neurons ($U < 0.001$, Mann-Whitney test). Right: bar graph representing the mean value of input resistance of Uninfected Putative DA and GABA neurons ($U = 13.0$, Mann-Whitney test). (b) Left: bar graph representing the mean value of cell capacitance of shShank3 infected Putative DA and GABA neurons ($U < 0.001$, Mann-Whitney test). Right: bar graph representing the mean value of input resistance of shShank3 infected Putative DA and GABA neurons (U = 10, Mann-Whitney test). The numbers indicate cells and mice.

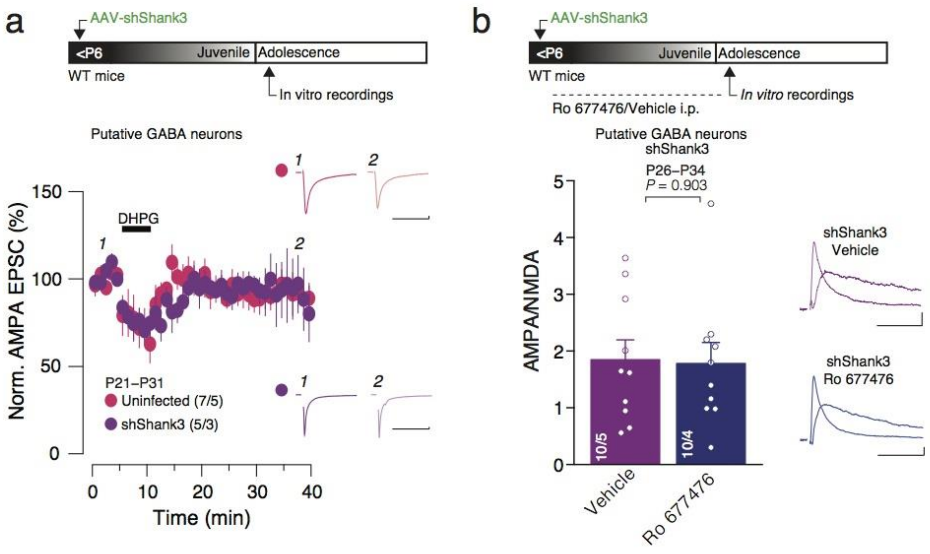

Supplementary Figure 3

Group I mGluR activation does not rescue synaptic deficits onto putative GABA neurons in the VTA

(a) Top: schematics of the experiment. Time course of AMPAR-EPSCs recorded at –60 mV before and after 5 minutes DHPG (20 μM) bath application from Uninfected and shShank3 infected VTA Putative GABA neurons. Inset: *1/2* example traces before and 25 minutes after DHPG application. (**b**) Top: schematics of the experiment. Bar graph representing the mean value of AMPA/NMDA recorded from shShank3 infected Putative GABA neurons from Vehicle and mGluR1-PAM Ro 677476 treated animals (t_{18} = 0.123, unpaired t-test). Right: example traces of AMPAR- and NMDAR-EPSCs recorded at +40 mV.

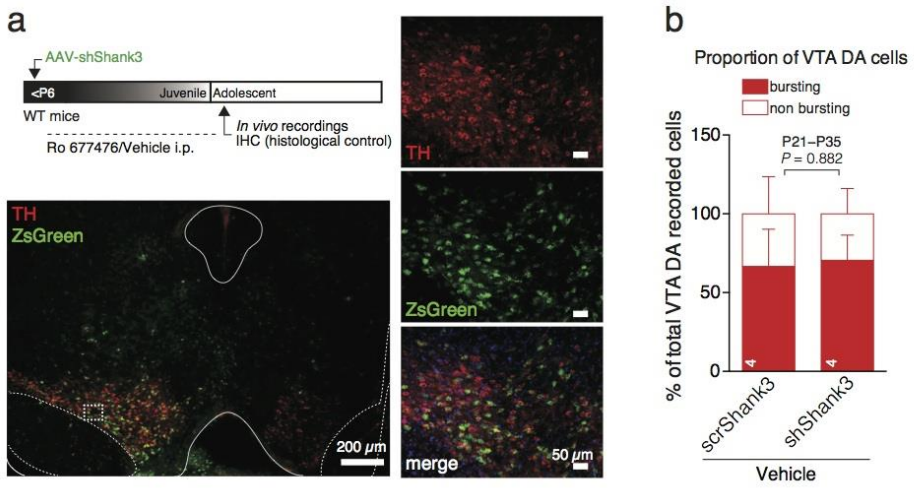

Supplementary Figure 4

Proportion of bursting and non-bursting DA neurons

(a) Experimental protocol and histological control of the injection site of the AAV-shShank3 virus in the VTA. Representative TH-immunostaining performed to delineate VTA dopaminergic area (red labeling).. Right: co-localisation of TH positive neurons with shShank3 positive neurons in the VTA. (b) Graph representing the proportion of VTA DA neurons with a bursting pattern compared to VTA DA neurons without bursting activity in scrShank3 and in shShank3 mice treated with i.p. injection of Vehicle (U = 8, Mann-Whitney test). The numbers indicate the mice.

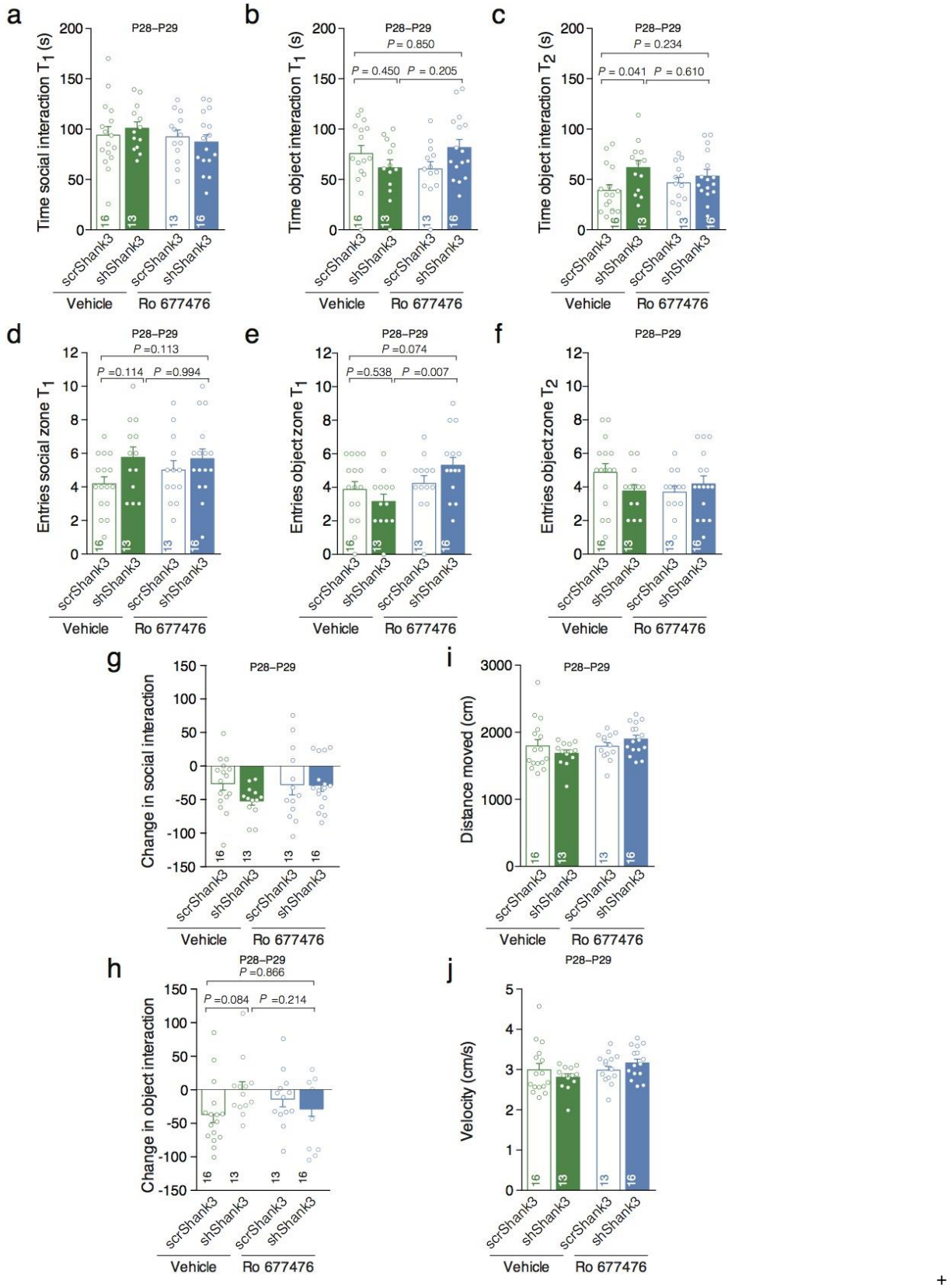
a
P28–P29
Time social interaction T1 (s)
b
P28–P29
P = 0.850
P = 0.450
P = 0.205
Time object interaction T1 (s)
c
P28–P29
P = 0.234
P = 0.041
P = 0.610
Time object interaction T2 (s)
d
P28–P29
P =0.113
P =0.114
P =0.994
Entries social zone T1
e
P28–P29
P =0.074
P =0.538
P =0.007
Entries object zone T1
f
P28–P29
Entries object zone T2
g
P28–P29
Change in social interaction
h
P28–P29
P =0.866
P =0.084
P =0.214
Change in object interaction
i
P28–P29
Distance moved (cm)
j
P28–P29
Velocity (cm/s)
scrShank3
shShank3
Vehicle
Ro 677476

Supplementary Figure 5

Additional parameters of social behavior and locomotor activity in VTA SHANK3 mice

(a) Bar graph representing the duration of interaction with the social stimulus during the first half of the three-chamber social preference test (T_1) (two-way ANOVA; no main effects and no interactions) **(b)** Bar graph representing the duration of interaction with the object during T_1 (two-way ANOVA; Virus × drug interaction: $F_{1,54} = 4.96$, $p = 0.030$; main effect virus: $F_{1,54} = 0.20$, p = 0.655 ; main effect drug: $F_{1,54} = 0.09$, $p = 0.763$; followed by Tukey HSD post-hoc test). **(c)** Bar graph representing the duration of interaction with the object during the second half of the three-chamber social preference test (T_2) (two-way ANOVA; Virus × drug interaction: $F_{1,54} = 1.74$, $p = 0.192$; main effect virus: $F_{1,54} = 5.76$, p = 0.020 ; main effect drug: $F_{1,54} = 0.01$, $p = 0.931$; followed by Tukey HSD post-hoc test) **(d)** Bar graph representing the number of entries in the virtual zone surrounding the social stimulus during T_1. (two-way ANOVA; Virus × drug interaction: $F_{1,54} = 0.67$, $p = 0.416$; main effect virus: $F_{1,54} = 4.33$, p = 0.042 ; main effect drug: $F_{1,54} = 0.45$, $p = 0.506$; followed by Tukey HSD post-hoc test) **(e)** Bar graph representing the number of entries in the virtual zone surrounding the object during T_1. (two-way ANOVA; Virus × drug interaction: $F_{1,54} = 3.68$, $p = 0.060$; main effect virus: $F_{1,54} = 0.15$, p = 0.703 ; main effect drug: $F_{1,54} = 7.15$, $p = 0.010$; followed by Tukey HSD post-hoc test) **(f)** Bar graph representing the number of entries in the virtual zone surrounding the object during T_2. (two-way ANOVA; no main effects and no interactions). (**g-h)** Bar graphs reporting the change in social and object interaction from T_2 to T_1 between scrShank3 and shShank3 mice treated with Vehicle. (Social: two-way ANOVA; no main effects and no interactions; Object: two-way ANOVA; Virus × drug interaction: $F_{1,54} = 4.88$, $p = 0.031$; main effect virus: $F_{1,54} = 0.90$, p = 0.346 ; main effect drug: $F_{1,54} = 0.06$, $p = 0.802$; followed by Tukey HSD post-hoc test) **(i)** Bar graph representing the distance moved during the social preference test (two-way ANOVA; no main effects and no interactions). **(j)** Bar graph representing the velocity during the social preference test (two-way ANOVA; no main effects and no interactions). Error bars show SEM.

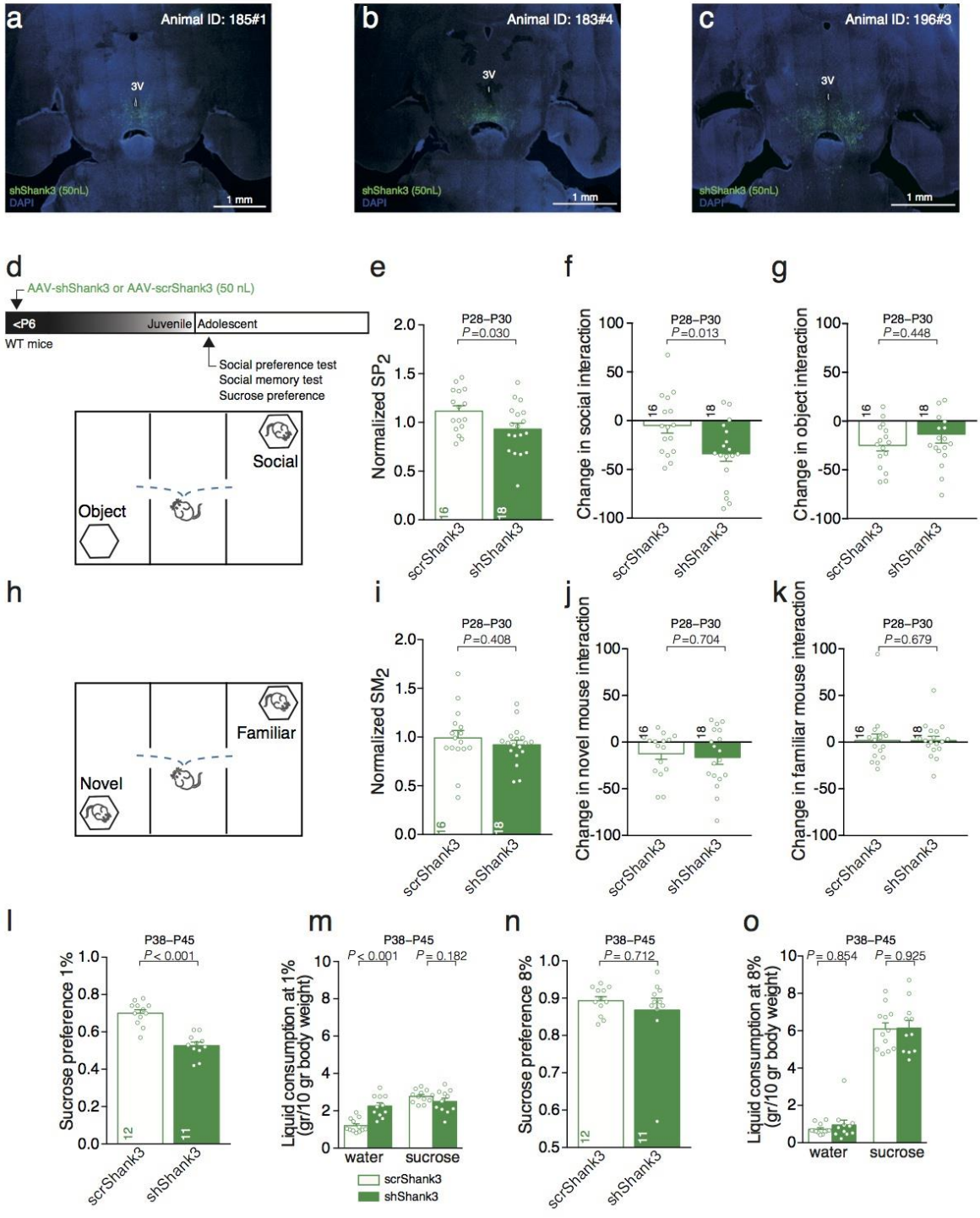
a
Animal ID: 185#1
3V
shShank3 (50nL)
DAPI
1 mm
b
Animal ID: 183#4
3V
shShank3 (50nL)
DAPI
1 mm
c
Animal ID: 196#3
3V
shShank3 (50nL)
DAPI
1 mm
d
AAV-shShank3 or AAV-scrShank3 (50 nL)
<P6
Juvenile
Adolescent
WT mice
Social preference test
Social memory test
Sucrose preference
Social
Object
e
P28–P30
P=0.030
Normalized SP2
scrShank3
shShank3
f
P28–P30
P=0.013
Change in social interaction
scrShank3
shShank3
g
P28–P30
P=0.448
Change in object interaction
scrShank3
shShank3
h
Familiar
Novel
i
P28–P30
P=0.408
Normalized SM2
scrShank3
shShank3
j
P28–P30
P=0.704
Change in novel mouse interaction
scrShank3
shShank3
k
P28–P30
P=0.679
Change in familiar mouse interaction
scrShank3
shShank3
l
P38–P45
P< 0.001
Sucrose preference 1%
scrShank3
shShank3
m
P38–P45
P< 0.001
P= 0.182
Liquid consumption at 1% (gr/10 gr body weight)
water
sucrose
scrShank3
shShank3
n
P38–P45
P= 0.712
Sucrose preference 8%
scrShank3
shShank3
o
P38–P45
P= 0.854
P= 0.925
Liquid consumption at 8% (gr/10 gr body weight)
water
sucrose

Supplementary Figure 6

Low volume of AAV-shShank3 alters social and sucrose preference

(a-c) Representative images of midbrain horizontal sections from three animals that underwent behavioral characterization injected with 50 nL of AAV-shShank3. **(d)** Schematic of the time course of the experiments and behavioral protocol of the social preference test. **(e)** Bar graph representing the normalized social preference at T_2 (t_{32} = 2.27, unpaired t-test). **(f)** Bar graph representing the change in social interaction from T_1 to T_2 (t_{32} = 2.64, unpaired t-test). **(g)** Bar graph representing the change in object interaction from T_1 to T_2 (U = 122.00, Mann-Whitney test). **(h)** Schematic of the social memory test protocol in the three-chamber apparatus. **(i)** Bar graph representing the normalized social memory at T_2 (t_{32} = 0.84, unpaired t-test). **(j)** Bar graph representing the change in novel mouse interaction from T_1 to T_2 (U = 133.00, Mann-Whitney test). **(k)** Bar graph representing the change in familiar mouse interaction from T_1 to T_2 (U = 132.00, Mann-Whitney test). **(l)** Bar graph representing the sucrose preference ratio at 1% sucrose concentration (t_{21} = 6.83, unpaired t-test). **(m)** Bar graphs representing water and sucrose consumption at 1% sucrose (water: t_{21} = 5.26; sucrose: t_{21} = -1.38, unpaired t-tests). **(n)** Bar graph representing the sucrose preference ratio at 8% sucrose concentration (U = 60.00, Mann-Whitney test). **(o)** Bar graphs representing water and sucrose consumption at 8% sucrose (water: U = 63.00, Mann-Whitney test; sucrose: t_{21} = 0.09, unpaired t-test). Error bars show SEM. The numbers indicate the mice.

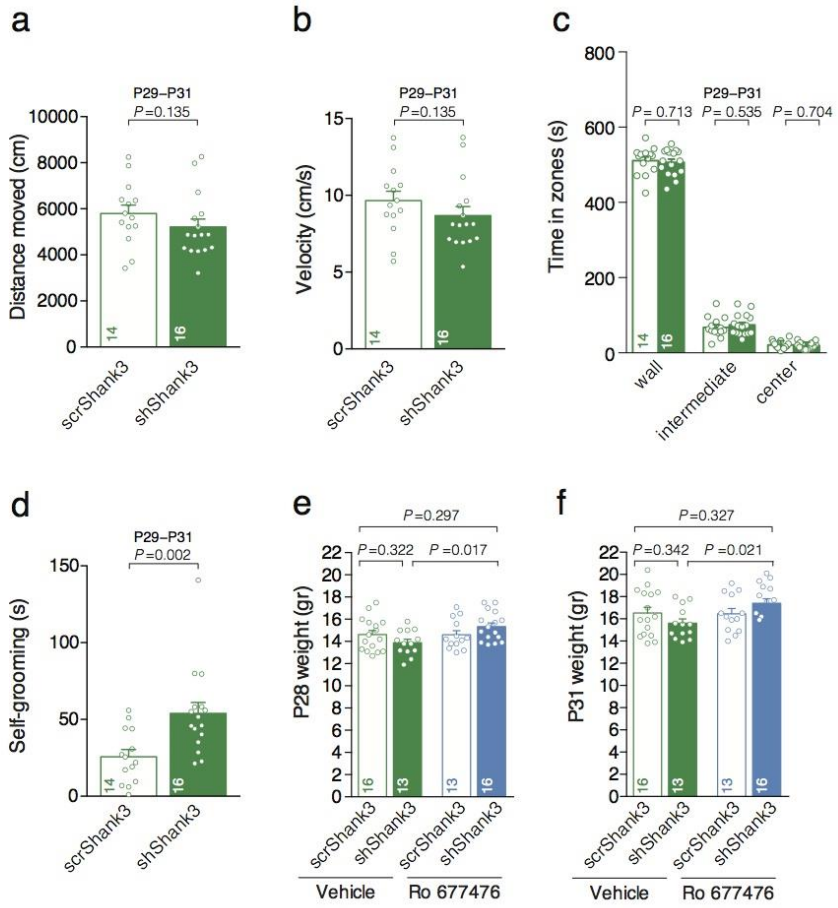

Supplementary Figure 7

Further behavioral characterization of AAV-Shank3 infection in the VTA

(a) Bar graph of the distance moved during the open field test, which was performed with a separate cohort of scrShank3 and shShank3 mice (not treated with Vehicle or PAM i.p.) (U = 76.00, Mann-Whitney test). **(b)** Bar graph of the velocity during the open field test (U = 76.00, Mann-Whitney test). **(c)** Bar graphs representing the time in the virtual zones of the open field (wall: t_{28} = 0.37; intermediate: t_{28} = -0.63; center: t_{28} = 0.38; unpaired t-test) **(d)** Bar graph of self-grooming scored manually during the open field test (U = 38.50, Mann-Whitney test). **(e)** Bar graph with the weight of the animals at P28 (two-way ANOVA; Virus × drug interaction: $F_{1,54}$ = 4.27, p = 0.044; main effect virus: $F_{1,54}$ < 0.001, p = 0.995 ; main effect drug: $F_{1,54}$ = 4.05, p = 0.049; followed by Tukey HSD post-hoc test). **(f)** Bar graph representing the weight of the animals at P31 (two-way ANOVA; Virus × drug interaction: $F_{1,54}$ = 4.20, p = 0.045; main effect virus: $F_{1,54}$ < 0.001, p = 0.971 ; main effect drug: $F_{1,54}$ = 3.65, p = 0.061; followed by Tukey HSD post-hoc test). Error bars show SEM.

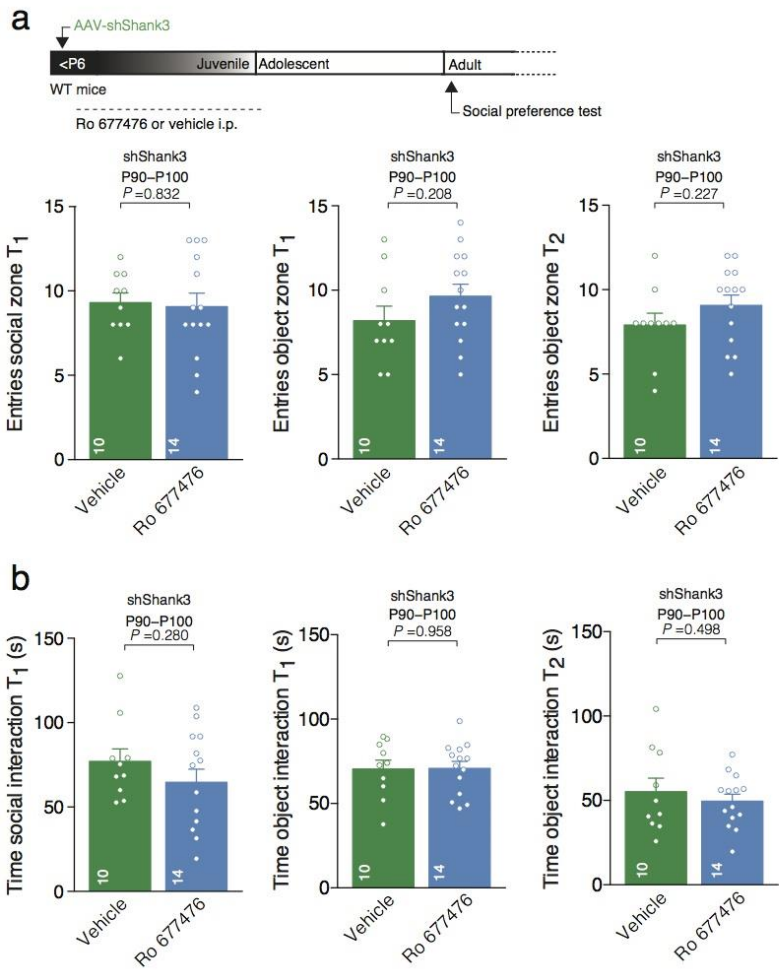

Supplementary Figure 8

Further behavioral characterization of AAV-Shank3 infection in the VTA during adulthood

(a) Left: Entries in the virtual zone around the social enclosure in T_1 in adult shShank3 animals treated with Vehicle or Ro 677476 (t_{22} = 0.21, unpaired t-test). Middle: Bar graph representing the entries around the object enclosure during T_1 (t_{22} = -1.30, unpaired t-test) Right**:** Bar graph representing the entries around the object enclosure in T_2 (t_{22} = -1.24, unpaired t-test). **(b)** Left: Bar graph representing the time in social interaction in T_1 in adult animals treated with Vehicle or Ro 677476 (t_{22} = 1.11, unpaired t-test). Middle: Time in object interaction in T_1 (t_{22} = -0.05, unpaired t-test). Right: Time in object interaction in T_2 (t_{22} = 0.69, unpaired t-test). Error bars show SEM. The numbers indicate the mice.

nature neuroscience

Corresponding Author: Camilla Bellone

Manuscript Number: NN-A53462

Manuscript Type: Article

Main Figures: 8

Supplementary Figures: 8

Supplementary Tables: 0

Supplementary Videos: 0

Reporting Checklist for Nature Neuroscience

This checklist is used to ensure good reporting standards and to improve the reproducibility of published results. For more information, please read Reporting Life Sciences Research.

Please note that in the event of publication, it is mandatory that authors include all relevant methodological and statistical information in the manuscript.

Statistics reporting, by figure

- Please specify the following information for each panel reporting quantitative data, and where each item is reported (section, e.g. Results, & paragraph number).
- Each figure legend should ideally contain an exact sample size (n) for each experimental group/condition, where n is an exact number and not a range, a clear definition of how n is defined (for example x cells from x slices from x animals from x litters, collected over x days), a description of the statistical test used, the results of the tests, any descriptive statistics and clearly defined error bars if applicable.
- For any experiments using custom statistics, please indicate the test used and stats obtained for each experiment.
- Each figure legend should include a statement of how many times the experiment shown was replicated in the lab; the details of sample collection should be sufficiently clear so that the replicability of the experiment is obvious to the reader.
- For experiments reported in the text but not in the figures, please use the paragraph number instead of the figure number.

Note: Mean and standard deviation are not appropriate on small samples, and plotting independent data points is usually more informative. When technical replicates are reported, error and significance measures reflect the experimental variability and not the variability of the biological process; it is misleading not to state this clearly.

		TEST USED		n			DESCRIPTIVE STATS (AVERAGE, VARIANCE)		P VALUE		DEGREES OF FREEDOM & F/t/z/R/ETC VALUE	
	FIGURE NUMBER	WHICH TEST?	SECTION & PARAGRAPH #	EXACT VALUE	DEFINED?	SECTION & PARAGRAPH #	REPORTED?	SECTION & PARAGRAPH #	EXACT VALUE	SECTION & PARAGRAPH #	VALUE	SECTION & PARAGRAPH #
example	1a	one-way ANOVA	Fig. legend	9, 9, 10, 15	mice from at least 3 litters/group	Methods para 8	error bars are mean +/- SEM	Fig. legend	p = 0.044	Fig. legend	F(3, 36) = 2.97	Fig. legend
example	results, para 6	unpaired t-test	Results para 6	15	slices from 10 mice	Results para 6	error bars are mean +/- SEM	Results para 6	p = 0.0006	Results para 6	t(28) = 2.808	Results para 6
+ -	1c	Mann-Whitney test	Fig. 1 Legend	6,7	VTA samples from 6 scrShank3 and 7 shShank3 mice	Fig. 1c Graph	errors bars are mean +/- SEM and scatter plot	Fig. 1c Graph	p = 0.008	Fig. 1c graph	U = 3	Fig. 1 Legend

Nature Neuroscience: doi:10.1038/nn.4319

		TEST USED		n			DESCRIPTIVE STATS (AVERAGE, VARIANCE)		P VALUE		DEGREES OF FREEDOM & F/t/z/R/ETC VALUE	
	FIGURE NUMBER	WHICH TEST?	SECTION & PARAGRAPH #	EXACT VALUE	DEFINED?	SECTION & PARAGRAPH #	REPORTED?	SECTION & PARAGRAPH #	EXACT VALUE	SECTION & PARAGRAPH #	VALUE	SECTION & PARAGRAPH #
+ -	Fig. 1c	Mann-Whitney test	Fig. 1 Legend	4,5	SN samples from 4 scrShank3 and 5 shShank3 mice	Fig. 1c Graph	errors bars are mean +/- SEM and scatter plot	Fig. 1c Graph	p > 0.999	Fig. 1c graph	U = 10	Fig. 1 Legend
+ -	Fig. 2a	Kruskal-Wallis	Fig.2 Legend	9, 10, 4	9 Uninfected cells from 7 mice, 10 shShank3 infected cells from 9 mice, 4 scrShank3 cells from 3 mice	Fig. 2a Graph	errors bars are mean +/- SEM and scatter plot	Fig. 2a Graph	p = 0.005	Fig. 2a Legend	K (2) = 10.47	Fig. 1 Legend
+ -	Fig. 2a	Dunn's test	Fig. 2 Legend	9, 10	9 Uninfected cells from 7 mice, 10 shShank3 infected cells from 9 mice	Fig. 2a Graph	errors bars are mean +/- SEM and scatter plot	Fig. 2a Graph	p = 0.013	Fig. 2a Graph		
+ -	Fig. 2a	Dunn's test	Fig. 2 Legend	10, 4	10 shShank3 infected cells from 9 mice, 4 scrShank3 cells from 3 mice	Fig. 2a Graph	errors bars are mean +/- SEM and scatter plot	Fig. 2a Graph	p = 0.043	Fig. 2a Graph		
+ -	Fig. 2b	unpaired t-test	Fig. 2 Legend	9,11	9 Uninfected cells from 6 mice, 11 shShank3 cells from 6 mice	Fig. 2b Graph	errors bars are mean +/- SEM and scatter plot	Fig. 2b Graph	p = 0.960	Fig. 2a Graph	t (18) = 0.05	Fig. 2 Legend
+ -	Fig. 2c	One-Way ANOVA	Fig. 2 Legend	12,12,6	12 Uninfected from 8 mice, 12 shShank3 from 10 mice, 6 scrShank3 from 3 mice	Fig.2c Graph	errors bars are mean +/- SEM and scatter plot	Fig. 2c Graph	p < 0.001	Fig. 2c Legend	F (2, 27) = 11.66	Fig. 2 Legend
+ -	Fig. 2c	Tukey HSD	Fig. 2 Legend	12, 12	12 Uninfected from 8 mice, 12 shShank3 from 10 mice	Fig. 2c Graph	errors bars are mean +/- SEM and scatter plot	Fig. 2c Graph	p < 0.001	Fig. 2c Graph		
+ -	Fig. 2c	Tukey HSD	Fig. 2 Legend	12, 6	12 shShank3 from 10 mice, 6 scrShank3 from 3 mice	Fig. 2c Graph	errors bars are mean +/- SEM and scatter plot	Fig. 2c Graph	p = 0.003	Fig. 2c Graph		
+ -	Fig. 2e	unpaired t-test	Fig. 2 legend	6, 6	6 Uninfected from 4 mice, 4 shShank3 from 4 mice	Fig. 2e Graph	errors bars are mean +/- SEM and scatter plot	Fig. 2e Graph	p = 0.837	Fig. 2e Graph	t (10) = -0.21	Fig. 2 Legend
+ -	Fig. 2f	unpaired t-test	Fig. 2 legend	14, 16	14 Uninfected from 10 mice, 16 shShank3 from 8 mice	Fig. 2f Graph	errors bars are mean +/- SEM and scatter plot	Fig. 2e Graph	p = 0.872	Fig. 2f Graph	t (28) = -0.16	Fig. 2 Legend
+ -	Fig. 2g	Mann-Whitney test	Fig. 2 Legend	9, 6	9 Uninfected cells from 6 mice, 6 shShank3 from 5 mice	Fig. 2g Graph	errors bars are mean +/- SEM and scatter plot	Fig. 2g Graph	p = 0.316	Fig. 2g Graph	U = 18.50	Fig. 2 Legend
+ -	Fig. 2h	unpaired t-test	Fig. 2 Legend	7, 7	7 Uninfected from 6 mice, 7 shShank3 from 5 mice	Fig.2h Graph	errors bars are mean +/- SEM and scatter plot	Fig. 2h Graph	p = 0.712	Fig. 2h Graph	t (12) = 0.38	Fig. 2 Legend
+ -	Fig. 3a	unpaired t-test	Fig. 3 Legend	9, 7	9 Uninfected from 8 mice, 7 shShank3 from 6 mice	Fig. 3a Graph	errors bars are mean +/- SEM and scatter plot	Fig. 3a Graph	p = 0.008	Fig. 3a Graph	t (14) = -3.11	Fig. 3 Legend
+ -	Fig. 3b	unpaired t-test	Fig. 3 Legend	12, 15	12 Uninfected cells from 6 mice, 15 shShank3 from 4 mice	Fig. 3b Graph	errors bars are mean +/- SEM and scatter plot	Fig. 3b Graph	p = 0.455	Fig. 3b Graph	t (25) = -0.76	Fig. 3 Legend

Nature Neuroscience: doi:10.1038/nn.4319

+ -	Fig. 3c	unpaired t-test	Fig. 3 Legend	7, 5	7 Uninfected cells from 5 mice, 5 shShank3 from 3 mice	Fig. 3c Graph	errors bars are mean +/- SEM and scatter plot	Fig. 3c Graph	p = 0.993	Fig. 3c Graph	t (10) = 0.01	Fig. 3 Legend
+ -	Fig. 4b	paired t-test	Fig. 4 Legend	6	6 shShank3 from 5 mice	Fig. 4b Graph	errors bars are mean +/- SEM and scatter plot	Fig. 4b Graph	p = 0.016	Fig. 4b Graph	t (5) = 3.60	Fig. 4 Legend
+ -	Fig. 4b	paired t-test	Fig. 4 Legend	5	5 Uninfected cells from 3 mice	Fig. 4b Graph	errors bars are mean +/- SEM and scatter plot	Fig. 4b Graph	p = 0.230	Fig. 4b Graph	t (4) = 1.42	Fig. 4 Legend
+ -	Fig. 4c	Two-Way ANOVA	Fig. 4 Legend	5, 8, 5,8	5 scrShank3 vehicle from 4 mice, 8 shShank3 vehicle cells from 3 mice, 5 scrShank3 Ro from 5 mice, 8 shShank3 Ro from 5 mice	Fig. 4c Graph	errors bars are mean +/- SEM and scatter plot	Fig. 4c Graph	virus x drug interaction p =0.019 virus main effect p < 0.001 drug main effect p = 0.015	Fig. 4c Legend	virus x drug interaction F (1,22) =6.41 virus main effect F (1,22) = 20.54 drug main effect F (1,22) = 7.02	Fig. 4 Legend
+ -	Fig. 4 c	Tukey HSD	Fig. 4 Legend	5,8	5 scrShank3 vehicle from 4 mice, 8 shShank3 vehicle cells from 3 mice	Fig. 4c Graph	errors bars are mean +/- SEM and scatter plot	Fig. 4c Graph	p < 0.001	Fig. 4c Graph		
+ -	Fig. 4 c	Tukey HSD	Fig. 4 Legend	8,8	8 shShank3 vehicle cells from 3 mice, 8 shShank3 Ro from 5 mice	Fig. 4c Graph	errors bars are mean +/- SEM and scatter plot	Fig. 4c Graph	p = 0.002	Fig. 4c Graph		
+ -	Fig 4c	Tukey HSD	Fig. 4 Legend	5, 8	5 scrShank3 vehicle from 4 mice, 8 shShank3 Ro from 5 mice	Fig. 4c Graph	errors bars are mean +/- SEM and scatter plot	Fig. 4c Graph	p = 0.554	Fig. 4c Graph		
+ -	Fig. 4d	Two-Way ANOVA	Fig. 4 Legend	9,9,6,10	9 scrShank3 vehicle cells from 5 mice, 9 shShank3 vehicle cells from 3 mice, 6 scrShank3 Ro cells from 4 mice, 10 shShank3 Ro cells from 7 mice	Fig. 4d Graph	errors bars are mean +/- SEM and scatter plot	Fig. 4d Graph	virus x drug interaction p =0.040 virus main effect p = 0.001 drug main effect p = 0.029	Fig. 4d Legend	virus x drug interaction F (1,30) =4.62 virus main effect F (1,30) = 14.93 drug main effect F (1,30) = 5.26	Fig. 4d Legend
+ -	Fig. 4d	Tukey HSD	Fig. 4 Legend	9,9	9 scrShank3 vehicle cells from 5 mice, 9 shShank3 vehicle cells from 3 mice	Fig. 4d Graph	errors bars are mean +/- SEM and scatter plot	Fig. 4d Graph	p = 0.001	Fig. 4d Graph		
+ -	Fig. 4d	Tukey HSD	Fig. 4 Legend	9, 10	9 shShank3 vehicle cells from 3 mice, 10 shShank3 Ro cells from 7 mice	Fig. 4d Graph	errors bars are mean +/- SEM and scatter plot	Fig. 4d Graph	p = 0.010	Fig. 4d Graph		
+ -	Fig. 4d	Tukey HSD	Fig. 4 Legend	9, 10	9 scrShank3 vehicle cells from 5 mice, 10 shShank3 Ro cells from 7 mice	Fig. 4d Graph	errors bars are mean +/- SEM and scatter plot	Fig. 4d Graph	p = 0.635	Fig. 4 Graph		
+ -	Fig. 5d	Kruskal-Wallis Test	Fig. 5 Legend , left	15, 15, 24, 21	15 scrShank3 vehicle cells from 4 mice, 15 shShank3 vehicle cells from 9 mice, 24 scrShank3 Ro cells from 6 mice, 21 shShank3 Ro cells from 4 mice	Fig. 5d Graph	errors bars are mean +/- SEM and scatter plot	Fig. 5d Graph	p = 0.003	Fig.5 Legend	K (3) = 14.09	Fig. 5d Legend

Nature Neuroscience: doi:10.1038/nn.4319

+ -	Fig. 5d	Dunn's test	Fig. 5 Legend	15,15	15 scrShank3 vehicle cells from 4 mice, 15 shShank3 vehicle cells from 9 mice	Fig. 5d, Graph	errors bars are mean +/- SEM and scatter plot	Fig. 5d Graph	p = 0.035	Fig. 5d Graph		
+ -	Fig. 5d	Dunn's test	Fig.5 Legend	24,21	24 scrShank3 Ro cells from 6 mice, 21 shShank3 Ro cells from 4 mice	Fig. 5d, Graph	errors bars are mean +/- SEM and scatter plot	Fig. 5c Graph	p = 0.208	Fig. 5d Graph		
+ -	Fig. 5d	Kruskal-Wallis test	Fig. 5d, right, Legend	15, 15, 24, 21	15 scrShank3 vehicle cells from 4 mice, 15 shShank3 vehicle cells from 9 mice, 24 scrShank3 Ro cells from 6 mice, 21 shShank3 Ro cells from 4 mice	Fig. 5d Graph	errors bars are mean +/- SEM and scatter plot	Fig. 5d Graph	p = 0.002	Fig. 5d Legend	K (3) = 14.62	Fig. 5d Legend
+ -	Fig. 5d	Dunn's test	Fig. 5d, Legend	15, 15	15 scrShank3 vehicle cells from 4 mice, 15 shShank3 vehicle cells from 9 mice	Fig. 5d Graph	errors bars are mean +/- SEM and scatter plot	Fig. 5d Graph	p = 0.035	Fig.5d Graph		
+ -	Fig. 5d	Dunn's test	Fig. 5d Legend	24, 21	24 scrShank3 Ro cells from 6 mice, 21 shShank3 Ro cells from 4 mice	Fig. 5d Graph	errors bars are mean +/- SEM and scatter plot	Fig. 5d Graph	p = 0.251	Fig. 5d Graph		
+ -	Fig. 5c	Kruskal-Wallis test	Fig. 5c Legend	15, 15, 24, 21	15 scrShank3 vehicle cells from 4 mice, 15 shShank3 vehicle cells from 9 mice, 24 scrShank3 Ro cells from 6 mice, 21 shShank3 Ro cells from 4 mice	Fig. 5c Graph	errors bars are mean +/- SEM and scatter plot	Fig. 5c Graph	p = 0.013	Fig. 5c Legend	K (3) = 10.85	Fig. 5c Legend
+ -	Fig. 5c	Dunn's test	Fig. 5c Legend	15,15	15 scrShank3 vehicle cells from 4 mice, 15 shShank3 vehicle cells from 9 mice	Fig. 5c Graph	errors bars are mean +/- SEM and scatter plot	Fig. 5c Graph	p = 0.151	Fig. 5c Graph		
+ -	Fig. 5c	Dunn's test	Fig. 5c Legend	24, 21	24 scrShank3 Ro cells from 6 mice, 21 shShank3 Ro cells from 4 mice	Fig. 5c Graph	errors bars are mean +/- SEM and scatter plot	Fig. 5c Graph	p = 0.908	Fig. 5c Graph		
+ -	Fig. 5f	Mann-Whitney test	Fig. 5f Legend	34, 35	34 scrShank3 vehicle cells from 8 mice, 35 shShank3 vehicle cells from 7 mice	Fig. 5f Graph	errors bars are mean +/- SEM and scatter plot	Fig. 5f Graph	p = 0.043	Fig. 5f Graph	U = 425.5	Fig. 5f Legend
+ -	Fig. 6 c	RM Two-Way ANOVA	Fig. 6c Legend	16, 13, 13, 16	16 scrShank3 vehicle mice, 13 shShank3 vehicle mice, 13 scrShank3 Ro mice, 16 shShank3 Ro mice	Fig. 6c Graph	errors bars are mean +/- SEM and scatter plot	Fig. 6c Graph	time x virus x drug interaction p =0.039 virus main effect p = 0.030	Fig. 6c Legend	time x virus x drug interaction F(1,54) = 4.48 virus main effect F (1,54) = 4.99	Fig. 6c Legend
+ -	Fig. 6c	RM ANOVA within subjects	Fig. 6c Legend	16	16 scrShank3 vehicle mice	Fig. 6c Graph	errors bars are mean +/- SEM and scatter plot	Fig. 6c Graph	time main effect p = 0.261	Fig. 6c Graph	F (1,15) = 1.36	Fig. 6c Legend
+ -	Fig. 6c	RM ANOVA within subjects	Fig. 6c Legend	13	13 shShank3 vehicle mice	Fig. 6c Graph	errors bars are mean +/- SEM and scatter plot	Fig. 6c Graph	time main effect p = 0.016	Fig. 6c Graph	F (1,12) = 7.87	Fig. 6c Legend
+ -	Fig. 6c	RM ANOVA within subjects	Fig. 6c Legend	13	13 scrShank3 Ro mice	Fig. 6c Graph	errors bars are mean +/- SEM and scatter plot	Fig. 6c Graph	time main effect p = 0.623	Fig. 6c Graph	F (1,12) = 0.26	Fig. 6c Legend

Nature Neuroscience: doi:10.1038/nn.4319

+ -	Fig. 6c	RM ANOVA within subjects	Fig. 6c Legend	16	16 shShank3 Ro mice	Fig. 6c Graph	errors bars are mean +/- SEM and scatter plot	Fig. 6c Graph	time main effect p = 0.877	Fig. 6c Graph	F (1,15) = 0.03	Fig. 6c Legend
+ -	Fig. 6f	Two-Way ANOVA	Fig. 6f Legend	16, 13, 13, 16	16 scrShank3 vehicle mice, 13 shShank3 vehicle mice, 13 scrShank3 Ro mice, 16 shShank3 Ro mice	Fig. 6f Graph	errors bars are mean +/- SEM and scatter plot	Fig. 6f Graph	virus x drug interaction p = 0.012 virus main effect p = 0.442 drug main effect p = 0.182	Fig. 6f Legend	virus x drug interaction F(1,54) = 6.76 virus main effect F(1,54) = 0.60 drug main effect F (1,54) = 1.83	Fig. 6f Legend
+ -	Fig. 6f	Tukey HSD	Fig. 6f Legend	16, 13	16 scrShank3 vehicle mice, 13 shShank3 vehicle mice	Fig. 6f Graph	errors bars are mean +/- SEM and scatter plot	Fig. 6f Graph	p = 0.070	Fig. 6f Graph		
+ -	Fig. 6f	Tukey HSD	Fig. 6f Legend	13, 16	13 shShank3 vehicle mice, 16 shShank3 Ro mice	Fig. 6f Graph	errors bars are mean +/- SEM and scatter plot	Fig. 6f Graph	p = 0.029	Fig 6f Graph		
+ -	Fig. 6f	Tukey HSD	Fig. 6f Legend	16, 16	16 scrShank3 vehicle mice, 16 shShank3 Ro mice	Fig. 6f Graph	errors bars are mean +/- SEM and scatter plot	Fig. 6f Graph	p = 0.912	Fig 6f Graph		
+ -	Fig. 6e	Two-Way ANOVA	Fig. 6e Legend	16, 13, 13, 16	16 scrShank3 vehicle mice, 13 shShank3 vehicle mice, 13 scrShank3 Ro mice, 16 shShank3 Ro mice	Fig. 6e Graph	errors bars are mean +/- SEM and scatter plot	Fig. 6e Graph	virus x drug interaction p = 0.305 virus main effect p = 0.055 drug main effect p = 0.606	Fig. 6e Legend	virus x drug interaction F(1,54) = 1.07 virus main effect F(1,54) = 3.84 drug main effect F (1,54) = 0.27	Fig. 6e Legend
+ -	Fig. 6e	Tukey HSD	Fig. 6e Legend	16, 13	16 scrShank3 vehicle mice, 13 shShank3 vehicle mice	Fig. 6e Graph	errors bars are mean +/- SEM and scatter plot	Fig. 6e Graph	p = 0.040	Fig. 6e Graph		
+ -	Fig. 6e	Tukey HSD	Fig. 6e Legend	13, 16	13 shShank3 vehicle mice, 16 shShank3 Ro mice	Fig. 6e Graph	errors bars are mean +/- SEM and scatter plot	Fig. 6e Graph	p = 0.397	Fig. 6e Graph		
+ -	Fig. 6e	Tukey HSD	Fig. 6e Legend	16, 16	16 scrShank3 vehicle mice, 16 shShank3 Ro mice	Fig. 6e Graph	errors bars are mean +/- SEM and scatter plot	Fig. 6e Graph	p = 0.411	Fig. 6e Graph		
+ -	Fig. 6d	Two-Way ANOVA	Fig. 6d Legend	16, 13, 13, 16	16 scrShank3 vehicle mice, 13 shShank3 vehicle mice, 13 scrShank3 Ro mice, 16 shShank3 Ro mice	Fig. 6d Graph	errors bars are mean +/- SEM and scatter plot	Fig. 6d Graph	virus x drug interaction p = 0.018 virus main effect p = 0.194 drug main effect p = 0.875	Fig. 6d Legend	virus x drug interaction F(1,54) = 5.98 virus main effect F(1,54) = 1.73 drug main effect F (1,54) = 0.03	Fig. 6d Legend
+ -	Fig. 6d	Tukey HSD	Fig. 6d Legend	16, 13	16 scrShank3 vehicle mice, 13 shShank3 vehicle mice	Fig. 6d Graph	errors bars are mean +/- SEM and scatter plot	Fig. 6d Graph	p = 0.028	Fig. 6d Graph		
+ -	Fig. 6d	Tukey HSD	Fig. 6d Legend	13, 16	13 shShank3 vehicle mice, 16 shShank3 Ro mice	Fig. 6d Graph	errors bars are mean +/- SEM and scatter plot	Fig. 6d Graph	p = 0.166	Fig. 6d Graph		
+ -	Fig. 6d	Tukey HSD	Fig. 6d Legend	16, 16	16 scrShank3 vehicle mice, 16 shShank3 Ro mice	Fig. 6d Graph	errors bars are mean +/- SEM and scatter plot	Fig. 6d Graph	p = 0.664	Fig. 6d Graph		

Nature Neuroscience: doi:10.1038/nn.4319

+ -	Fig. 7b	unpaired t-test	Fig. 7b Legend	8, 10	8 shShank3 vehicle cells from 4 mice, 10 shShank3 Ro cells from 5 mice	Fig. 7b Graph	errors bars are mean +/- SEM and scatter plot	Fig. 7b Graph	p = 0.049	Fig. 7b Graph	t (8.33) = 2.30	Fig. 7b Legend
+ -	Fig. 7c	RM ANOVA	Fig. 7c Legend	10, 14	10 shShank3 vehicle mice, 14 shShank3 Ro mice	Fig. 7c Graph	errors bars are mean +/- SEM and scatter plot	Fig. 7c Graph	time x group interaction p = 0.028 group main effect p = 0.644	Fig. 7c Graph	time x group interaction F (1,22) = 5.56 group main effect F(1,22) = 0.22	Fig. 7c Legend
+ -	Fig. 7c	RM ANOVA within subjects	Fig.7c	10	10 shShank3 vehicle mice	Fig. 7c Graph	errors bars are mean +/- SEM and scatter plot	Fig. 7c Graph	time main effect p = 0.017	Fig. 7c Graph	time main effect F(1,9) = 8.58	Fig. 7c Legend
+ -	Fig. 7c	RM ANOVA within subjects	Fig.7c	14	14 shShank3 Ro mice	Fig. 7c Graph	errors bars are mean +/- SEM and scatter plot	Fig. 7c Graph	time main effect p = 0.634	Fig. 7c Graph	time main effect F(1,13) = 0.24	Fig. 7c Legend
+ -	Fig. 7d	unpaired t-test	Fig.7d	10, 14	10 shShank3 vehicle mice, 14 shShank3 Ro mice	Fig. 7d Graph	errors bars are mean +/- SEM and scatter plot	Fig. 7d Graph	p = 0.009	Fig. 7d Graph	t (22) = -2.88	Fig. 7d Graph
+ -	Fig. 7d	Mann-Whitney test	Fig.7d Legend	10, 14	10 shShank3 vehicle mice, 14 shShank3 Ro mice	Fig. 7d Graph	errors bars are mean +/- SEM and scatter plot	Fig. 7d Graph	p = 0.069	Fig. 7d Graph	U = 39	Fig. 7d Graph
+ -	Fig. 7d	unpaired t-test	Fig.7d Legend	10, 14	10 shShank3 vehicle mice, 14 shShank3 Ro mice	Fig. 7d Graph	errors bars are mean +/- SEM and scatter plot	Fig. 7d Graph	p = 0.023	Fig. 7d Graph	t (22) = -2.44	Fig. 7d Graph
+ -	Fig. 8f	RM Two-Way ANOVA	Fig. 8f Legend	10, 11, 8, 6	10 scrShank3 off mice, 11 shShank3 off mice, 8 scrShank3 on mice, 6 shShank3 on mice	Fig. 8f Graph	errors bars are mean +/- SEM and scatter plot	Fig. 8f Graph	time x drug x virus interaction p = 0.300 light x virus interaction p = 0.025 virus main effect p = 0.141 light main effect p = 0.001	Fig. 8f Legend	time x drug x virus interaction F (1,31) = 1.11 light x virus interaction F (1,31) = 5.52 virus main effect F (1,31) = 2.28 light main effect F (1,31) = 14.17	Fig. 8f Legend
+ -	Fig. 8f	RM ANOVA within subjects	Fig. 8f	10	10 scrShank3 off	Fig. 8f Graph	errors bars are mean +/- SEM and scatter plot	Fig. 8f Graph	time main effect p = 0.640	Fig. 8f Graph	time main effect F(1,9) = 0.23	Fig. 8f Legend
+ -	Fig. 8f	RM ANOVA within subjects	Fig. 8f	11	11 shShank3 off	Fig. 8f Graph	errors bars are mean +/- SEM and scatter plot	Fig. 8f Graph	time main effect p = 0.006	Fig. 8f Graph	time main effect F(1,10) = 11.77	Fig. 8f Legend
+ -	Fig. 8f	RM ANOVA within subjects	Fig. 8f	8	8 scrShank3 on	Fig. 8f Graph	errors bars are mean +/- SEM and scatter plot	Fig. 8f Graph	time main effect p < 0.001	Fig. 8f Graph	time main effect F(1,7) = 55.14	Fig. 8f Legend
+ -	Fig. 8f	RM ANOVA within subjects	Fig. 8f	6	6 shShank3 on mice	Fig. 8f Graph	errors bars are mean +/- SEM and scatter plot	Fig. 8f Graph	time main effect p = 0.030	Fig. 8f Graph	time main effect F(1,5) = 9.03	Fig. 8f Legend
+ -	Fig. 8g	Two-Way ANOVA	Fig. 8g Legend	10, 11, 8, 6	10 scrShank3 off mice, 11 shShank3 off mice, 8 scrShank3 on mice, 6 shShank3 on mice	Fig. 8g Graph	errors bars are mean +/- SEM and scatter plot	Fig. 8g Graph	virus x light interaction p = 0.267 virus main effect p = 0.038 light main effect p < 0.001	Fig. 8g Legend	virus x light interaction F(1,31) = 1.28 virus main effect F(1,31) = 4.70 light main effect F(1,31) = 16.93	Fig. 8g Legend
+ -	Fig. 8g	Dunnett test	Fig. 8g Legend	10,11	10 scrShank3 off mice, 11 shShank3 off mice	Fig. 8g Graph	errors bars are mean +/- SEM and scatter plot	Fig. 8g Graph	p = 0.047	Fig. 8g Graph		

Nature Neuroscience: doi:10.1038/nn.4319

+ -	Fig. 8g	Dunnett test	Fig. 8g Legend	10, 6	10 scrShank3 off mice, 6 shShank3 on mice	Fig. 8g Graph	errors bars are mean +/- SEM and scatter plot	Fig. 8g Graph	p = 0.405	Fig. 8g Graph		
+ -	Fig.4 c	Tukey HSD	Fig. 4c Legend	5, 5	5 scrShank3 vehicle from 4 mice, 5 scrShank3 Ro from 5 mice	Fig. 4c Graph	errors bars are mean +/- SEM and scatter plot	Fig. 4c Graph	p > 0.999	Fig. 4c Graph		
+ -	Fig. 4c	Tukey HSD	Fig. 4d Legend	9,6	9 scrShank3 Vehicle from 5 mice, 6 scrShank3 Ro from 4 mice	Fig. 4d	errors bars are mean +/- SEM and scatter plot	Fig. 4d Graph	p > 0.999	Fig. 4d Graph		
+ -	Fig. S1c	Mann-Whitney	Fig. S1c Legend	5,5	5 infected side from 5 shShank3 mice, 5 uninfected side from 5 shShank3 mice	Fig. S1c Graph	errors bars are mean +/- SEM and scatter plot	Fig. S1c Graph	p = 0.667	Fig. S1c Graph	U = 10.00	Fig. S1c Legend
+ -	Fig. S2a, left	Mann-Whitney	Fig. S2a, Legend	14, 12	14 putative DA from 9 mice, 12 putative GABA from 11 mice	Fig. S2a, Graph	errors bars are mean +/- SEM and scatter plot	Fig. S2a, Graph	p < 0.001	Fig. S2a, Graph	U < 0.001	Fig. S2, Legend
+ -	Fig. S2a, right	Mann-Whitney	Fig. S2a, Legend	14, 12	14 putative DA from 9 mice, 12 putative GABA from 11 mice	Fig. S2a, Graph	errors bars are mean +/- SEM and scatter plot	Fig. S2a, Graph	p < 0.001	Fig. S2a, Graph	U = 13.00	Fig. S2, Legend
+ -	Fig. S2b, left	Mann-Whitney	Fig. S2b, Legend	14, 11	14 putative DA from 11 mice, 11 putative GABA from 8 mice	Fig. S2b Graph	errors bars are mean +/- SEM and scatter plot	Fig. S2b Graph	p < 0.001	Fig. S2b Graph	U < 0.001	Fig. S2b Legend
+ -	Fig. S2b, right	Mann-Whitney	Fig. S2b, Legend	14, 11	14 putative DA from 11 mice, 11 putative GABA from 8 mice	Fig. S2b Graph	errors bars are mean +/- SEM and scatter plot	Fig. S2b Graph	p < 0.001	Fig. S2b Graph	U = 10.00	Fig. S2b Legend
+ -	Fig. S3b	unpaired t-test	Fig. S3b, Legend	10, 10	10 shShank3 cells from 5 vehicle treated mice, 10 shShank3 cells from 4 Ro treated mice	Fig. S3b Graph	errors bars are mean +/- SEM and scatter plot	Fig. S3b Graph	p = 0.903	Fig. S3b Graph	t (18) = 0.123	Fig. S3b, Legend
+ -	Fig. S4b	Mann-Whitney test	Fig. S4b Legend	4, 4	4 scrShank3 vehicle mice, 4 shShank3 vehicle mice	Fig. S4b Graph	errors bars are mean +/- SEM and scatter plot	Fig. S4b Graph	p = 0.882	Fig. S4b Graph	U = 8.00	Fig. S4b Legend
+ -	Fig. S5a	Two-Way ANOVA	Fig. S5a Legend	16, 13, 13, 16	16 scrShank3 vehicle mice, 13 shShank3 vehicle mice, 13 scrShank3 Ro mice, 16 shShank3 Ro mice	Fig. S5a Graph	errors bars are mean +/- SEM and scatter plot	Fig. S5a Graph	virus x drug interaction p = 0.428 virus main effect p = 0.909 drug main effect p = 0.312	exact values not reported since significance not reached	virus x drug interaction F(1,54)=0.64 virus main effect F(1,54)=0.02 drug main effect F(1,54)=1.04	exact values not reported
+ -	Fig. S5b	Two-Way ANOVA	Fig. S5b Legend	16, 13, 13, 16	16 scrShank3 vehicle mice, 13 shShank3 vehicle mice, 13 scrShank3 Ro mice, 16 shShank3 Ro mice	Fig. S5b Graph	errors bars are mean +/- SEM and scatter plot	Fig. S5b Graph	virus x drug interaction p = 0.030 virus main effect p = 0.655 drug main effect p = 0.763	Fig. S5b Legend	virus x drug interaction F(1,54)= 4.96 virus main effect F(1,54)= 0.20 drug main effect F(1,54)=0.09	Fig. S5b Legend
+ -	Fig. S5b	Tukey HSD	Fig. S5b Legend	16, 13	16 scrShank3 vehicle mice, 13 shShank3 Vehicle mice	Fig. S5b Graph	errors bars are mean +/- SEM and scatter plot	Fig. S5b Graph	p = 0.450	Fig. S5b Graph		

Nature Neuroscience: doi:10.1038/nn.4319

+ -	Fig. S5b	Tukey HSD	Fig. S5b Legend	13, 16	13 shShank3 vehicle, 16 shShank3 Ro mice	Fig. S5b Graph	errors bars are mean +/- SEM and scatter plot	Fig. S5b Graph	p = 0.205	Fig. S5b Graph		
+ -	Fig. S5b	Tukey HSD	Fig. S5b Legend	16, 16	16 scrShank3 vehicle mice, 16 shShank3 Ro mice	Fig. S5b Graph	errors bars are mean +/- SEM and scatter plot	Fig. S5b Graph	p = 0.850	Fig. S5b Graph		
+ -	Fig. S5c	Two-Way ANOVA	Fig. S5c Legend	16, 13, 13, 16	16 scrShank3 vehicle mice, 13 shShank3 vehicle mice, 13 scrShank3 Ro mice, 16 shShank3 Ro mice	Fig. S5c Graph	errors bars are mean +/- SEM and scatter plot	Fig. S5c Graph	virus x drug interaction p = 0.192 virus main effect p = 0.020 drug main effect p = 0.931	Fig. S5c Legend	virus x drug interaction F(1,54)= 1.74 virus main effect F(1,54)= 5.76 drug main effect F(1,54)=0.01	Fig. S5c Legend
+ -	Fig. S5c	Tukey HSD	Fig. S5c Legend	16, 13	16 scrShank3 vehicle mice, 13 shShank3 Vehicle mice	Fig. S5c Graph	errors bars are mean +/- SEM and scatter plot	Fig. S5c Graph	p = 0.041	Fig. S5c Graph		
+ -	Fig. S5c	Tukey HSD	Fig. S5c Legend	13, 16	13 shShank3 vehicle, 16 shShank3 Ro mice	Fig. S5c Graph	errors bars are mean +/- SEM and scatter plot	Fig. S5c Graph	p = 0.610	Fig. S5c Graph		
+ -	Fig. S5c	Tukey HSD	Fig. S5c Legend	16, 16	16 scrShank3 vehicle mice, 16 shShank3 Ro mice	Fig. S5c Graph	errors bars are mean +/- SEM and scatter plot	Fig. S5c Graph	p = 0.234	Fig. S5c Graph		
+ -	Fig. S5d	Two-Way ANOVA	Fig. S5d Legend	16, 13, 13, 16	16 scrShank3 vehicle mice, 13 shShank3 vehicle mice, 13 scrShank3 Ro mice, 16 shShank3 Ro mice	Fig. S5d Graph	errors bars are mean +/- SEM and scatter plot	Fig. S5d Graph	virus x drug interaction p = 0.416 virus main effect p = 0.042 drug main effect p = 0.406	Fig. S5d Legend	virus x drug interaction F(1,54)= 0.67 virus main effect F(1,54)= 4.33 drug main effect F(1,54)=0.45	Fig. S5d Legend
+ -	Fig. S5d	Tukey HSD	Fig. S5d Legend	16, 13	16 scrShank3 vehicle mice, 13 shShank3 Vehicle mice	Fig. S5d Graph	errors bars are mean +/- SEM and scatter plot	Fig. S5d Graph	p = 0.114	Fig. S5d Graph		
+ -	Fig. S5d	Tukey HSD	Fig. S5d Legend	13, 16	13 shShank3 vehicle, 16 shShank3 Ro mice	Fig. S5d Graph	errors bars are mean +/- SEM and scatter plot	Fig. S5d Graph	p = 0.994	Fig. S5d Graph		
+ -	Fig. S5d	Tukey HSD	Fig. S5d Legend	16, 16	16 scrShank3 vehicle mice, 16 shShank3 Ro mice	Fig. S5d Graph	errors bars are mean +/- SEM and scatter plot	Fig. S5d Graph	p = 0.113	Fig. S5d Graph		
+ -	Fig. S5e	Two-Way ANOVA	Fig. S5e Legend	16, 13, 13, 16	16 scrShank3 vehicle mice, 13 shShank3 vehicle mice, 13 scrShank3 Ro mice, 16 shShank3 Ro mice	Fig. S5e Graph	errors bars are mean +/- SEM and scatter plot	Fig. S5e Graph	virus x drug interaction p = 0.016 virus main effect p = 0.703 drug main effect p = 0.010	Fig. S5e Legend	virus x drug interaction F(1,54)= 3.68 virus main effect F(1,54)= 0.15 drug main effect F(1,54)=7.15	Fig. S5e Legend
+ -	Fig. S5e	Tukey HSD	Fig. S5e Legend	16, 13	16 scrShank3 vehicle mice, 13 shShank3 Vehicle mice	Fig. S5e Graph	errors bars are mean +/- SEM and scatter plot	Fig. S5e Graph	p = 0.538	Fig. S5e Graph		
+ -	Fig. S5e	Tukey HSD	Fig. S5e Legend	13, 16	13 shShank3 vehicle, 16 shShank3 Ro mice	Fig. S5e Graph	errors bars are mean +/- SEM and scatter plot	Fig. S5e Graph	p = 0.007	Fig. S5e Graph		

Nature Neuroscience: doi:10.1038/nn.4319

+ -	Fig. S5e	Tukey HSD	Fig. S5e Legend	16, 16	16 scrShank3 vehicle mice, 16 shShank3 Ro mice	Fig. S5e Graph	errors bars are mean +/- SEM and scatter plot	Fig. S5e Graph	p = 0.074	Fig. S5e Graph		
+ -	Fig. S5f	Two-Way ANOVA	Fig. S5f Legend	16, 13, 13, 16	16 scrShank3 vehicle mice, 13 shShank3 vehicle mice, 13 scrShank3 Ro mice, 16 shShank3 Ro mice	Fig. S5f Graph	errors bars are mean +/- SEM and scatter plot	Fig. S5f Graph	virus x drug interaction p = 0.085 virus main effect p = 0.506 drug main effect p = 0.406	exact values not reported since significance not reached	virus x drug interaction F(1,54)= 3.08 virus main effect F(1,54)= 0.45 drug main effect F(1,54)=0.70	exact values not reported
+ -	Fig. S5g	Two-Way ANOVA	Fig. S5g Legend	16, 13, 13, 16	16 scrShank3 vehicle mice, 13 shShank3 vehicle mice, 13 scrShank3 Ro mice, 16 shShank3 Ro mice	Fig. S5g Graph	errors bars are mean +/- SEM and scatter plot	Fig. S5g Graph	virus x drug interaction p = 0.240 virus main effect p = 0.215 drug main effect p = 0.304	exact values not reported since significance not reached	virus x drug interaction F(1,54)= 1.41 virus main effect F(1,54)= 1.57 drug main effect F(1,54)=1.07	exact values not reported
+ -	Fig. S5h	Two-Way ANOVA	Fig. S5h Legend	16, 13, 13, 16	16 scrShank3 vehicle mice, 13 shShank3 vehicle mice, 13 scrShank3 Ro mice, 16 shShank3 Ro mice	Fig. S5h Graph	errors bars are mean +/- SEM and scatter plot	Fig. S5h Graph	virus x drug interaction p = 0.031 virus main effect p = 0.346 drug main effect p = 0.802	Fig. S5h Legend	virus x drug interaction F(1,54)= 4.88 virus main effect F(1,54)= 0.90 drug main effect F(1,54)=0.06	Fig. S5h Legend
+ -	Fig. S5h	Tukey HSD	Fig. S5h Legend	16, 13	16 scrShank3 vehicle mice, 13 shShank3 Vehicle mice	Fig. S5h Graph	errors bars are mean +/- SEM and scatter plot	Fig. S5h Graph	p = 0.084	Fig. S5h Graph		
+ -	Fig. S5h	Tukey HSD	Fig. S5h Legend	13, 16	13 shShank3 vehicle, 16 shShank3 Ro mice	Fig. S5h Graph	errors bars are mean +/- SEM and scatter plot	Fig. S5h Graph	p = 0.214	Fig. S5h Graph		
+ -	Fig. S5h	Tukey HSD	Fig. S5h Legend	16, 16	16 scrShank3 vehicle mice, 16 shShank3 Ro mice	Fig. S5h Graph	errors bars are mean +/- SEM and scatter plot	Fig. S5h Graph	p = 0.866	Fig. S5h Graph		
+ -	Fig. S5i	Two-Way ANOVA	Fig. S5h Legend	16, 13, 13, 16	16 scrShank3 vehicle mice, 13 shShank3 vehicle mice, 13 scrShank3 Ro mice, 16 shShank3 Ro mice	Fig. S5h Graph	errors bars are mean +/- SEM and scatter plot	Fig. S5h Graph	virus x drug interaction p = 0.122 virus main effect p = 0.976 drug main effect p = 0.143	exact values not reported since significance not reached	virus x drug interaction F(1,54)= 2.47 virus main effect F(1,54) = 0.001 drug main effect F(1,54)= 2.21	exact values not reported
+ -	Fig. S5j	Two-Way ANOVA	Fig. S5j Legend	16, 13, 13, 16	16 scrShank3 vehicle mice, 13 shShank3 vehicle mice, 13 scrShank3 Ro mice, 16 shShank3 Ro mice	Fig. S5j Graph	errors bars are mean +/- SEM and scatter plot	Fig. S5j Graph	virus x drug interaction p = 0.122 virus main effect p = 0.976 drug main effect p = 0.143	exact values not reported since significance not reached	virus x drug interaction F(1,54)= 2.47 virus main effect F(1,54) = 0.001 drug main effect F(1,54)= 2.21	exact values not reported

Nature Neuroscience: doi:10.1038/nn.4319

+ -	Fig. S6e	unpaired t-test	Fig. S6e Legend	16, 18	16 scrShank3 mice, 18 shShank3 mice	Fig. S6e Graph	errors bars are mean +/- SEM and scatter plot	Fig. S6e Graph	p = 0.030	Fig. S6e Graph	t (32) = 2.27	Fig. S6e Legend
+ -	Fig. S6f	unpaired t-test	Fig. S6f Legend	16, 18	16 scrShank3 mice, 18 shShank3 mice	Fig. S6f Graph	errors bars are mean +/- SEM and scatter plot	Fig. S6f Graph	p = 0.013	Fig. S6f Graph	t (32) = 2.64	Fig. S6f Legend
+ -	Fig. S6g	Mann-Whitney	Fig. S6g Legend	16, 18	16 scrShank3 mice, 18 shShank3 mice	Fig. S6g Graph	errors bars are mean +/- SEM and scatter plot	Fig. S6g Graph	p = 0.448	Fig. S6g Graph	U = 122.00	Fig. S6g Legend
+ -	Fig. S6i	unpaired t-test	Fig. S6i Legend	16, 18	16 scrShank3 mice, 18 shShank3 mice	Fig. S6i Graph	errors bars are mean +/- SEM and scatter plot	Fig. S6i Graph	p = 0.408	Fig. S6i Graph	t (32) = 0.84	Fig. S6i Legend
+ -	Fig. S6j	Mann-Whitney	Fig. S6j Legend	16, 18	16 scrShank3 mice, 18 shShank3 mice	Fig. S6j graph	errors bars are mean +/- SEM and scatter plot	Fig. S6j graph	p = 0.704	Fig. S6j graph	U = 133.00	Fig. S6j Legend
+ -	Fig. S6k	Mann-Whitney	Fig. S6k Legend	16, 18	16 scrShank3 mice, 18 shShank3 mice	Fig. S6k graph	errors bars are mean +/- SEM and scatter plot	Fig. S6k graph	p = 0.679	Fig. S6k graph	U = 132.00	Fig. S6k Legend
+ -	Fig. S6l	unpaired t-test	Fig. S6l	12, 11	12 scrShank3 mice, 11 shShank3 mice	Fig. S6l graph	errors bars are mean +/- SEM and scatter plot	Fig. S6l graph	p < 0.001	Fig. S6l graph	t (21) = 6.83	Fig. S6l Legend
+ -	Fig. S6m	unpaired t-tests	Fig. S6l	12, 11	12 scrShank3 mice, 11 shShank3 mice	Fig. S6m Graph	errors bars are mean +/- SEM and scatter plot	Fig. S6m Graph	water p < 0.001 sucrose p = 0.182	Fig. S6m Graph	water t (21) = 5.26 sucrose t (21) = -1.38	Fig. S6m Legend
+ -	Fig. S6n	Mann-Whitney	Fig. S6n Legend	12, 11	12 scrShank3 mice, 11 shShank3 mice	Fig. S6n Graph	errors bars are mean +/- SEM and scatter plot	Fig. S6n Graph	p = 0.712	Fig. S6n Graph	U = 60.00	Fig. S6n Legend
+ -	Fig. S6o	Mann-Whitney and unpaired t-tests	Fig. S6o Legend	12, 11	12 scrShank3 mice, 11 shShank3 mice	Fig. S6o Graph	errors bars are mean +/- SEM and scatter plot	Fig. S6o Graph	water p=0.854 sucrose p=0.925	Fig. S6o Graph	water U = 63.00 sucrose t(21) = 0.09	Fig. S6o Legend
+ -	Fig. S7a	Mann-Whitney	Fig. S7a Legend	14, 16	14 scrShank3 mice, 16 shShank3 mice	Fig. S7a Graph	errors bars are mean +/- SEM and scatter plot	Fig. S7a Graph	p = 0.135	Fig. S7a Graph	U = 76.00	Fig. S7a Legend
+ -	Fig. S7b	Mann-Whitney	Fig. S7b Legend	14, 16	14 scrShank3 mice, 16 shShank3 mice	Fig. S7b Graph	errors bars are mean +/- SEM and scatter plot	Fig. S7b Graph	p = 0.135	Fig. S7b Graph	U = 76.00	Fig. S7b Legend
+ -	Fig. S7c	unpaired t-tests	Fig. S7c Legend	14, 16	14 scrShank3 mice, 16 shShank3 mice	Fig. S7c Graph	errors bars are mean +/- SEM and scatter plot	Fig. S7c Graph	wall p = 0.713 intermediate p = 0.535 center p = 0.704	Fig. S7c Graph	wall t (28) = 0.37 intermediate t(28) = -0.63 center t(28) = 0.38	Fig. S7c Legend
+ -	Fig. S7d	Mann-Whitney	Fig. S7d Legend	14, 16	14 scrShank3 mice, 16 shShank3 mice	Fig. S7d Graph	errors bars are mean +/- SEM and scatter plot	Fig. S7d Graph	p = 0.002	Fig. S7d Graph	U = 38.50	Fig. S7d Legend
+ -	Fig. S7e	Two-Way ANOVA	Fig. S7e Legend	16, 13, 13, 16	16 scrShank3 vehicle mice, 13 shShank3 vehicle mice, 13 scrShank3 Ro mice, 16 shShank3 Ro mice	Fig. S7e Graph	errors bars are mean +/- SEM and scatter plot	Fig. S7e Graph	virus x drug interaction p = 0.044 virus main effect p = 0.995 drug main effect p = 0.049	Fig. S7e legend	virus x drug interaction F (1,54) = 4.27 virus main effect F (1,54) <0.001 drug main effect F (1,54) = 4.05	Fig. S7e legend
+ -	Fig. S7e	Tukey HSD	Fig. S7e Legend	16, 13	16 scrShank3 vehicle mice, 13 shShank3 vehicle mice	Fig. S7e Graph	errors bars are mean +/- SEM and scatter plot	Fig. S7e Graph	p = 0.322	Fig. S7e graph		

Nature Neuroscience: doi:10.1038/nn.4319

+ -	Fig. S7e	Tukey HSD	Fig. S7e Legend	13, 16	13 shShank3 vehicle mice, 16 shShank3 Ro mice	Fig. S7e Graph	errors bars are mean +/- SEM and scatter plot	Fig. S7e Graph	p = 0.017	Fig. S7e graph		
+ -	Fig. S7e	Tukey HSD	Fig. S7e Legend	16, 16	16 scrShank3 vehicle mice, 16 shShank3 Ro mice	Fig. S7e Graph	errors bars are mean +/- SEM and scatter plot	Fig. S7e Graph	p = 0.297	Fig. S7e graph		
+ -	Fig. S7f	Two-Way ANOVA	Fig. S7f Legend	16, 13, 13, 16	16 scrShank3 vehicle mice, 13 shShank3 vehicle mice, 13 scrShank3 Ro mice, 16 shShank3 Ro mice	Fig. S7f Graph	errors bars are mean +/- SEM and scatter plot	Fig. S7f Graph	virus x drug interaction p = 0.045 virus main effect p = 0.971 drug main effect p = 0.061	Fig. S7f legend	virus x drug interaction F (1,54) = 4.20 virus main effect F (1,54) <0.001 drug main effect F (1,54) = 3.65	Fig. S7f legend
+ -	Fig. S7f	Tukey HSD	Fig. S7f Legend	16, 13	16 scrShank3 vehicle mice, 13 shShank3 vehicle mice	Fig. S7f Graph	errors bars are mean +/- SEM and scatter plot	Fig. S7f Graph	p = 0.342	Fig. S7f Graph		
+ -	Fig. S7f	Tukey HSD	Fig. S7f Legend	13, 16	13 shShank3 vehicle mice, 16 shShank3 Ro mice	Fig. S7f Graph	errors bars are mean +/- SEM and scatter plot	Fig. S7f Graph	p = 0.021	Fig. S7f Graph		
+ -	Fig. S7f	Tukey HSD	Fig. S7f Legend	16, 16	16 scrShank3 vehicle mice, 16 shShank3 Ro mice	Fig. S7f Graph	errors bars are mean +/- SEM and scatter plot	Fig. S7f Graph	p = 0.327	Fig. S7f Graph		
+ -	Fig. S8a left	unpaired t-test	Fig. S8a Legend	10, 14	10 shShank3 vehicle, 14 shShank3 Ro	Fig. S8a Graph	errors bars are mean +/- SEM and scatter plot	Fig. S8a Graph	p = 0.832	Fig. S8a Graph	t (22) = 0.21	Fig. S8a Legend
+ -	Fig. S8a middle	unpaired t-test	Fig. S8a Legend	10, 14	10 shShank3 vehicle, 14 shShank3 Ro	Fig. S8a Graph	errors bars are mean +/- SEM and scatter plot	Fig. S8a Graph	p = 0.208	Fig. S8a Graph	t (22) = -1.30	Fig. S8a Legend
+ -	Fig. S8a right	unpaired t-test	Fig. S8a Legend	10, 14	10 shShank3 vehicle, 14 shShank3 Ro	Fig. S8a Graph	errors bars are mean +/- SEM and scatter plot	Fig. S8a Graph	p = 0.227	Fig. S8a Graph	t (22) = -1.24	Fig. S8a Legend
+ -	Fig. S8b left	unpaired t-test	Fig. S8b Legend	10, 14	10 shShank3 vehicle, 14 shShank3 Ro	Fig. S8b Graph	errors bars are mean +/- SEM and scatter plot	Fig. S8b Graph	p = 0.280	Fig. S8b Graph	t (22) = 1.11	Fig. S8b Legend
+ -	Fig. S8b, middle	unpaired t-test	Fig. S8b Legend	10, 14	10 shShank3 vehicle, 14 shShank3 Ro	Fig. S8b Graph	errors bars are mean +/- SEM and scatter plot	Fig. S8b Graph	p = 0.958	Fig. S8b Graph	t (22) = -0.05	Fig. S8b legend
+ -	Fig. S8b, right	unpaired t-test	Fig. S8b Legend	10, 14	10 shShank3 vehicle, 14 shShank3 Ro	Fig. S8b Graph	errors bars are mean +/- SEM and scatter plot	Fig. S8b Graph	p = 0.498	Fig. S8b Graph	t (22) = 0.69	Fig. S8b legend
+ -	Fig. 6c	Two-way ANOVA	Fig. 6c Legend	16, 16, 13, 13	16 scrShank3 Vehicle T1, 16 scrShank3 Vehicle T2, 13 shShank3 Vehicle T1, 13 shShank3 Vehicle T2	Fig. 6c Graph	errors bars are mean +/- SEM and scatter plot	Fig. 6c Graph	time main effect p = 0.368 virus main effect p = 0.220 time x virus p = 0.006	Fig. 6c Legend	time main effect F (1,54) = 0.83 virus main effect F (1,54) = 1.54 time x virus F (1.54) = 8.30	Fig. 6c Legend
+ -	Fig. 6c	Two-way ANOVA	Fig. 6c Legend	13, 13, 16, 16	13 scrShank3 Ro T1, 13 scrShank3 Ro T2, 16 shShank3 Ro T1, 16 shShank3 Ro T2	Fig. 6c Graph	errors bars are mean +/- SEM and scatter plot	Fig. 6c Graph	time main effect p = 0.683 virus main effect p = 0.207 time x virus p = 0.531	Fig. 6c Legend	time main effect F (1,54) = 0.17 virus main effect F (1,54) = 1.63 time x virus F (1,54) = 0.40	Fig. 6c Legend

Nature Neuroscience: doi:10.1038/nn.4319

+ -	Fig. 8f	Two-way ANOVA	Fig. 8f Legend	10, 10, 11, 11	10 scrShank3 off T1, 10 scrShank3 off T2, 11 shShank3 off T1, 11 shShank3 off T2	Fig. 8f Graph	errors bars are mean +/- SEM and scatter plot	Fig. 8f Graph	time main effect p = 0.204 virus main effect p = 0.003 time x virus p = 0.044	Fig. 8f Legend	time main effect F (1,38) = 1.67 virus main effect F (1,38) = 9.88 time x virus F (1,38) = 4.34	Fig. 8f Legend
+ -	Fig. 8f	Two-way ANOVA	Fig. 8f Legend	8, 8, 6, 6	8 scrShank3 on T1, 8 scrShank3 on T2, 6 shShank3 on T1, 6 shShank3 on T2	Fig. 8f Graph	errors bars are mean +/- SEM and scatter plot	Fig. 8f Graph	time main effect p < 0.001 virus main effect p = 0.527 time x virus p = 0.558	Fig. 8f Legend	time main effect F (1,24) = 31.08 virus main effect F (1,24) = 0.41 time x virus F (1,24) = 0.35	Fig. 8f Legend

Representative figures

1. Are any representative images shown (including Western blots and immunohistochemistry/staining) in the paper?

   If so, what figure(s)?

   Yes, Fig.1, Fig.8, S1, S4, S6

2. For each representative image, is there a clear statement of how many times this experiment was successfully repeated and a discussion of any limitations in repeatability?

   If so, where is this reported (section, paragraph #)?

   No, but the infection site has been validated for each animal used for the behavioral test and the in vivo electrophysiology. The WB image is from 4 mice. See table above for details.

Statistics and general methods

1. Is there a justification of the sample size?

   If so, how was it justified?

   Where (section, paragraph #)?

   Even if no sample size calculation was performed, authors should report why the sample size is adequate to measure their effect size.

   Based on previous experiments and publications, we have used a sample size that allow acceptable variability in order to draw valid conclusion.

2. Are statistical tests justified as appropriate for every figure?

   Where (section, paragraph #)?

   Yes, the appropriate statistical analysis is justified in details in Materials and Methods. The specific tests applied for each graph are also reported in the Figure legends.

   a. If there is a section summarizing the statistical methods in the methods, is the statistical test for each experiment clearly defined?

   Yes, in Materials and Methods section there is a paragraph entitled Statistical Analysis where we justified each test for each experiment. For each experiment the statistical test is detailed in the corresponding figure legend.

   b. Do the data meet the assumptions of the specific statistical test you chose (e.g. normality for a parametric test)?

   Where is this described (section, paragraph #)?

   Yes, as reported in the Statistical Analysis paragraph of Materials and Methods we report that the Shapiro-Wilk test was used to assess the normality for all the data. If violated, non-parametric tests were used.

Nature Neuroscience: doi:10.1038/nn.4319

c. Is there any estimate of variance within each group of data? Is the variance similar between groups that are being statistically compared? Where is this described (section, paragraph #)?	For each experiment the equality of variances has been assessed with Levene's test and when violated, the corrected degree of freedom for the t-test has been reported. As described in the Statistical Analysis session.
d. Are tests specified as one- or two-sided?	Yes, two-sided tests were used for all the experiments.
e. Are there adjustments for multiple comparisons?	Yes, following Two-Way ANOVA post hoc tests that correct for multiple comparisons were used.
3. Are criteria for excluding data points reported? Was this criterion established prior to data collection? Where is this described (section, paragraph #)?	Yes, the criteria were established prior to data collection and reported in the Material and Methods section.
4. Define the method of randomization used to assign subjects (or samples) to the experimental groups and to collect and process data. If no randomization was used, state so. Where does this appear (section, paragraph #)?	The day of the viral infection, we randomly assigned within the same litter the mice to their experimental group. This information appears in the text in the Material and methods session.
5. Is a statement of the extent to which investigator knew the group allocation during the experiment and in assessing outcome included? If no blinding was done, state so. Where (section, paragraph #)?	The behavioral experiments were performed, assessed and analyzed by an experimenter that was blind to the treatments and conditions. For the physiology either the viral infection or the treatment was blind to the experimenter. This information appears in the text in the Materials and methods session.
6. For experiments in live vertebrates, is a statement of compliance with ethical guidelines/regulations included? Where (section, paragraph #)?	Yes it is state in the Material and Methods session, first paragrapher "Animals"
7. Is the species of the animals used reported? Where (section, paragraph #)?	Yes it is state in the Material and Methods section, first paragrapher "Animals"
8. Is the strain of the animals (including background strains of KO/ transgenic animals used) reported? Where (section, paragraph #)?	Yes it is state in the Material and Methods section, first paragrapher "Animals"
9. Is the sex of the animals/subjects used reported? Where (section, paragraph #)?	We balanced female and male in this study according to the experimental groups and we now report it in the Materals and Methods section.
10. Is the age of the animals/subjects reported? Where (section, paragraph #)?	Yes we report the age of the animals in the figures when we indicate the experimental protocol, above the graphs and it is also stated in the result session
11. For animals housed in a vivarium, is the light/dark cycle reported? Where (section, paragraph #)?	Yes, we now report a standard light/dark cycle in the Materials and methods session.

Nature Neuroscience: doi:10.1038/nn.4319

12. For animals housed in a vivarium, is the housing group (i.e. number of animals per cage) reported? Where (section, paragraph #)?	We state that the animals were housed in groups in the Materials and Methods session.
13. For behavioral experiments, is the time of day reported (e.g. light or dark cycle)? Where (section, paragraph #)?	We did the experiments during the light cycle. We now report it into the Materials and methods session.
14. Is the previous history of the animals/subjects (e.g. prior drug administration, surgery, behavioral testing) reported? Where (section, paragraph #)?	The history of the animals is reported in result, material and methods and legend sessions.
a. If multiple behavioral tests were conducted in the same group of animals, is this reported? Where (section, paragraph #)?	No
15. If any animals/subjects were excluded from analysis, is this reported? Where (section, paragraph #)?	Yes, is reported in the material and methods session.
a. How were the criteria for exclusion defined? Where is this described (section, paragraph #)?	The animals were excluded if no virus infection was detected at the end of the experiment. In the behavioral experiments we excluded one animal that did not show any social preference during the test. This is stated in the Material and Methods session.
b. Specify reasons for any discrepancy between the number of animals at the beginning and end of the study. Where is this described (section, paragraph #)?	NA

Reagents

1. Have antibodies been validated for use in the system under study (assay and species)?	Yes, the antibodies used in the study were validated in IHC and WB experiments in mouse and rat.
a. Is antibody catalog number given? Where does this appear (section, paragraph #)?	Yes, in the Materials and Methods session.
b. Where were the validation data reported (citation, supplementary information, Antibodypedia)? Where does this appear (section, paragraph #)?	The validation data is reported in the data sheet of the company.

Nature Neuroscience: doi:10.1038/nn.4319

2. Cell line identity

a. Are any cell lines used in this paper listed in the database of commonly misidentified cell lines maintained by ICLAC and NCBI Biosample?

Where (section, paragraph #)?

NA

b. If yes, include in the Methods section a scientific justification of their use--indicate here in which section and paragraph the justification can be found.

NA

c. For each cell line, include in the Methods section a statement that specifies:

- the source of the cell lines
- have the cell lines been authenticated? If so, by which method?
- have the cell lines been tested for mycoplasma contamination?

Where (section, paragraph #)?

NA

Data deposition

Data deposition in a public repository is mandatory for:

a. Protein, DNA and RNA sequences
b. Macromolecular structures
c. Crystallographic data for small molecules
d. Microarray data

Deposition is strongly recommended for many other datasets for which structured public repositories exist; more details on our data policy are available here. We encourage the provision of other source data in supplementary information or in unstructured repositories such as Figshare and Dryad.

We encourage publication of Data Descriptors (see Scientific Data) to maximize data reuse.

1. Are accession codes for deposit dates provided?

Where (section, paragraph #)?

Yes, we reported the GeneBank code in the accession code session.

Computer code/software

Any custom algorithm/software that is central to the methods must be supplied by the authors in a usable and readable form for readers at the time of publication. However, referees may ask for this information at any time during the review process.

1. Identify all custom software or scripts that were required to conduct the study and where in the procedures each was used.

NA

2. If computer code was used to generate results that are central to the paper's conclusions, include a statement in the Methods section under "**Code availability**" to indicate whether and how the code can be accessed. Include version information as necessary and any restrictions on availability.

NA

Nature Neuroscience: doi:10.1038/nn.4319

Human subjects

1. Which IRB approved the protocol?

   Where is this stated (section, paragraph #)?

   NA

2. Is demographic information on all subjects provided?

   Where (section, paragraph #)?

   NA

3. Is the number of human subjects, their age and sex clearly defined?

   Where (section, paragraph #)?

   NA

4. Are the inclusion and exclusion criteria (if any) clearly specified?

   Where (section, paragraph #)?

   NA

5. How well were the groups matched?

   Where is this information described (section, paragraph #)?

   NA

6. Is a statement included confirming that informed consent was obtained from all subjects?

   Where (section, paragraph #)?

   NA

7. For publication of patient photos, is a statement included confirming that consent to publish was obtained?

   Where (section, paragraph #)?

   NA

fMRI studies

For papers reporting functional imaging (fMRI) results please ensure that these minimal reporting guidelines are met and that all this information is clearly provided in the methods:

1. Were any subjects scanned but then rejected for the analysis after the data was collected?

   NA

   a. If yes, is the number rejected and reasons for rejection described?

      Where (section, paragraph #)?

      NA

2. Is the number of blocks, trials or experimental units per session and/or subjects specified?

   Where (section, paragraph #)?

   NA

3. Is the length of each trial and interval between trials specified?

   NA

Nature Neuroscience: doi:10.1038/nn.4319

4. Is a blocked, event-related, or mixed design being used? If applicable, please specify the block length or how the event-related or mixed design was optimized.	NA
5. Is the task design clearly described? Where (section, paragraph #)?	NA
6. How was behavioral performance measured?	NA
7. Is an ANOVA or factorial design being used?	NA
8. For data acquisition, is a whole brain scan used? If not, state area of acquisition.	NA
a. How was this region determined?	NA
9. Is the field strength (in Tesla) of the MRI system stated?	NA
a. Is the pulse sequence type (gradient/spin echo, EPI/spiral) stated?	NA
b. Are the field-of-view, matrix size, slice thickness, and TE/TR/ flip angle clearly stated?	NA
10. Are the software and specific parameters (model/functions, smoothing kernel size if applicable, etc.) used for data processing and pre-processing clearly stated?	NA
11. Is the coordinate space for the anatomical/functional imaging data clearly defined as subject/native space or standardized stereotaxic space, e.g., original Talairach, MNI305, ICBM152, etc? Where (section, paragraph #)?	NA
12. If there was data normalization/standardization to a specific space template, are the type of transformation (linear vs. nonlinear) used and image types being transformed clearly described? Where (section, paragraph #)?	NA
13. How were anatomical locations determined, e.g., via an automated labeling algorithm (AAL), standardized coordinate database (Talairach daemon), probabilistic atlases, etc.?	NA
14. Were any additional regressors (behavioral covariates, motion etc) used?	NA
15. Is the contrast construction clearly defined?	NA
16. Is a mixed/random effects or fixed inference used?	NA

Nature Neuroscience: doi:10.1038/nn.4319

a. If fixed effects inference used, is this justified?	NA
17. Were repeated measures used (multiple measurements per subject)?	NA
a. If so, are the method to account for within subject correlation and the assumptions made about variance clearly stated?	NA
18. If the threshold used for inference and visualization in figures varies, is this clearly stated?	NA
19. Are statistical inferences corrected for multiple comparisons?	NA
a. If not, is this labeled as uncorrected?	NA
20. Are the results based on an ROI (region of interest) analysis?	NA
a. If so, is the rationale clearly described?	NA
b. How were the ROI's defined (functional vs anatomical localization)?	NA
21. Is there correction for multiple comparisons within each voxel?	NA
22. For cluster-wise significance, is the cluster-defining threshold and the corrected significance level defined?	NA

Additional comments

Additional Comments	NA

Nature Neuroscience: doi:10.1038/nn.4319